

UNIVERSIDADE FEDERAL DO RIO GRANDE DO SUL
INSTITUTO DE INFORMÁTICA
PROGRAMA DE PÓS-GRADUAÇÃO EM COMPUTAÇÃO

GUSTAVO MELLO MACHADO

**A Model for Simulation of Color Vision
Deficiency and A Color Contrast
Enhancement Technique for Dichromats**

Thesis presented in partial fulfillment
of the requirements for the degree of
Master of Computer Science

Prof. Dr. Manuel Menezes de Oliveira Neto
Advisor

Porto Alegre, September 2010

CIP – CATALOGING-IN-PUBLICATION

Machado, Gustavo Mello

A Model for Simulation of Color Vision Deficiency and A Color Contrast Enhancement Technique for Dichromats / Gustavo Mello Machado. – Porto Alegre: PPGC da UFRGS, 2010.

94 f.: il.

Thesis (Master) – Universidade Federal do Rio Grande do Sul. Programa de Pós-Graduação em Computação, Porto Alegre, BR–RS, 2010. Advisor: Manuel Menezes de Oliveira Neto.

1. Models of Color Vision. 2. Color Perception. 3. Simulation of Color Vision Deficiency. 4. Recoloring Algorithm. 5. Color-Contrast Enhancement. 6. Color Vision Deficiency. 7. Dichromacy. 8. Anomalous Trichromacy. I. Oliveira Neto, Manuel Menezes de. II. Título.

UNIVERSIDADE FEDERAL DO RIO GRANDE DO SUL

Reitor: Prof. Carlos Alexandre Netto

Vice-Reitor: Prof. Rui Vicente Oppermann

Pró-Reitora de Pós-Graduação: Prof. Aldo Bolten Lucion

Diretor do Instituto de Informática: Prof. Flávio Rech Wagner

Coordenador do PPGC: Prof. Álvaro Freitas Moreira

Bibliotecária-Chefe do Instituto de Informática: Beatriz Regina Bastos Haro

“...Galega, tento descrever o que é estar com você...”
— FRED ZERO QUATRO (MEU ESQUEMA)

ACKNOWLEDGMENTS

I am deeply grateful to professor Manuel for his dedication as my advisor in this work, for the precision and lucidity of his teachings and suggestions that provided significant help to reach the outcomes, for his understanding and encouragement in times of difficulty and the severity in moments of weakness. With hard work and study, he introduced me to the academic life, showed me a career and became an example of life.

I would also like to express my thanks to Leandro A. F. Fernandes who efficiently drove the various experiments with volunteers and to the volunteers including my father. For all the moments of study and academic living, I thank my colleagues and professors, especially the ones from the Computer Graphics Group of PPGC-UFRGS.

I thank Giovane Kuhn for many fruitful discussions and suggestions, and Francisco Pinto for providing the visualization software. The many reference images used in this work were kindly provided by Francisco Pinto, CCSE at LBNL, Martin Falk e Daniel Weiskopf, Karl Rasche and <http://commons.wikimedia.org>. This work was sponsored by CNPq-Brazil (grants 200284/2009-6, 131327/2008-9, 476954/2008-8, 305613/2007-3 and 142627/2007-0). Nvidia kindly donated the Quadro FX 5800 card used in this research. I also thank the anonymous reviewers for their insightful comments on the submissions.

I would like to express special thanks to my wife, Sharon C. Andrade, for the mutual love, for always supporting me, for her company that was fundamental to my effective participation in all stages of this work, and for accepting to be my “evolutionary partner” forever. I also thank my parents, Christiano H. L. Machado and Tereza M. Mello Machado, who were my advisors in life; my brother and sisters, Rodrigo, Denise and Camila, for the eternal friendship and trust; my mother-in-law Maria do Carmo Dias Custodio for her friendship and warm accommodation; and my grandmother, Lygia T. C. Mello, fan of Fluminense, for her love and for teaching me that we can lose everything but we must never lose the joke.

CONTENTS

LIST OF FIGURES	9
LIST OF TABLES	13
ABSTRACT	15
RESUMO	17
1 INTRODUCTION	19
1.1 Thesis Contributions	21
1.2 Structure of the Thesis	21
2 BACKGROUND ON COLOR VISION DEFICIENCY	23
2.1 Photoreceptor Cells	23
2.2 Stage Theories of Human Color Vision	24
2.3 Genetic of Human Photopigments	25
2.4 Color Vision Deficiency	25
3 RELATED WORK	29
3.1 Simulation Techniques	29
3.2 Recoloring Techniques	32
3.2.1 User-Assisted Techniques	32
3.2.2 Optimization-based Techniques	32
3.2.3 Color-to-Grayscale Mappings	33
3.3 Summary	35
4 A PHYSIOLOGICALLY-BASED MODEL FOR SIMULATION OF COLOR VISION DEFICIENCY	37
4.1 Quantification of The Stage Theory	37
4.2 Simulating Color Vision Deficiency	38
4.2.1 Simulating Anomalous Trichromacy	39
4.2.2 Simulating Dichromacy	42
4.2.3 The Algorithm for Simulating CVD	45
4.3 Results	46
4.3.1 Experimental Validation	47
4.3.2 Discussion	50
4.4 Summary and Conclusions	52

5	A REAL-TIME TEMPORAL-COHERENT COLOR CONTRAST ENHANCEMENT FOR DICHROMATS	55
5.1	The Color-Contrast Enhancing Technique	56
5.1.1	Direction that Maximizes Contrast Loss	57
5.1.2	Computing the Final Colors	58
5.1.3	Exaggerated Contrast	59
5.1.4	Enforcing Temporal Coherence	59
5.2	Results	59
5.2.1	Limitations	63
5.3	Summary and Conclusions	65
6	CONCLUSIONS AND FUTURE WORK	67
6.1	Future Work	67
	REFERENCES	69
	APPENDIX A PRE-COMPUTED MATRICES FOR SIMULATION OF CVD	73
	APPENDIX B EXPERIMENTAL DATA	75
	APPENDIX C SIMULATION OF CVD USING SPD OF AN LCD	79
	APPENDIX D UM MODELO PARA SIMULAÇÃO DAS DEFICIÊNCIAS NA PERCEPÇÃO DE CORES E UMA TÉCNICA DE AU- MENTO DO CONTRASTE DE CORES PARA DICROMÁ- TAS	83
D.1	O Modelo para Simulação da Percepção de Cores	85
D.2	A Técnica de Realce de Contraste de Cores	88
D.3	Conclusões	91

LIST OF FIGURES

Figure 1.1	(left) Europe's map with colors used to encode the percentage of population growth/decline of different countries in 2006. (right) simulation of deuteranopes' perception of left image.	19
Figure 1.2	(left) the reference scientific visualization image (Brain dataset). (center) simulation of deuteranopes' perception of left image. (right) simulation of deuteranopes' perception of recolored image. Simulation technique used for center and right images were the proposed by Brettel <i>et al.</i> and recoloring technique for right image was the proposed by Kuhn <i>et al.</i> . Reference image provided by Francisco Pinto.	20
Figure 2.1	Spectral sensitivity functions of the three cone types and the rods (after Smith and Pokorny) concerning an average normal trichromat individual. These curves represent a ratio of probability of photon capture as a function of wavelength.	24
Figure 2.2	Spectral response functions for the opponent channels concerning an average normal trichromat.	25
Figure 2.3	Spectral sensitivity functions of cones in anomalous trichromats. Figures from left to right refer to protanomaly, deuteranomaly, and tritanomaly, respectively. They illustrate the spectral shifts of anomalous cones, which occur in the three kinds of anomalous trichromacy.	26
Figure 2.4	Illustration simulating the perception of dichromats. (left) reference image (color wheel). The subsequent wheels refer from left to right to the perception of protanopes, deuteranopes, and tritanopes, respectively. Wheels were simulated using Brettel <i>et al.</i> 's approach.	26
Figure 3.1	The three graphs illustrate the technique for simulating the perception of individuals with dichromacy proposed by Brettel <i>et al.</i> . In the LMS color space, the original colors are orthographically projected to corresponding semi-planes, along the direction defined by the axis representing the affected cone. Illustrations of the technique for simulating protanopia (left), deuteranopia (center), and tritanopia (right).	30
Figure 3.2	Examples showing the results obtained with Brettel <i>et al.</i> 's simulation technique. (a) a reference image showing a set of color pencils. The subsequent images show the simulation of the perception of protanopes (b), deuteranopes (c), and tritanopes (d).	31

Figure 3.3	Images demonstrating the simulation of the perception of Figure 3.2 (left) by individuals with anomalous trichromacy according to the approach proposed by Yang <i>et al.</i> . First row shows simulations of protanomalous' perceptions while the second row shows simulations of deuteranomalous' perceptions. The four columns, from left to right, concerns anomalous trichromacy with severities (spectral shift in wavelength) of 8 nm, 12 nm, 16 nm, and 20 nm, respectively. To compare with the perception of severe anomalous trichromacy, the last column shows simulations according to Brettel <i>et al.</i> 's approach for protanopes and deuteranopes in the first and second rows, respectively.	31
Figure 3.4	Demonstration of the results of two recently developed recoloring techniques. (a) the reference image showing natural scene with some flowers in foreground. (b) simulation of the perception of individuals with deuteranopia according to Brettel <i>et al.</i> . Subsequently, simulations of deuteranope's perception of the recolored images according to the approaches proposed by Rasche <i>et al.</i> in (c) and Kuhn <i>et al.</i> in (d). Images extracted from Kuhn <i>et al.</i> 's paper.	34
Figure 4.1	Scientific visualization under color vision deficiency. Simulation, for a normal trichromat, of the color perception of individuals with color vision deficiency (protanomaly) at different degrees of severity. The image on the left (turbulent flows) illustrates the perception of a normal trichromat and is used for reference. The numbers in parenthesis indicate the amount of shift, in nanometers, applied to the spectral response of the L cones. The image on the right shows the simulated perception of a dichromat (protanope), which is approximately equivalent to the perception of protanomalous with a spectral shift of 20 nm. Note the progressive loss of color contrast as the degree of severity increases. Images simulated using the proposed model. Reference image was provided by CCSE at LBNL.	38
Figure 4.2	Ingling and Tsou's two-stage model of human color vision. The output of the photoreceptor stage (L , M and S cones) is linearly combined in the opponent stage (V_λ , $y - b$, and $r - g$ nodes).	39
Figure 4.3	(left) Cone spectral sensitivity functions for an average normal trichromat (after Smith and Pokorny). (right) Spectral response functions for the opponent channels of the average normal trichromat according to Ingling and Tsou's model. These functions are obtained by evaluating Equation 4.1 for the LMS triples resulting from the cone spectral sensitivity functions at all wavelengths in the visible range.	40
Figure 4.4	Exon arrangements of the L , M , and hybrid photopigment genes. X-linked anomalous photopigment spectral sensitivity are interpreted as interpolations of the normal L and M photopigment spectra. Adapted from Sharpe <i>et al.</i>	40
Figure 4.5	Spectral opponent functions for anomalous trichromats. (left) Protanomaly ($\Delta\lambda_L = 15 \text{ nm}$). (right) Deuteranomaly ($\Delta\lambda_M = -19 \text{ nm}$).	41

Figure 4.6	Reference images. (a) Flower. (b) Brain. (c) Cat's Eye nebula. (d) Scatter plot. (e) Slice of the HSV color space ($V=1$). (f) Tornado.	43
Figure 4.7	Simulation of dichromatic perception for the flower shown in Figure 4.6(a) according to four different models. From left to right: empty space / empty cones, photopigment substitution (replacement model), photopigment substitution with scaling according to Equation 4.15, same as previous but also scaled by 0.96, Brettel <i>et al.</i> 's (for reference).	43
Figure 4.8	Comparison of the plausible dichromacy models considering the entire RGB space (protanopia case). A surface obtained using Brettel <i>et al.</i> 's algorithm is shown for reference in all images. (a) Empty Space / Empty Cones model. (b) Replacement model. (c) Replacement model using Equation 4.15. (d) Same as (c) but also scaled by 0.96.	45
Figure 4.9	Simulation of protanomalous and deuteranomalous vision for several degrees of severity (expressed in nm). Last column: result of Brettel <i>et al.</i> 's algorithm for reference. <i>P/D (Model)</i> : Protanomaly/Deuteranomaly simulated with the proposed technique. <i>P/D (Yang)</i> : Protanomaly/Deuteranomaly simulated with Yang <i>et al.</i> 's technique.	48
Figure 4.10	Simulation of protanomalous and deuteranomalous vision in scientific visualization. From top to bottom: brain dataset, Tornado, Scatter plot, and Cat's Eye nebula. The degrees of severity are expressed in nm . Last column: Brettel <i>et al.</i> 's dichromatic simulation for reference. <i>Pnomaly</i> : Protanomaly. <i>Dnomaly</i> : Deuteranomaly.	49
Figure 4.11	Averaged results of the Farnsworth-Munsell 100H test performed by 17 normal trichromats using the test original colors.	50
Figure 4.12	Averaged results of the Farnsworth-Munsell 100H test. (a) Normal trichromats simulating protan vision. (b) Protan results for the original colors. (c) Normal trichromats simulating deutan vision. (d) Deutan results for the original colors.	51
Figure 4.13	Visualization of the Visible Male's head using the same transfer function (bottom) defined over the color gamut (top row) of a normal trichromat, a protanomalous (10 nm), and a protanope.	52
Figure 5.1	Comparison of the results produced by the proposed recoloring technique and by Kuhn <i>et al.</i> 's for a set of scientific visualization images. The "Dichromat" column shows the simulated perception of dichromats for the corresponding "Reference" image obtained using the approach presented in Chapter 4 The simulation and recolorings of the Flame and Nebula images are for deuteranopes, while the Tornado ones are for protanopes.	56
Figure 5.2	Planar approximation for the color gamut of dichromats in the CIE $L^*a^*b^*$ color space. (a) Protanope ($\theta_p = -11.48^\circ$). (b) Deuteranope ($\theta_d = -8.11^\circ$). (c) Tritanope ($\theta_t = 46.37^\circ$).	57

Figure 5.3	The steps of the proposed recoloring algorithm. (a) Colors c_1 to c_4 are perceived by a dichromat as c'_1 to c'_4 , respectively (their projections on the dichromat's gamut plane). The relative loss of contrast experienced by a dichromat for a pair of colors (c_i, c_j) is given by $l_{(c_i, c_j)} = (\ c_i - c_j\ - \ c'_i - c'_j\) / (\ c_i - c_j\)$, which happens along the direction $\vartheta_{ij} = c_i - c_j$. (b) Direction v_{ab} (shown in blue) that maximizes the loss of local contrast (in a least-square sense) is computed as the main eigenvector of the matrix $M^T M$, where M is defined in Equation 5.2. (c) Projection of the original colors on the plane defined by v_{ab} and L^* . (d) Final colors obtained after rotating the projected colors c''_k in (c) around L^* so that they align with the dichromat's plane.	58
Figure 5.4	Comparison of the results produced by the proposed technique and by Kuhn <i>et al.</i> 's. First row, from left to right: reference image, simulated perception of a deuteranope, and recolored images using various algorithms. Second row: Perceptual errors according to the DRIM metric. Third row: Local contrast differences according to the RMS metric of Equation 5.3 (for $k = 100$). According to both metrics, the proposed recoloring technique is less prone to noticeable changes in contrast.	60
Figure 5.5	Recoloring of information visualization images for protanopes. . . .	61
Figure 5.6	Integration of the proposed technique with an existing visualization application. (left) Reference image as perceived by an individual with normal color vision. (center) Simulation of the perception of a deuteranope for the reference image using the model explained in chapter 4. (right) Recolored image for a deuteranope using the proposed technique.	61
Figure 5.7	Example of a situation that causes the proposed technique to fail. Note that deuteranopes (and protanopes) already perceive the reference image as having sufficient contrast, and no recoloring is necessary.	63
Figure 5.8	Comparison of the results produced by the proposed technique and the ones obtained with Kuhn <i>et al.</i> 's approach for a set of medical visualization images. The even rows show the estimated changes in contrast perceived by an observer in the recolored images (with respect to the reference images), according to the DRIM metric. Green indicates <i>loss of contrast</i> , blue represents <i>contrast amplification</i> , and red shows regions with <i>contrast reversal</i> . The metric favors the proposed technique's results in all examples. Reference images Knee and Foot were provided by Francisco Pinto.	64

LIST OF TABLES

Table 1.1	Incidence of red-green color blindness among different ethnic groups.	20
Table 2.1	Incidence of CVD types among Caucasian population.	27
Table 5.1	Performance comparison (in sec.) of the proposed technique and Kuhn <i>et al.</i> 's for both CPU and GPU versions of the algorithms executed on several images. Due to the linear cost of the proposed approach, the relative speedup improves as the image size increases. .	62
Table 5.2	Times (in sec.) for the quantization and reconstruction phases of the technique of Kuhn <i>et al.</i> for several images. K-means used in the CPU version of the technique, and uniform quantization used in its GPU version. The column Clusters shows the number of clusters identified in the quantization phase.	63

ABSTRACT

Color vision deficiency (CVD) affects approximately 200 million people worldwide, compromising the ability of these individuals to effectively perform color and visualization-related tasks. This has a significant impact on their private and professional lives.

This thesis presents a physiologically-based model for simulating color perception. Besides modeling normal color vision, it also accounts for the hereditary and most prevalent cases of color vision deficiency (*i.e.*, protanopia, deuteranopia, protanomaly, and deuteranomaly), which together account for approximately 99.96% of all CVD cases. This model is based on the stage theory of human color vision and is derived from data reported in electrophysiological studies. It is the first model to consistently handle normal color vision, anomalous trichromacy, and dichromacy in a unified way. The proposed model was validated through an experimental evaluation involving groups of color vision deficient individuals and normal color vision ones. This model can provide insights and feedback on how to improve visualization experiences for individuals with CVD. It also provides a framework for testing hypotheses about some aspects of the retinal photoreceptors in color vision deficient individuals.

This thesis also presents an automatic image-recoloring technique for enhancing color contrast for dichromats whose computational cost varies linearly with the number of input pixels. This approach can be efficiently implemented on GPUs, and for typical image sizes it is up to two orders of magnitude faster than the current state-of-the-art technique. Unlike previous approaches, the proposed technique preserves temporal coherence and, therefore, is suitable for video recoloring. This thesis demonstrates the effectiveness of the proposed technique by integrating it into a visualization system and showing, for the first time, real-time high-quality recolored visualizations for dichromats.

Keywords: Models of Color Vision, Color Perception, Simulation of Color Vision Deficiency, Recoloring Algorithm, Color-Contrast Enhancement, Color Vision Deficiency, Dichromacy, Anomalous Trichromacy.

Um Modelo para Simulação das Deficiências na Percepção de Cores e Uma Técnica de Aumento do Contraste de Cores para Dicromátas

RESUMO

As Deficiências na Percepção de Cores (DPC) afetam aproximadamente 200 milhões de pessoas em todo o mundo, comprometendo suas habilidades para efetivamente realizar tarefas relacionadas com cores e com visualização. Isto impacta significativamente os âmbitos pessoais e profissionais de suas vidas.

Este trabalho apresenta um modelo baseado na fisiologia para simulação da percepção de cores. Além de modelar visão de cores normal, ele também compreende os tipos mais predominantes de deficiências na visão de cores (*i.e.*, protanopia, deuteranopia, protanomalia e deuteranomalia), cujas causas são hereditárias. Juntos estes representam aproximadamente 99.96% de todos os casos de DPC. Para modelar a percepção de cores da visão humana, este modelo é baseado na teoria dos estágios e é derivado de dados reportados em estudos eletrofisiológicos. Ele é o primeiro modelo a consistentemente tratar visão de cores normal, tricromacia anômala e dicromacia de modo unificados. Seus resultados foram validados por avaliações experimentais envolvendo grupos de indivíduos com deficiência na percepção de cores e outros com visão de cores normal. Além disso, ele pode proporcionar a melhor compreensão e um *feedback* sobre como aperfeiçoar as experiências de visualização por indivíduos com DPC. Ele também proporciona um *framework* para se testar hipóteses sobre alguns aspectos acerca das células fotoreceptoras na retina de indivíduos com deficiência na percepção de cores.

Este trabalho também apresenta uma técnica automática de recoloração de imagens que visa realçar o contraste de cores para indivíduos dicromatas com custo computacional variando linearmente com o número de pixels. O algoritmo proposto pode ser eficientemente implementado em GPUs, e para imagens com tamanhos típicos ele apresenta performance de até duas ordens de magnitude mais rápida do que as técnicas estado da arte atuais. Ao contrário das abordagens anteriores, a técnica proposta preserva coerência temporal e, portanto, é adequado para recoloração de vídeos. Este trabalho demonstra a efetividade da técnica proposta ao integrá-la a um sistema de visualização e apresentando, pela primeira vez, cenas de visualização recoloridas para dicromatas em tempo-real e com alta qualidade.

Palavras-chave: Modelos da Visão de Cores, Percepção de Cores, Simulação de Deficiências na Percepção de Cores, Algoritmo de Recoloração, Aumento de Contraste de Cores, Deficiências na Percepção de Cores, Dicromacia, Tricromacia Anômala.

1 INTRODUCTION

Color Vision Deficiency (CVD) affects one's ability to distinguish between certain colors. Such condition is predominantly caused by hereditary reasons, while, in some rare cases, it is believed to be acquired by neurological injuries. Estimates indicate that about two hundred million people worldwide have some kind of CVD. Furthermore, there is no known treatment or cure for these dysfunctions.

Individuals with CVD have difficulties in performing color related tasks, which interferes with their personal and professional lives. For example, the map shown in Figure 1.1 (left) aims to illustrate population growth/decline in Europe's countries in 2006 using colors, whose contrast allows the correlation between percentage ranges and countries. Such combination of colors seems to be reasonable to represent the data when the map is read by individuals with normal color vision. But, for individuals with deuteranopia¹, the colors representing population growth of up to 0.5% and population decline of up to 0.5% are indistinguishable (Figure 1.1 right). This example demonstrates a recurring situation in information visualization and scientific visualization images.

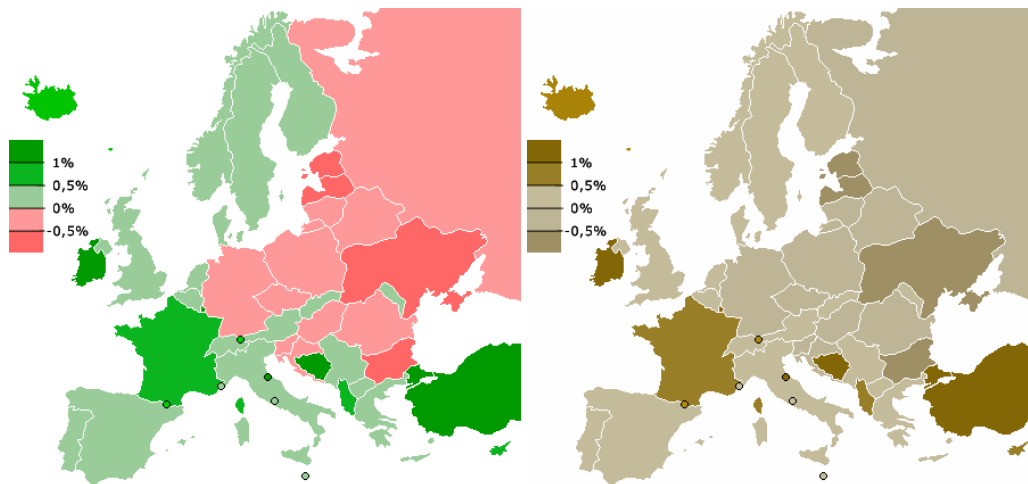


Figure 1.1: (left) Europe's map with colors used to encode the percentage of population growth/decline of different countries in 2006. (right) simulation of deuteranopes' perception of left image. Left image is from (WIKIMEDIA COMMONS, 2010).

Red-green color vision deficiency comprises the most common types of CVD (approximately 99.96% of all cases), which are characterized by malfunction of *L*- or *M*-cones opsins. Such opsins are encoded by genes located on the X chromosome. Thus, such types

¹Deuteranopia is a CVD type characterized by the absence of *M*-photopigments in retina.

are caused by X-linked inheritance and are more prevailing among the male population. Table 1.1 shows the incidence of red-green CVD among different ethnic groups.

Ethnic Groups	Incidence of red-green CVD (%)	
	Male	Female
Caucasians	7.9	0.42
Asians	4.2	0.58
Africans	2.6	0.54

Table 1.1: Incidence of red-green color blindness among different ethnic groups (RIGDEN, 1999; SHARPE et al., 1999).

The most relevant works dealing with CVD can be broadly classified as techniques for *simulation* and *recoloring*. The first group aims to provide tools for demonstrating for individuals with normal color vision how some color stimuli are perceived by individuals with CVD. Such tools help to better understand the difficulties faced by these individuals. Moreover, they can provide insights and feedback, for example, on how to improve visualization experiences for individuals with color vision deficiency. Recoloring algorithms, on the other hand, aim to change image colors so that individuals with CVD can recover (as much as possible) the lost color contrast. No previous techniques are capable to provide real-time recoloring. Besides, an efficient technique could be integrated to portable devices, which would impact these individuals' daily lives.

The results of state-of-art techniques for simulation and recoloring are illustrated in Figure 1.2. It uses as reference (Figure 1.2 left) a scientific visualization image. Figure 1.2 (center) shows the simulation of deuteranopes' perception for the reference image according to Brettel *et al.* (BRETTEL; VIÉNOT; MOLLON, 1997). For these individuals, the ability to distinguish between certain colors vanishes compromising their capacity to identify the image features. Note, however, how a recoloring technique (Figure 1.2 right) offers a good possibility for these individuals to perceive the contrasts. This image was recolored according to the exaggerated approach proposed by Kuhn *et al.* (KUHN; OLIVEIRA; FERNANDES, 2008a), which preserves image naturalness.

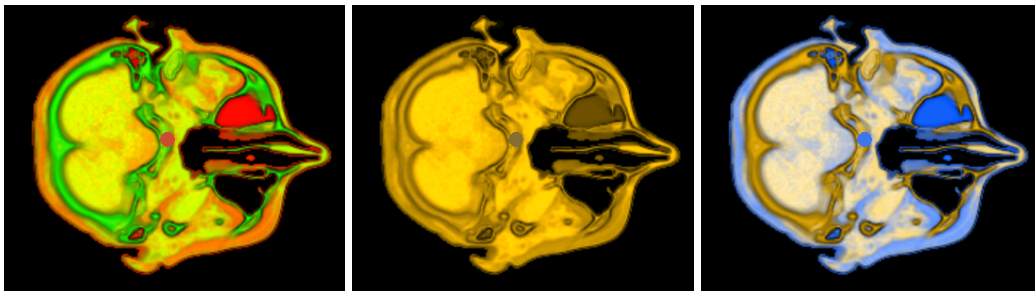


Figure 1.2: (left) the reference scientific visualization image (Brain dataset). (center) simulation of deuteranopes' perception of left image. (right) simulation of deuteranopes' perception of recolored image. Simulation technique used for center and right images were the proposed by Brettel *et al.* (BRETTEL; VIÉNOT; MOLLON, 1997) and recoloring technique for right image was the proposed by Kuhn *et al.* (KUHN; OLIVEIRA; FERNANDES, 2008a). Reference image provided by Francisco Pinto.

1.1 Thesis Contributions

This thesis presents two novel techniques (*i.e.*, a simulation and a recoloring) to solve the main limitations of the state-of-art techniques. Both techniques were successfully integrated into a visualization system, which allowed the practical validation of its results. Both works were published in visualization journals (MACHADO; OLIVEIRA; FERNANDES, 2009; MACHADO; OLIVEIRA, 2010). The simulation technique introduced in this thesis presents the following contributions:

- First model that consistently simulates normal trichromacy, dichromacy², and anomalous trichromacy³ while previous model addressed only dichromacy.
- A single model for simulation that comprises about 99.96% of all cases of CVD while previous approaches addressed only 27.46% of the cases.

And the recoloring technique presented in this thesis has the following contributions:

- High-quality results comparable to results obtained with the state-of-art technique.
- Real-time recoloring. Performance of up to two orders of magnitude faster than the state-of-art technique.
- Temporal coherence preservation, not requiring prior knowledge of subsequent frames.

1.2 Structure of the Thesis

This dissertation is organized as follows: Chapter 2 introduces the color vision deficiencies by addressing the concepts and theories of color perception in humans and provides some useful terminologies. Chapter 3 describes the related works emphasizing the most relevant ones to this thesis. It introduces the state-of-art techniques among simulation and recoloring approaches. Besides, it presents some relevant color-to-grayscale techniques, as they represent algorithms involving dimensionality reduction, a technique akin to recoloring techniques for dichromats. Chapter 4 presents a physiologically-based model for simulation of the perception of individuals with CVD. Moreover, it explains how this model is supported by known theories of color perception and knowledge about color vision deficiencies. It also compares its results with the state-of-art simulation techniques and describes an experiment used to validate the proposed model. Chapter 5 presents a recoloring algorithm that can produce high-quality results in real-time, as well as temporal coherence. It compares its results with the state-of-art recoloring technique and shows the benchmark results, that validated the techniques performance. Moreover, it demonstrates the successful integration with a visualization system. Finally, Chapter 6 concludes the thesis and suggests some possibilities of future work.

²Dichromacy is a CVD type characterized by absence of one type of photopigment in the human retina.

³Anomalous trichromacy is a CVD type characterized by an abnormal cone type in the retina.

2 BACKGROUND ON COLOR VISION DEFICIENCY

This chapter reviews the concepts involving color vision deficiency. It provides some background for the techniques presented in this thesis and summarizes the theories and fundamentals of color perception. Finally, it explains details about each type of CVD, emphasizing the most relevant ones.

2.1 Photoreceptor Cells

Photoreceptor cells are present in the retina and are characterized for being sensitive to light. Their sensitivities are defined by spectral absorption functions, which depend on the photopigment type contained. In the human retina, these cells are broadly classified as *cones* and *rods*.

The rods are primarily responsible for night vision, *i.e.*, low light environment sight. The photopigment type contained in the rods is called rhodopsin¹. This name concerns the red color reflected by the pigment, while the color absorbed by it corresponds mainly to regions of the spectrum with bluish tones. But the rods do not contribute to color perception in humans except under special conditions (SHARPE et al., 1999).

Cones are the photoreceptors responsible for color perception in humans. They act primarily in highly-illuminated environments. Cones are classified as *L*, *M*, and *S*, depending on their sensitivity to the spectrum regions with Long, Medium, and Short wavelengths, respectively.

The spectral sensitivity functions of the four photoreceptors types (*i.e.*, the three cone types and the rods) concerning an average normal trichromat individual are illustrated through the curves in Figure 2.1. These functions are usually graphically represented for ease of reading while define a relationship between probability of photons capture and the wavelength (SHARPE et al., 1999).

Spectral sensitivity functions associated to the *L*, *M*, and *S* cones overlap each other for some wavelength ranges, as can be noticed in Figure 2.1. This is more relevant for the *L*- and *M*-cones. Actually, a photoreceptor is only able to measure the total amount of incident light, responding according to its sensitivity function. For instance, two hypothetical radiations with 600 nm and 500 nm separately will result in equivalent stimuli to *M* cones, since its sensitivities to both wavelengths are approximately equal. Thus, the human visual system will distinguish between these two radiations by combining the responses of the three cone types.

¹ Rhodopsin: from Greek, *Rhodo* means red and *Opsin* means sight.

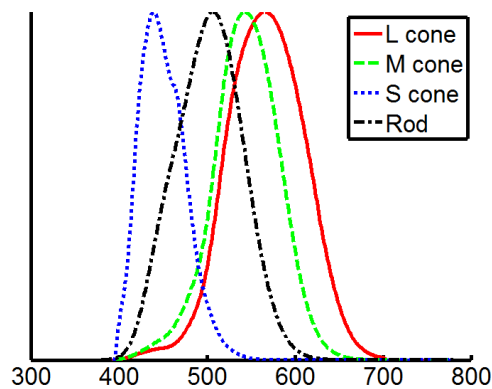


Figure 2.1: Spectral sensitivity functions of the three cone types and the rods (after Smith and Pokorny (SMITH; POKORNY, 1975)) concerning an average normal trichromat individual. These curves represent a ratio of probability of photon capture as a function of wavelength (SHARPE et al., 1999).

2.2 Stage Theories of Human Color Vision

There are some theories about how cone cells sensitivity are interpreted as colors by the human visual system. The *trichromatic theory* of color vision assumes the existence of three kinds of photoreceptors (cone types) with different spectral sensitivities. The responses produced by these photoreceptors would then be sent to the central nervous system and perceived as color sensations (WYSZECKI; STILES, 2000). Also known as the *Young-Helmholtz three-component theory*, it is based on the analysis of the stimuli required to evoke color sensations and provides satisfactory explanation for additive color-matching experiments.

Unfortunately, the theory cannot explain some perceptual issues, such as the opponent nature of visual afterimages, as well as why some hues are never perceived together while others (*e.g.*, green and yellow, green and blue, red and yellow, and red and blue) are easily found (FAIRCHILD, 1997). All these effects can be satisfactorily explained by Hering's *opponent-color theory*, which assumes the existence of six basic colors (white, black, red, green, yellow, and blue). According to Hering, light is absorbed by photopigments but, instead of having six separate channels, the visual system uses only three opposing channels: white-black (*WS*), red-green (*RG*), and yellow-blue (*YB*). While equal amounts of black and white produce a gray sensation, equal amounts of yellow and blue cancel to zero. Likewise, equal amounts of red and green also cancel out. Zero in this context means that the spectral response functions for the opponent channels (Figure 2.2) become zero at the points where opponent colors take equal values.

Considered separately, neither the trichromatic theory nor the opponent-color theory satisfactorily explains several important color-vision phenomena. When combined, however, they could explain and predict many color vision phenomena involving color matching, color discrimination, color appearance, and chromatic adaptation, among others, for both normal color vision and color vision deficient observers (WYSZECKI; STILES, 2000). von Kries suggested that the trichromatic theory should be valid at the photoreceptor level, but the resulting signals should be further processed in a later stage according to the opponent-color theory (JUDD, 1966). This so-called *stage theory* (also known as *zone theory*) provides the best models for human color vision. Besides the two-stage the-

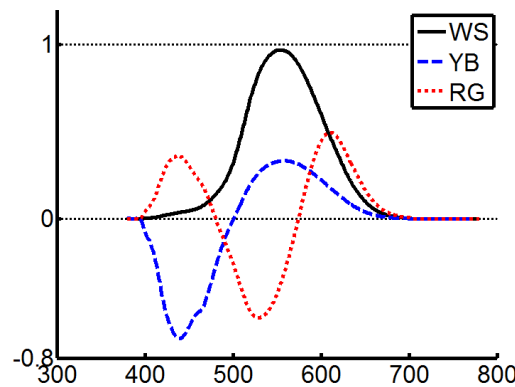


Figure 2.2: Spectral response functions for the opponent channels concerning an average normal trichromat.

ory suggested by von Kries, other two- and three-stage theories of color vision have been proposed, including Müller three-stage theory. A discussion of some of these theories can be found in (JUDD, 1966).

2.3 Genetic of Human Photopigments

Besides being closely located in the X chromosome, exons² concerning both *L*- and *M*-cones photopigments are similarly encoded. Actually, anomalous combinations of these exons are supposed to be responsible for all cases of red-green color vision deficiencies. Explanations for all these similarities can be supported by the evolution of opsin genes as described in (SHARPE et al., 1999). The *L*- and *M*-cones photopigments are very similar. They were the last to emerge throughout the evolutionary process of human color vision. About the evolution of genes responsible for production of rhodopsin, contained in the rods, little is known. It is believed that it has evolved from the *S*-opsin gene, but it is known that in humans it is located on chromosome 3 (SHARPE et al., 1999).

2.4 Color Vision Deficiency

Color vision deficiencies are broadly classified as *anomalous trichromacy*, *dichromacy* and *monochromacy*. Anomalous trichromacy is characterized by the presence in retina of one anomalous cone type. The anomalous cone contains a different photopigment type which spectrally deviates the cone's sensitivity. Anomalous trichromacy is further classified as *protanomaly*, *deutanomaly* and *tritanomaly*³ depending on whether the anomalous are the *L*, *M*, or *S* cones, respectively. In these cases, the sensitivities of the anomalous cones are shifted to different bands of the spectrum. Figure 2.3 illustrates these shifts for the three kinds of anomalous trichromacy. In cases of protanomaly (Figure 2.3 left), the sensitivities of the anomalous *L* cones are much similar to that of normal *M* cones, as it is shifted toward shorter wavelengths spectrum bands. Sensitivity functions of anomalous *M* cones in deutanomalous (Figure 2.3 center) resemble the sensitivity functions of normal *L* cones, as they are shifted toward longer wavelengths.

²Exon is an active sequence of genes, *i.e.*, it encodes information for protein synthesis.

³*Prot*, *Deut*, and *Trit* prefixes origins from Greek meaning One, Two and Three, respectively. These prefixes refers to *L*, *M*, and *S* cones, respectively.

The cases of tritanomaly are very rare, and the *S*-cones sensitivities are shifted toward longer wavelengths (Figure 2.3 right).

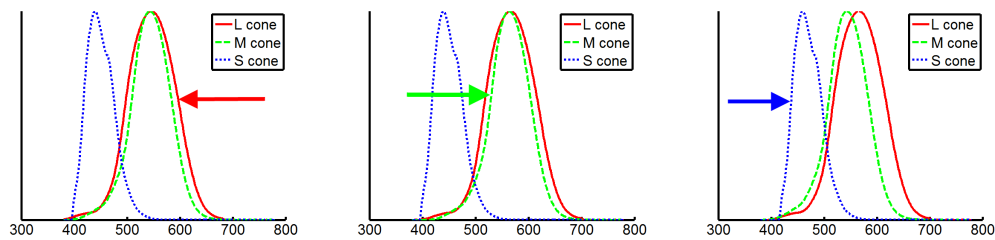


Figure 2.3: Spectral sensitivity functions of cones in anomalous trichromats. Figures from left to right refer to protanomaly, deuteranomaly, and tritanomaly, respectively. They illustrate the spectral shifts of anomalous cones, which occur in the three kinds of anomalous trichromacy.

In dichromatic retina there are only two types of photopigments. Dichromacy is further classified as *protanopia*, *deutanopia*, and *tritanopia*, depending on whether the absent photopigment concerns the *L*-, *M*-, or *S*-cone type, respectively. The perceived colors by individuals with both protanopia and deuteranopia are similar. As reported by unilateral dichromats⁴, protanopes and deuteranopes can only experience yellowish and blueish hues including gray shades (MEYER; GREENBERG, 1988; BRETTEL; VIÉNOT; MOLLON, 1997; VIÉNOT; BRETTEL; MOLLON, 1999). For tritanopia, a much rarer condition, individuals will always experience colors between a blueish-green and a reddish hue. Figure 2.4 illustrates the colors experienced by the three types of dichromacy. Figure 2.4 (left) shows a color wheel which is used as reference. The three subsequent images illustrate from left to right, the perception of the reference image by protanopes, deuteranopes, and tritanopes, respectively. Note how their color gamuts are reduced if compared to the gamut of individuals with normal color vision.

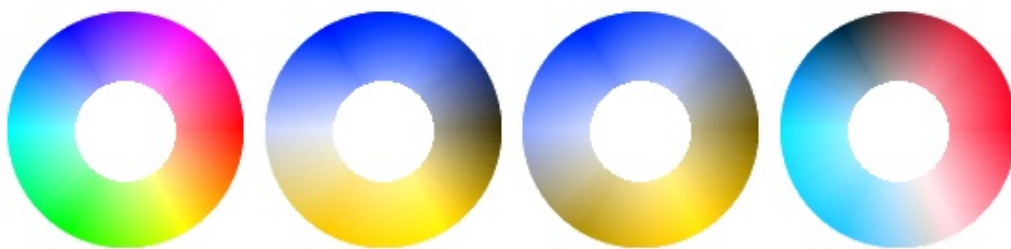


Figure 2.4: Illustration simulating the perception of dichromats. (left) reference image (color wheel). The subsequent wheels refer from left to right to the perception of protanopes, deuteranopes, and tritanopes, respectively. Wheels were simulated using Brettel *et al.*'s approach (BRETTEL; VIÉNOT; MOLLON, 1997).

The cases of monochromacy are classified as *rod-monochromacy*, when there are no cones in the retina; and *cone-monochromacy*, when there is only one cone type in the retina. Monochromacy cases are very rare and are not treated in this thesis.

⁴Unilateral dichromats are individuals with dichromacy in only one eye while the other has normal color vision.

CVD Type	Incidence (%)	
	Male	Female
Anomalous trichromacy	5.71	0.39
Protanomaly	1.08	0.03
Deuteranomaly	4.63	0.36
Tritanomaly	0.0001	0.0001
Dichromacy	2.28	0.03
Protanopia	1.01	0.02
Deuteranopia	1.27	0.01
Tritanopia	0.002	0.001
Monochromacy	0.003	0.00001

Table 2.1: Incidence of CVD types among Caucasian population (RIGDEN, 1999; SHARPE et al., 1999).

The incidences of the CVD types among the caucasian population, which is the only ethnic group for which there are some reliable statistics available, are shown in Table 2.1. Note that red-green color vision deficiencies (comprising protanopia, deuteranopia, and protanomaly deuteranomaly) are more prevailing while tritanopia, tritanomaly, and monochromacy are very rare.

3 RELATED WORK

This chapter describes the most relevant works on simulation and recoloring for color vision deficiency, emphasizing their strengths and limitations. Some works in color-to-grayscale conversion are also discussed in this chapter, since they deal with dimensionality reduction, and, as such, are akin to recoloring algorithms for dichromats.

3.1 Simulation Techniques

Despite the relevance of understanding how individuals with CVD perceive colors, little work has been done in simulating their perception for normal trichromats. In particular, none of the previous approaches is capable of handling both dichromacy and anomalous trichromacy while the simulation technique proposed in this thesis does. One should also note that the simulation process is not symmetrical: in general, it is not possible to simulate a normal trichromatic color experience for individuals with CVD, due to the reduced color gamuts of deficient color vision systems.

The first techniques that simulate the perception of individuals with CVD were developed based on the report of *unilateral dichromat* individuals. According to their report (GRAHAM; HSIA, 1959; JUDD, 1949a; SLOAN; WOLLACH, 1948) achromatic colors as well as some other hues are perceived similarly by both eyes (approximately wavelengths of 475 nm and 575 nm by individuals with protanopia and deuteranopia, and 485 nm and 660 nm by tritanopes). Meyer and Greenberg (MEYER; GREENBERG, 1988) mapped this gamut in the XYZ color space. They also mapped confusion lines in this color space, which represent directions along which there is no color variation according to dichromats perception. By projecting colors through confusion lines into the reduced gamut, they defined an accurate technique for simulating dichromacy.

Latter, some other similar works have been developed (BRETTEL; VIÉNOT; MOLLON, 1997; VIÉNOT; BRETTEL; MOLLON, 1999). The technique proposed by Brettel *et al.* (BRETTEL; VIÉNOT; MOLLON, 1997) is the most referenced of all existing simulation techniques. In this technique, the color gamut of dichromats is mapped to two semi-planes in the LMS color space, while the authors constrained the direction of confusion lines to be parallel to the direction of the color space axes L , M , or S , depending on whether the dichromacy type is protanopia, deuteranopia, or tritanopia, respectively. Figure 3.1 illustrates the process of projecting colors onto the semi-planes. For example, when simulating deuteranopia (Figure 3.1 center) the colors are projected onto the semi-planes through the direction of the M axis. This process is analogous for protanopia (Figures 3.1 left) and tritanopia (Figures 3.1 right). Figure 3.2 shows examples of some results of this simulation technique using Figure 3.2 (a) as reference image. Figures 3.2 (b), (c), and (d) shows the simulation of the perception of protanopes, deuteranopes, and tri-

tanopes, respectively. Note how the perception of color contrasts vanishes for some hues in different types of dichromacy.

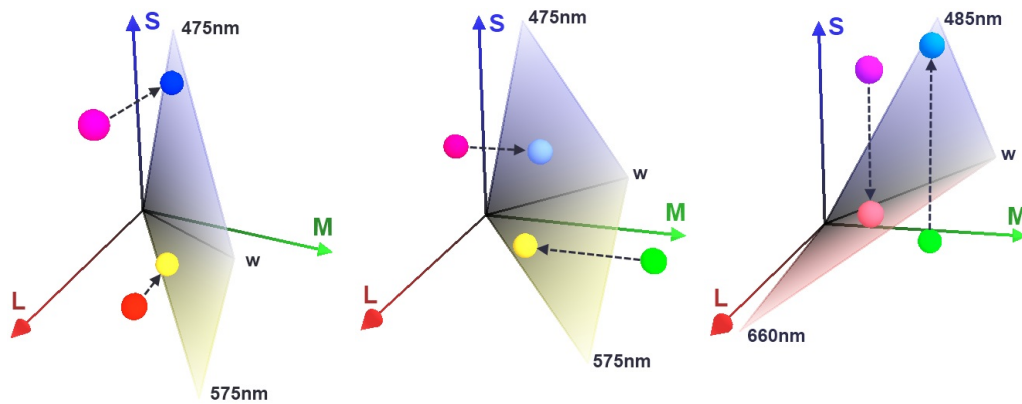


Figure 3.1: The three graphs illustrate the technique for simulating the perception of individuals with dichromacy proposed by Brettel *et al.* (BRETTEL; VIÉNOT; MOLLON, 1997). In the LMS color space, the original colors are orthographically projected to corresponding semi-planes, along the direction defined by the axis representing the affected cone. Illustrations of the technique for simulating protanopia (left), deuteranopia (center), and tritanopia (right).

These techniques produce very good results for the cases of dichromacy, but it can not be generalized to the cases of anomalous trichromacy, which comprises about 71% of the cases of CVD (RIGDEN, 1999; SHARPE *et al.*, 1999). With this, some authors attempted to simulate perception of anomalous trichromats.

Kondo (KONDO, 1990) proposed a model to simulate the perception of individuals with anomalous trichromacy based on dichromatic vision, given the similarities between the perception of both dichromats and individuals with severe anomalous trichromacy. However, the results of his model do not preserve achromatic colors, which are known to be perceived similarly by both dichromats and normal trichromats individuals. While the model proposed in this thesis preserves achromatic colors.

The approach proposed by Yang *et al.* (YANG *et al.*, 2008) for simulating the perception of individuals with anomalous trichromacy consists of defining a process for converting colors from RGB color space, regarding the spectral emission of a typical CRT monitor, to a LMS color space, regarding the sensitivity of the *L*, *M*, and *S* cones. With such conversion, the simulation occurs by the displacement of the spectral sensitivity of anomalous cones. By applying a conversion of colors from RGB to anomalous LMS and a subsequent conversion back from normal LMS to RGB, Yang *et al.* defined their simulation technique. By limiting the computation to the photoreceptor level, the algorithm does not agree with the opponent processing in the human visual system. As a result, the simulated images tend to contain colors that are not the ones perceived by individuals with CVD (Figure 3.3). The last column of Figure 3.3 shows the perception of individuals with severe protanomaly and deuteranomaly, which should be similar to the perception of protanopes and deuteranopes, respectively. The results obtained with Brettel *et al.*'s simulation technique for protanopia and deuteranopia (Figure 3.3 last column) differ from the results obtained with Yang *et al.*'s approach for severe anomalous trichromacy (Figure 3.3 20 nm).

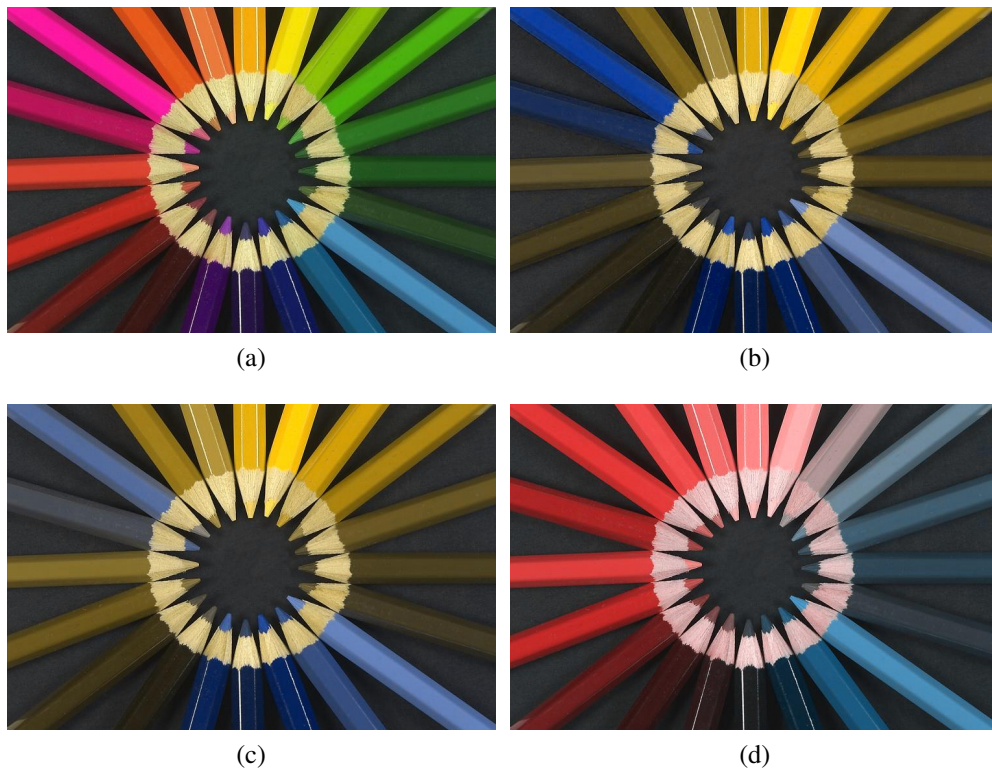


Figure 3.2: Examples showing the results obtained with Brettel *et al.*'s simulation technique (BRETTEL; VIÉNOT; MOLLON, 1997). (a) a reference image showing a set of color pencils. The subsequent images show the simulation of the perception of protanopes (b), deuteranopes (c), and tritanopes (d). Reference image is from (WIKIMEDIA COMMONS, 2010).

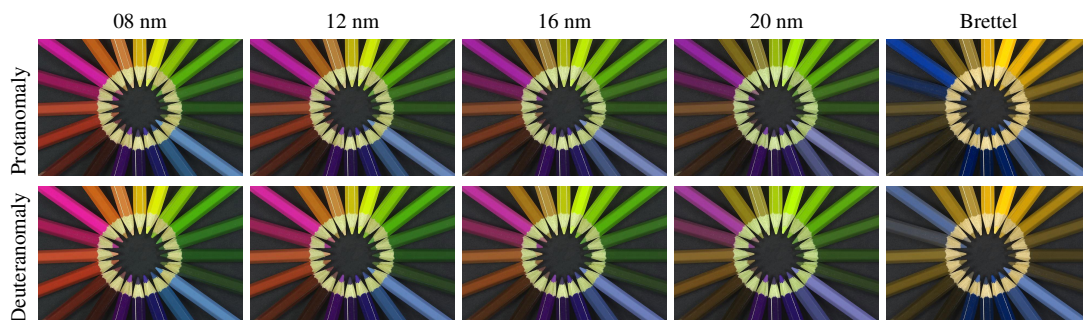


Figure 3.3: Images demonstrating the simulation of the perception of Figure 3.2 (left) by individuals with anomalous trichromacy according to the approach proposed by Yang *et al.* (YANG *et al.*, 2008). First row shows simulations of protanomalous' perceptions while the second row shows simulations of deuteranomalous' perceptions. The four columns, from left to right, concerns anomalous trichromacy with severities (spectral shift in wavelength) of 8 nm, 12 nm, 16 nm, and 20 nm, respectively. To compare with the perception of severe anomalous trichromacy, the last column shows simulations according to Brettel *et al.*'s approach for protanopes and deuteranopes in the first and second rows, respectively.

3.2 Recoloring Techniques

Several researchers have investigated the problem of image-recoloring for individuals with CVD. The existing techniques can be broadly classified as *user-assisted* and *optimization-based* approaches.

3.2.1 User-Assisted Techniques

The techniques in this class require assistance, in the form of user-provided parameters, to guide the recoloring process. Thus, the quality of their results is highly dependent on the provided parameters, making them unsuitable for real-time systems. Iaccarino *et al.* (IACCARINO *et al.*, 2006) employ six parameters to modulate the original colors of an input image. Daltonize (DOUGHERTY; WADE, 2002) uses three parameters to specify the recoloring process (for protanopes and deuteranopes). These parameters specify how the red-green channel should be stretched, projected into the luminance channel, and projected into the yellow-blue channel. Huang *et al.* (HUANG; WU; CHEN, 2008) enhance color contrast by remapping the Hue components in HSV color space aiming to provide wider dynamic ranges for the most confusing hues. This technique uses a control parameter to specify the degree of enhancement.

3.2.2 Optimization-based Techniques

These techniques operate without user intervention and consist of optimization procedures. Ichikawa *et al.* (ICHIKAWA *et al.*, 2003) used a genetic algorithm to recolor web pages for anomalous trichromats. Subsequently, the authors extended their work for image recoloring (ICHIKAWA *et al.*, 2004). Wakita and Shimamura (WAKITA; SHIMAMURA, 2005) presented a technique for recoloring documents (*e.g.*, web pages, charts, maps) for dichromats. Such a technique is based on three objective functions intended for: (i) color contrast preservation, (ii) maximum color contrast enforcement, and (iii) color naturalness preservation (for user-specified colors). The three objective functions are weighted according to user-specified parameters and optimized with simulated annealing. Wakita and Shimamura report that the optimization for documents with more than 10 colors could take several seconds. Jefferson and Harvey (JEFFERSON; HARVEY, 2006) use four objective functions to preserve brightness, color contrast, colors in the available gamut, and color naturalness. Their technique optimizes the combined objective functions using preconditioned conjugate gradients. The authors reported times of the order of several minutes for a set of 25 key colors (on a P4 2.0 GHz PC using Matlab).

In the perceptually uniform color space (CIE $L^*a^*b^*$), Euclidean distances represent perceptual differences. Rasche *et al.* (RASCHE; GEIST; WESTALL, 2005a) presented a technique of image-recoloring for dichromats consisting of an optimization that attempts to preserve the perceptual differences between all pairs of colors in the gamut of dichromats using an affine transformation. However, this transformation does not capture color variations along several directions and can not guarantee that the colors are kept in available mapped gamut. In a subsequent work, Rasche *et al.* (RASCHE; GEIST; WESTALL, 2005b) addressed these limitations applying a constrained multivariate optimization procedure to a reduced set of quantized colors. The resulting set of optimized quantized colors is then used to optimize the entire set of colors. Despite the improved results, this algorithm is prone to local minima, and does not scale well with the number of quantized colors and the size of the input images.

Kuhn *et al.* (KUHN; OLIVEIRA; FERNANDES, 2008a) presented a technique for

enhancing color contrast for dichromats preserving naturalness based on mass-spring optimization, which can be efficiently implemented on GPUs. Similar to the technique of Rasche *et al.* (RASCHE; GEIST; WESTALL, 2005b), the optimization is first performed on a set of quantized colors, which are then used to optimize the entire set of colors. Although their technique is about three orders of magnitude faster than previous approaches and can achieve interactive frame rates, it is still not sufficiently fast to allow real-time performance. Moreover, since the optimization is based on a set of quantized colors, it is not clear how one could preserve temporal coherence on the fly (*e.g.*, during an interactive scientific visualization session). The recoloring technique proposed in this thesis does not preserve image naturalness, but performs real-time recoloring and preserves temporal coherence.

Huang *et al.* (HUANG *et al.*, 2009) also present an optimization based approach for recoloring images. According to this technique, which works in CIE $L^*a^*b^*$ color space, the colors are first clustered using a Gaussian Mixture Model; then, the mean vector of each Gaussian component is relocated; and, to compute the final colors, a hue interpolation in CIE LCH color space is performed. But, as the authors reported, this technique takes about 5 seconds to recolor a 300x300 image on a Pentium 4 3.4 GHz PC, while the approach proposed in this thesis recolors an 800x800 image in 0.614 second on a Core 2 Extreme 3.0 GHz CPU, and in 0.028 second on a Quadro FX 5800 GPU.

Figure 3.4 compares the results produced using the techniques of Rasche *et al.* and Kuhn *et al.* when applied to the reference image shown in Figure 3.4 (a). Figure 3.4 (b) shows the simulation of deuteranopes' perception according to Brettel *et al.*'s approach, and Figures 3.4 (c) and (d) show the simulation of deuteranopes' perception of two images recolored according to Rasche *et al.*'s and Kuhn *et al.*'s recoloring techniques, respectively. Note how recoloring techniques can recover color contrasts. Note that Kuhn *et al.*'s results preserves naturalness by constraining the colors that are more similarly perceived by dichromats and normal trichromats.

3.2.3 Color-to-Grayscale Mappings

Image recoloring for dichromats is also a dimensionality reduction problem. In this sense, it is akin to the more constrained problem of color-to-grayscale mapping. Traditional techniques commonly used in commercial applications (BROWN, 2006; JESCHKE, 2002) perform this mapping by simply taking the color's luminance value computed on some color space (*e.g.*, XYZ, YCbCr, $L^*a^*b^*$, or HSL). An important aspect of all these techniques is that they preserve achromatic colors, which is a desirable feature for printing. Since no chrominance information is taken into account, these approaches map all isoluminant colors to the same shade of gray, despite of their perceptual differences. Recently, several techniques have been proposed to address this limitation (GOOCH *et al.*, 2005; RASCHE; GEIST; WESTALL, 2005b; GRUNDLAND; DODGSON, 2007; KUHN; OLIVEIRA; FERNANDES, 2008b).

Gooch *et al.* (GOOCH *et al.*, 2005) use an optimization procedure whose cost is quadratic in the number of pixels in the image. Although the technique produces some good results, its computational cost precludes it from being used for interactive applications. Moreover, it does not preserve achromatic colors. Gooch *et al.* report that they have explored the use of principal component analysis (PCA) to estimate an ellipsoid in color space that best approximates the set of colors found in the image. The grayscale image would then be computed by projecting all image colors on the axis of the ellipsoid with the largest variance. According to the authors (GOOCH *et al.*, 2005) and also pointed



Figure 3.4: Demonstration of the results of two recently developed recoloring techniques. (a) the reference image showing natural scene with some flowers in foreground. (b) simulation of the perception of individuals with deuteranopia according to Brettel *et al.* (BRETEL; VIÉNOT; MOLLON, 1997). Subsequently, simulations of deuteranope’s perception of the recolored images according to the approaches proposed by Rasche *et al.* (RASCHE; GEIST; WESTALL, 2005b) in (c) and Kuhn *et al.* (KUHN; OLIVEIRA; FERNANDES, 2008a) in (d). Images extracted from Kuhn *et al.*’s paper.

out by Rasche *et al.* (RASCHE; GEIST; WESTALL, 2005b), PCA fails to convert color images with variations along many directions, and an optimization step would be required to somehow combine the principal components.

Grundland and Dogdson (GRUNDLAND; DODGSON, 2007) perform the color-to-grayscale mapping by adding to the original luminance value Y_i of pixel p_i , some amount K_i that tries to compensate for the contrast loss. To compute K_i while avoiding a quadratic cost (as in previous techniques), the authors introduced a clever local sampling strategy called *Gaussian pairing*. It consists in choosing, for each pixel p_i , a pixel p_j in a circular neighborhood around p_i . The choice of p_j is based on a Gaussian probability distribution function. The size of the neighborhood is computed based on the image dimensions. For a given pair (p_i, p_j) , the relative contrast loss is computed as:

$$l_{(p_i, p_j)} = 1 - \frac{Y_i - Y_j}{\|p_i - p_j\|_{RGB}}, \quad (3.1)$$

where Y_i and Y_j are the luminance values of pixels p_i and p_j , respectively, and $\|p_i - p_j\|_{RGB}$ is the length of the color vector $v_{ij} = p_i - p_j$ computed in the *RGB* color space. Note that the distance computed in the denominator of Equation 3.1 has no perceptual meaning. In order to estimate the amount K_i , the authors map the original RGB colors to their own opponent-color space (*YPQ*), which, again, is not perceptually uniform. In the *YPQ* color

space, they estimate a direction d_{mcl} of maximum contrast loss (according to Equation 3.1) using a technique of their own, which they called *predominant component analysis*. The idea of predominant component analysis is to approximate the direction of maximum data dispersion using a sum of weighted vectors. Note, however, that its results are not equivalent to the solution of an eigenvector problem, such as done in PCA. As a result, for the same set of input vectors, the direction d_{mcl} is not the same as the direction of the main eigenvector obtained using PCA. For computing K_i , the authors essentially project the original pixel colors expressed in the YPQ space onto d_{mcl} .

3.3 Summary

This chapter has shown the state-of-art works related to this thesis emphasizing the most relevant simulation (BRETTEL; VIÉNOT; MOLLON, 1997) and recoloring (KUHN; OLIVEIRA; FERNANDES, 2008a) techniques. Color-to-grayscale conversion techniques were also covered as they perform dimensionality reduction and, therefore, are akin to image recoloring for dichromats. Among those, the technique proposed by Dodgson and Grundland (GRUNDLAND; DODGSON, 2007) presented significant advances in run-time performance, which is desirable for recoloring techniques.

4 A PHYSIOLOGICALLY-BASED MODEL FOR SIMULATION OF COLOR VISION DEFICIENCY

This chapter presents a model for simulating color perception based on the *stage theory* (JUDD, 1966) of human color vision. This model is the first to consistently handle normal color vision, anomalous trichromacy, and dichromacy in a unified way. Unlike previous techniques that are based on the reports of unilateral dichromats (BRETTEL; VIÉNOT; MOLLON, 1997; MEYER; GREENBERG, 1988) or on the spectral response of the photoreceptors only (YANG et al., 2008), this approach uses a two-stage model. It simulates color perception by combining a photoreceptor-spectral-response stage and an opponent-color stage defined according to data reported in electrophysiological studies (INGLING JR.; TSOU, 1977). This guarantees the generality of the proposed approach.

Figure 4.1 illustrates the results produced by the proposed model in the context of scientific visualization. The image on the left shows a reference image (*i.e.*, the perception of a normal trichromat). The two images in the middle show simulated views for two protanomalous individuals with different degrees of severity. The numbers in parenthesis indicate the amount of shift, in nanometers, applied to the spectral response of the *L* cones. The image on the right is a simulated view of a protanope (a dichromat), which is approximately equivalent to the perception of protanomalous with a spectral shift of 20 nm. Note the progressive loss of color contrast as the degree of severity increases.

4.1 Quantification of The Stage Theory

A stage theory can qualitatively explain human color vision. However, before one can use it to define a model for rendering images that simulate color perception, it needs to describe both stages using equations. While curves describing the spectral sensitivity of the cones can be measured *in vivo* and are available for an average individual (SMITH; POKORNY, 1975), one still needs the coefficients that define how the signals generated by the cones are combined to form the achromatic (*WS*) as well as the two chromatic channels (*RG* and *YB*). Such coefficients cannot be easily obtained, but fortunately Ingling and Tsou (INGLING JR.; TSOU, 1977) provided transformations for mapping cone responses (in the LMS color space) to an opponent-color space. The suprathreshold form of their transformation presents advantages over the threshold one, as it tries to take into account reports by psychophysical and electrophysiological studies regarding light adap-

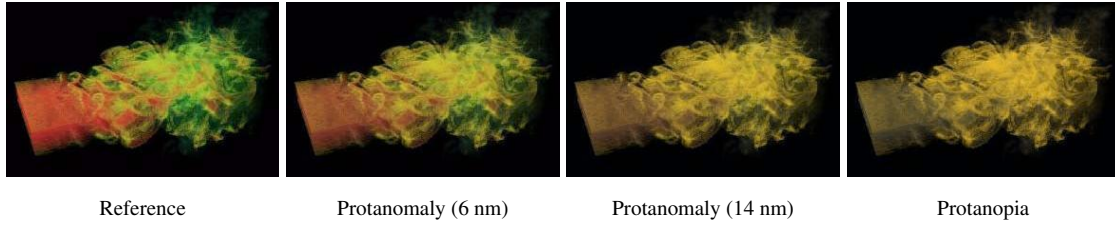


Figure 4.1: Scientific visualization under color vision deficiency. Simulation, for a normal trichromat, of the color perception of individuals with color vision deficiency (protanomaly) at different degrees of severity. The image on the left (turbulent flows) illustrates the perception of a normal trichromat and is used for reference. The numbers in parenthesis indicate the amount of shift, in nanometers, applied to the spectral response of the L cones. The image on the right shows the simulated perception of a dichromat (protanope), which is approximately equivalent to the perception of protanomalous with a spectral shift of 20 nm. Note the progressive loss of color contrast as the degree of severity increases. Images simulated using the proposed model. Reference image was provided by CCSE at LBNL.

tation. Equation 4.1 describes Ingling and Tsou’s suprathreshold transformation:

$$\begin{bmatrix} V_\lambda \\ y - b \\ r - g \end{bmatrix} = \begin{bmatrix} 0.600 & 0.400 & 0.000 \\ 0.240 & 0.105 & -0.700 \\ 1.200 & -1.600 & 0.400 \end{bmatrix} \begin{bmatrix} L \\ M \\ S \end{bmatrix} \quad (4.1)$$

where V_λ represents the luminance channel WS , and $r - g$ and $y - b$ represent the two opponent chromatic channels RG and YB , respectively. Figure 4.2 illustrates how the cones’ output signals are combined into the spectral response functions of the opponent channels WS , YB , and RG . Figure 4.3 (left) shows the spectral sensitivity functions for the cones of an average normal trichromat according to Smith and Pokorny (SMITH; POKORNY, 1975). The resulting spectral response functions of the opponent channels for this average normal trichromat according to Ingling and Tsou’s model are shown on Figure 4.3 (right).

4.2 Simulating Color Vision Deficiency

Except for the cases resulting from trauma, the causes of color vision deficiency are genetic and result from alterations in the cones’ photopigment spectral sensitivity (BERENDSCHOT; KRAATS; NORREN, 1996; SHARPE et al., 1999). The conditions involving the L and M cones are hereditary and associated with a gene array in the X chromosome (SHARPE et al., 1999). The conditions involving the S cones (tritanomaly and tritanopia) are considerably less frequent (RIGDEN, 1999; SHARPE et al., 1999) and are believed to be acquired (SHARPE et al., 1999).

The proposed physiologically-based model treats CVD as changes in the spectral absorption of the cones’ photopigments. While CVD is essentially modeled at the retinal photopigment stage, the opponent-color stage is crucial for producing the correct results and cannot be underestimated. For this, the proposed model uses Ingling and Tsou’s model (Figure 4.2) that, despite its simplicity, is useful for estimating the results of several color vision experiments, even though it is limited by insufficient knowledge (INGLING JR.; TSOU, 1977). One should note, however, that the proposed approach is not

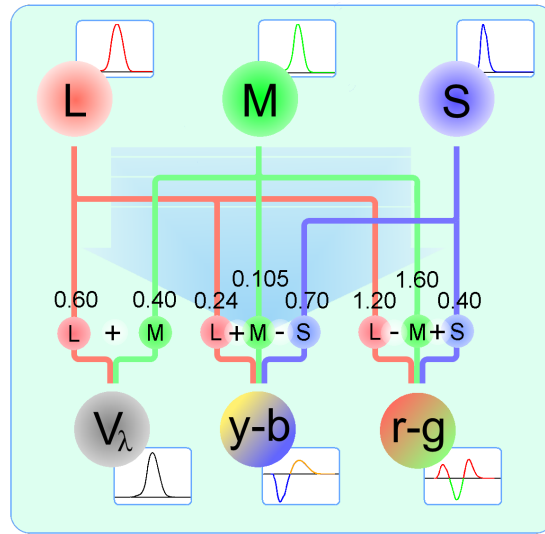


Figure 4.2: Ingling and Tsou's (INGLING JR.; TSOU, 1977) two-stage model of human color vision. The output of the photoreceptor stage (L, M and S cones) is linearly combined in the opponent stage (V_λ , $y - b$, and $r - g$ nodes).

tied to any particular stage model. For instance, the proposed model was also used with a three-stage model based on Müller's theory using the parameters derived by Judd (JUDD, 1949b). According to visual comparisons with Brettel *et al.*'s simulations, however, the parameters provided by Ingling and Tsou's model produce better results. Moreover, Müller's theory explanation for the occurrence of deuteranopia (JUDD, 1949b) does not seem to be in accordance with evidence reported in the literature (BERENDSCHOT; KRAATS; NORREN, 1996; CICERONE; NERGER, 1989; SHARPE et al., 1999; WESNER et al., 1991).

4.2.1 Simulating Anomalous Trichromacy

Anomalous trichromacy is explained by a shift in the spectral sensitivity function of the anomalous cones (DEMARCO; POKORNY; SMITH, 1992; NEITZ; NEITZ, 2000; POKORNY; SMITH, 1997; SHARPE et al., 1999; WYSZECKI; STILES, 2000). Arrangements of DNA bases called *exons* are involved in producing proteins which are responsible to define specific characteristics. The *L* and *M* photopigment characteristics in humans are defined by sequences of six exons from which the first and the last are invariant. The four intermediary exons in the sequence are responsible for the variability between the spectral responses of normal and anomalous photopigments (SHARPE et al., 1999). Hybrid genes contain exons from both *L* and *M* pigments as illustrated in Figure 4.4. The squares indicate gene-specific for *L* and *M* pigments. All hybrid genes produce photopigments with peak sensitivity between the peaks of normal *L* and *M* photopigments. Each exon contributes to the spectral shift of the produced hybrid photopigment, but exon five is determinant of the basic type of photopigment.

The proposed approach models anomalous trichromacy by shifting the spectral sensitivity function of the anomalous cone according to the degree of severity of the anomaly. A shift of approximately 20 nm represents a severe case of protanomaly or deuteranomaly (MCINTYRE, 2002; SHARPE et al., 1999), causing the spectral sensitivity functions of the anomalous *L* (or *M*) cones to almost completely overlap with the normal *M*

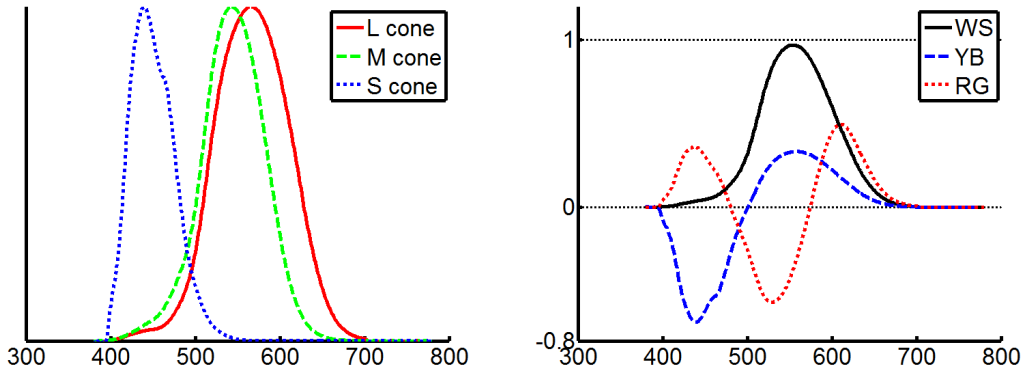


Figure 4.3: (left) Cone spectral sensitivity functions for an average normal trichromat (after Smith and Pokorny (SMITH; POKORNY, 1975)). (right) Spectral response functions for the opponent channels of the average normal trichromat according to Ingling and Tsou’s model (INGLING JR.; TSOU, 1977). These functions are obtained by evaluating Equation 4.1 for the LMS triples resulting from the cone spectral sensitivity functions at all wavelengths in the visible range.

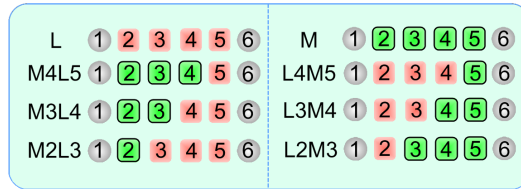


Figure 4.4: Exon arrangements of the L, M, and hybrid photopigment genes. X-linked anomalous photopigment spectral sensitivity are interpreted as interpolations of the normal L and M photopigment spectra. Adapted from Sharpe *et al.* (SHARPE *et al.*, 1999).

(or L) cones. As a result, the perception of a severe protanomalous (deutanomalous) is very similar to the perception of a protanope (deutanope). The much rarer case of tritanomaly can also be simulated by shifting the spectral sensitivity function of the S cones. The spectral sensitivity functions of the anomalous cones are represented as

$$L_a(\lambda) = L(\lambda + \Delta\lambda_L), \quad (4.2)$$

$$M_a(\lambda) = M(\lambda + \Delta\lambda_M), \quad (4.3)$$

$$S_a(\lambda) = S(\lambda + \Delta\lambda_S) \quad (4.4)$$

where $L(\lambda)$, $M(\lambda)$, and $S(\lambda)$ are the cone spectral sensitivity functions for an average normal trichromat (SMITH; POKORNY, 1975). $\Delta\lambda_L$, $\Delta\lambda_M$, and $\Delta\lambda_S$ represent the amount of shift applied to the L , M , and S anomalous cone, respectively. Since these curves represent the outcome of the photoreceptor level in the proposed two-stage model, they still need to be processed by the opponent-color stage. As previously noted, the proposed model uses the opponent-color space defined by Ingling and Tsou (INGLING JR.; TSOU, 1977), whose transformation from LMS to opponent space is represented by the 3×3 matrix shown in Equation 4.1, which will be referred to as $T_{LMS2Opp}$.

As CVD results from changes in the spectral properties of the photopigments, which happens at the retinal level, the proposed model assumes that the neural connections that link the photoreceptors themselves to the rest of the visual system are not affected. Thus, it uses the transformation $T_{LMS2Opp}$ to obtain anomalous spectral response functions for

the opponent channels, as shown by Equations 4.5 to 4.7. In those equations, pa , da , and ta stand for protanomalous, deuteranomalous, and tritanomalous, respectively. Figure 4.5 shows examples of the resulting spectral opponent functions for protanomaly and deuteranomaly instantiated for $\Delta\lambda_L = 15 \text{ nm}$, and $\Delta\lambda_M = -19 \text{ nm}$. Note that the transformation for normal trichromats is represented by Equation 4.1.

$$\begin{bmatrix} WS(\lambda) \\ YB(\lambda) \\ RG(\lambda) \end{bmatrix}_{pa} = T_{LMS_2Opp} \begin{bmatrix} L_a(\lambda) \\ M(\lambda) \\ S(\lambda) \end{bmatrix} \quad (4.5)$$

$$\begin{bmatrix} WS(\lambda) \\ YB(\lambda) \\ RG(\lambda) \end{bmatrix}_{da} = T_{LMS_2Opp} \begin{bmatrix} L(\lambda) \\ M_a(\lambda) \\ S(\lambda) \end{bmatrix} \quad (4.6)$$

$$\begin{bmatrix} WS(\lambda) \\ YB(\lambda) \\ RG(\lambda) \end{bmatrix}_{ta} = T_{LMS_2Opp} \begin{bmatrix} L(\lambda) \\ M(\lambda) \\ S_a(\lambda) \end{bmatrix} \quad (4.7)$$

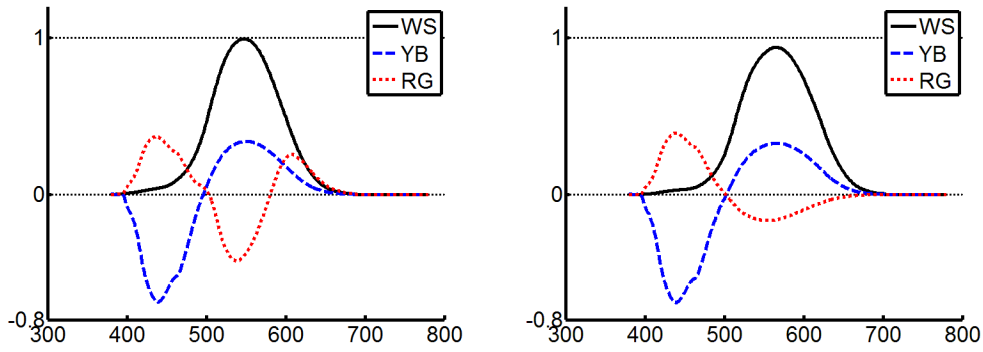


Figure 4.5: Spectral opponent functions for anomalous trichromats. (left) Protanomaly ($\Delta\lambda_L = 15 \text{ nm}$). (right) Deuteranomaly ($\Delta\lambda_M = -19 \text{ nm}$).

A transformation from an RGB color space to an opponent-color space is obtained simply by projecting the spectral power distributions $\phi_R(\lambda)$, $\phi_G(\lambda)$, and $\phi_B(\lambda)$ of the RGB primaries onto the set of basis functions $WS(\lambda)$, $YB(\lambda)$, and $RG(\lambda)$ that define the opponent-color space, as shown in Equation 4.8. By using the appropriate set of basis functions, Equation 4.8 transforms RGB triples to opponent colors for either normal trichromats, for anomalous trichromats, or for dichromats (discussed in Section 4.2.2). For instance, using the functions shown on the left-hand side of Equation 4.5 as basis functions, Equation 4.8 will produce the elements of a matrix that maps RGB to the opponent-color space of protanomalous with a spectral sensitivity shift of $\Delta\lambda_L$.

$$\begin{aligned} WS_R &= \rho_{WS} \int \phi_R(\lambda) WS(\lambda) d\lambda, \\ WS_G &= \rho_{WS} \int \phi_G(\lambda) WS(\lambda) d\lambda, \\ WS_B &= \rho_{WS} \int \phi_B(\lambda) WS(\lambda) d\lambda, \\ YB_R &= \rho_{YB} \int \phi_R(\lambda) YB(\lambda) d\lambda, \\ YB_G &= \rho_{YB} \int \phi_G(\lambda) YB(\lambda) d\lambda, \\ YB_B &= \rho_{YB} \int \phi_B(\lambda) YB(\lambda) d\lambda, \\ RG_R &= \rho_{RG} \int \phi_R(\lambda) RG(\lambda) d\lambda, \\ RG_G &= \rho_{RG} \int \phi_G(\lambda) RG(\lambda) d\lambda, \\ RG_B &= \rho_{RG} \int \phi_B(\lambda) RG(\lambda) d\lambda \end{aligned} \quad (4.8)$$

The normalization factors ρ_{WS} , ρ_{YB} , and ρ_{RG} are chosen to satisfy the restrictions in Equation 4.9. They guarantee that the achromatic colors (gray shades) have the exact same coordinates ranging from (0,0,0) to (1,1,1) both in RGB as well as in all possible versions of the opponent-color spaces (normal trichromatic, all anomalous trichromatic, and all dichromatic). This is key for the simulation algorithm.

$$\begin{aligned} WS_R + WS_G + WS_B &= 1, \\ YB_R + YB_G + YB_B &= 1, \\ RG_R + RG_G + RG_B &= 1 \end{aligned} \quad (4.9)$$

Thus, the general class of transformation matrices Γ that map the RGB color space to various instances of the opponent-color space can be expressed as:

$$\Gamma = \begin{bmatrix} WS_R & WS_G & WS_B \\ YB_R & YB_G & YB_B \\ RG_R & RG_G & RG_B \end{bmatrix} \quad (4.10)$$

Let Γ_{normal} be the matrix that maps RGB to the opponent-color space of a normal trichromat. Γ_{normal} is obtained by using the functions shown on Figure 4.3 (right) as basis functions for the projection operations represented by Equation 4.8. Thus, the simulation for a normal trichromat of the color perception of an anomalous trichromat is obtained with Equation 4.11. As will be shown next, the same general solution applies to the simulation of dichromatic vision.

$$\begin{bmatrix} R_s \\ G_s \\ B_s \end{bmatrix} = \Gamma_{normal}^{-1} \Gamma \begin{bmatrix} R \\ G \\ B \end{bmatrix} \quad (4.11)$$

4.2.2 Simulating Dichromacy

Measurements of visual pigment absorption using retinal densitometry showed that dichromats lack one type of photopigment (ALPERN; WAKE, 1977; RUSHTON, 1963). Currently, researchers work with three possible alternatives for explaining the lack of one kind of cone photopigment (BERENDSCHOT; KRAATS; NORREN, 1996): (i) the *empty spaces model*, which states that a given class of cones and its corresponding photopigment are lost, producing empty spaces in the cone mosaic. This hypothesis, however, is not supported by the findings of Wesner *et al.* (WESNER *et al.*, 1991) who verified that the foveal cone photoreceptor mosaics of dichromats are similar in structure to the ones of normal trichromats. (ii) The *replacement model* suggests that the cones are still there, but filled with one of the remaining kinds of photopigments. Finally, (iii) the *empty cones model* suggests that a given class of cones contains no photopigment. While the work of Vos and Walraven (VOS; WALRAVEN, 1971) may support models (i) or (iii), evidence supporting the replacement model can be found in the results of several researchers (BERENDSCHOT; KRAATS; NORREN, 1996; CICERONE; NERGER, 1989; WESNER *et al.*, 1991). This makes the photopigment substitution the most accepted model for explaining dichromacy, with genetic arguments for protanopia and deuteranopia.

The proposed model makes it easy to test these hypotheses. For instance, for simulating color appearance according to the empty space or to the empty cone models, all one needs to do is to zero the outcome of the corresponding cone type (either L , M , or S) before transforming these signals into opponent color space functions. Given such curves, a transformation matrix from RGB to opponent-color space is obtained using Equations 4.8

and 4.9, and a simulation of color perception is obtained using Equation 4.11. The cases of deuteranopia and tritanopia are similar. The first column of Figure 4.7 (*Empty*) shows the simulated results obtained for the flower image shown in Figure 4.6 (a) using the empty space and empty cone models, for protanopia (top row), and deuteranopia (bottom row). These results are incorrect. For reference, we show in the last column of this figure the results produced by Brettel *et al.*'s algorithm (BRETTEL; VIÉNOT; MOLLON, 1997).

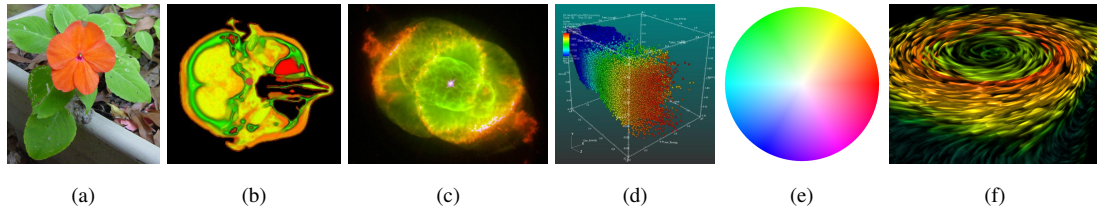


Figure 4.6: Reference images. (a) Flower. (b) Brain. (c) Cat's Eye nebula. (d) Scatter plot. (e) Slice of the HSV color space ($V=1$). (f) Tornado. Image (a) extracted from Rasche *et al.*'s paper. Image (b) provided by Francisco Pinto. Images (c) and (d) are from (WIKIMEDIA COMMONS, 2010). Image (f) provided by Martin Falk and Daniel Weiskopf.

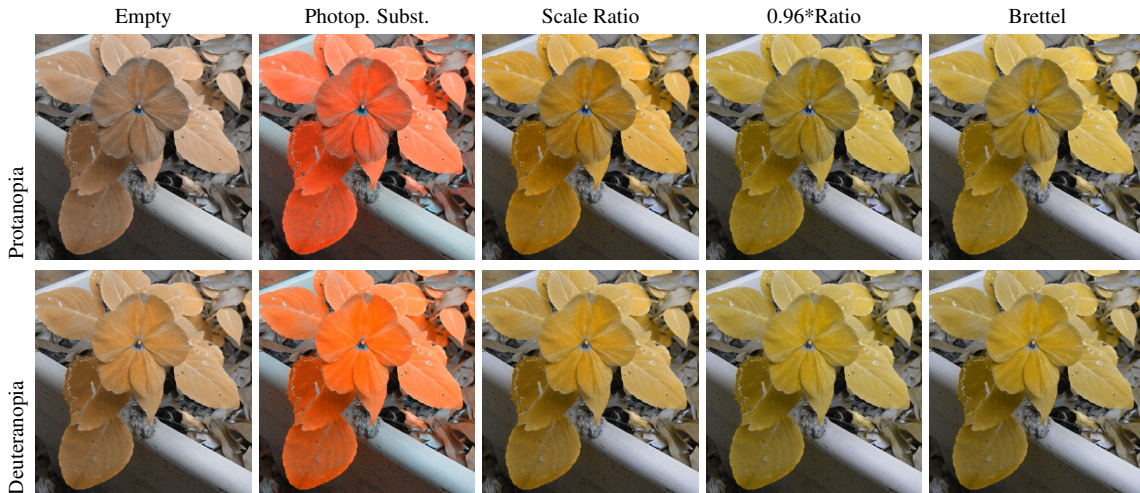


Figure 4.7: Simulation of dichromatic perception for the flower shown in Figure 4.6(a) according to four different models. From left to right: empty space / empty cones, photopigment substitution (replacement model), photopigment substitution with scaling according to Equation 4.15, same as previous but also scaled by 0.96, Brettel *et al.*'s (for reference).

4.2.2.1 The Replacement Model

The replacement model seems to be the most plausible hypothesis for explaining dichromacy (BERENDSCHOT; KRAATS; NORREN, 1996; CICERONE; NERGER, 1989; WESNER et al., 1991). The occurrence of a given photopigment in a “wrong” type of cone seems more plausible between the L and M cones, and less plausible when it involves

the S cones. For instance, L - and M -cone photopigment genes show 96% mutual identity (SHARPE et al., 1999). Moreover, the genes encoding the L - and M -cone photopigments reside in the X-chromosome (at location Xq28) and have similar exon arrangement coding. S -cone photopigments, on the other hand, reside in chromosome 7, and its coding is given by five exons, one less than L - and M -cone photopigment genes (SHARPE et al., 1999). Thus, there is no genetic basis for a photopigment substitution model of tritanopia. Tritanopia is generally considered an acquired, as opposed to inherited, condition (SHARPE et al., 1999). For this reason, the proposed model is not intended to handle tritanopia (which is expected to affect about 0.003% of the population, according to the data available for the Caucasian population (RIGDEN, 1999; SHARPE et al., 1999)).

The proposed model uses for dichromacy three cone types, but only two kinds of photopigments. The replacement model could be simulated simply by replacing the spectral sensitivity function of the L cones with the M cones for the case of protanopia, and the other way around for the case of deuteranopia. Equation 4.12 illustrates this for the case of protanopia. The second column of Figure 4.7 (*Photop. Subst.*) illustrates the results obtained with this technique, which, again, are clearly incorrect. This resulted from the fact that, even though the spectral sensitivity functions of all three types of cones had their peak sensitivity independently normalized to 1.0, the areas under these curves are sufficiently different (Figure 4.3 left) and need to be taken into account.

$$\begin{bmatrix} WS(\lambda) \\ YB(\lambda) \\ RG(\lambda) \end{bmatrix}_{\text{protanopia}} = T_{LMS_2Opp} \begin{bmatrix} M(\lambda) \\ M(\lambda) \\ S(\lambda) \end{bmatrix} \quad (4.12)$$

The replacement of the L -cone spectral sensitivity curve by the M -cone spectral sensitivity curve, which has a smaller area than L 's, causes the restrictions defined in Equation 4.9 to only be satisfied for $\rho_{RG} < 0$. In this case, the resulting coefficients RG_R , RG_G , and RG_B have their signs reversed (with respect to the corresponding coefficients for a normal trichromat), making it impossible to preserve the achromatic colors in the range from (0,0,0) to (1,1,1) in the opponent-color space. A similar phenomenon happens when the spectral sensitivity curve of the M cone is replaced by the L cone one. The solution to this problem lies in rescaling the replaced curves.

The rescaling of the curves is performed so that the new curves preserve the areas under the curves of the *host* cones (Equations 4.15 and 4.16). The third column of Figure 4.7 (*Scale Ratio*) illustrates the results obtained with this technique. Note that while the colors of the leaves and petals are approximately correct, they still contain some excessive redness.

$$Area_L = \int L(\lambda) d\lambda, \quad (4.13)$$

$$Area_M = \int M(\lambda) d\lambda, \quad (4.14)$$

$$L_{\text{protanope}}(\lambda) = \frac{Area_L}{Area_M} M(\lambda), \quad (4.15)$$

$$M_{\text{deuteranope}}(\lambda) = \frac{Area_M}{Area_L} L(\lambda) \quad (4.16)$$

A small adjustment in the area ratios in Equations 4.15 and 4.16 produces a significant improvement in image quality. For instance, the results shown in the fourth column of Figure 4.7 were obtained after scaling the ratio ($Area_L/Area_M$) in Equations 4.15 and 4.16 by 0.96. Such a scaling factor was used to improve the matching between the surfaces obtained when the entire RGB color space is simulated for dichromatic vision using Brettel et al.'s and the proposed model (Figure 4.8d). This seems to support the proposed

model's prediction that the correctness of the replacement model requires normalization by the ratio of the areas under the original spectral sensitivity curves of the L and M cones. Such a prediction still needs to be verified experimentally. While the prediction is off by a 0.04 factor, one should consider two important points: (i) the coefficients of the $T_{LMS2Opp}$ matrix (Equation 4.1) used in the current implementation of the proposed model are expected to contain some inaccuracies; and (ii) Brettel *et al.*'s model, used for reference, provides an approximation to the actual dichromat's perception and cannot be taken as ground truth. For a qualitative comparison of Brettel *et al.*'s and the proposed model's results, please see the last two columns of Figure 4.7.

Figure 4.8 compares the simulations of the protanopic vision for the entire RGB color space performed by the several models discussed in this section. A surface obtained using Brettel *et al.*'s (BRETTEL; VIÉNOT; MOLLON, 1997) algorithm is shown for reference (the blue-and-yellow surface). Figure 4.8 (a) shows a simulation of the empty space / empty cones models. (b) illustrates the result obtained with the use of a replacement model without normalization (photopigment substitution). The image in (c) shows the resulting surface after the original ratio ($Area_L/Area_M$) has been preserved using Equation 4.15. Figure 4.8 (d) shows the resulting surface obtained after the original ratio ($Area_L/Area_M$) has been scaled by 0.96. The two surfaces are now considerably closer, although not coincident.

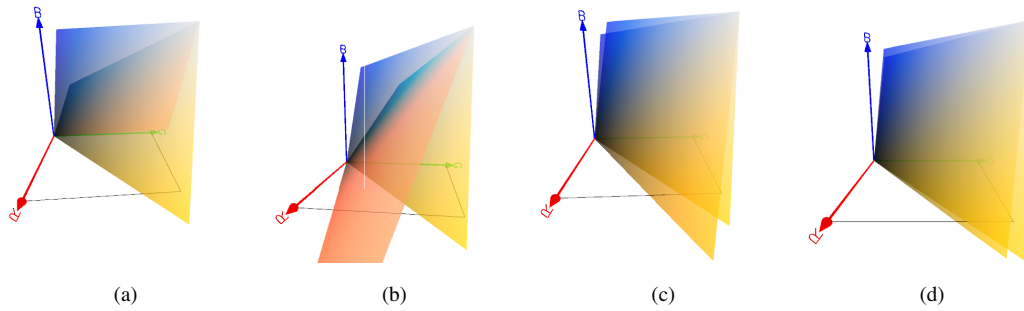


Figure 4.8: Comparison of the plausible dichromacy models considering the entire RGB space (protanopia case). A surface obtained using Brettel *et al.*'s (BRETTEL; VIÉNOT; MOLLON, 1997) algorithm is shown for reference in all images. (a) Empty Space / Empty Cones model. (b) Replacement model. (c) Replacement model using Equation 4.15. (d) Same as (c) but also scaled by 0.96.

4.2.3 The Algorithm for Simulating CVD

As discussed in Section 4.2.1, anomalous trichromacy can vary from mild to severe depending the amount of shift found in the peak sensitivity of the photopigments. Such shifts are caused by the exon arrangements (Figure 4.4) and the color perception of a severe anomalous trichromat is similar to the perception of a dichromat of the same class (*i.e.*, protan or deutan). Thus, it is reasonable to speculate that as the peak sensitivity of the L (or M) cones gets shifted toward the peak sensitivity of the M (or L) cone, the rescaling of the associated curve required for the case of protanopia and deuteranopia, also needs to be performed, in proportion to the amount of shift. This is justified considering that as one transitions between the spectral sensitivity curves of the L and M cones, there should also be a corresponding transition in the bandwidths and areas under the intermediate curves. Such a gradual rescaling guarantees a smooth transition between the various degrees of

protanomaly (deuteranomaly) and protanopia (deutanopia). Equations 4.17 and 4.18 model this smooth transition:

$$L_a(\lambda) = \alpha L(\lambda) + (1 - \alpha) 0.96 \frac{Area_L}{Area_M} M(\lambda) \quad (4.17)$$

$$M_a(\lambda) = \alpha M(\lambda) + (1 - \alpha) \frac{1}{0.96} \frac{Area_M}{Area_L} L(\lambda) \quad (4.18)$$

$$S_a(\lambda) = S(\lambda + \Delta\lambda_S) \quad (4.19)$$

where $\alpha = (20 - \Delta\lambda)/20$, for $\Delta\lambda \in [0, 20]$. Note that the 0.96 factor has been added to try to compensate for the inaccuracies of the available data, assuming Brettel *et al.*'s model as reference. As more accurate data describing the mapping from cones responses into opponent channels and/or a more accurate reference model become available, the need for such a factor might be eliminated.

Since there are no strong biological explanations yet to justify the causes of tritanopia and tritanomaly, tritanomaly is simulated based on the shift paradigm only (Equation 4.19) as an approximation to the actual phenomenon and restrain the proposed model from trying to model tritanopia. Likewise, simulation of monochromacy (either rod or cone) is not supported by this model. One should note, however, that the conditions covered by the proposed model (*i.e.*, anomalous trichromacy and dichromacy) correspond to approximately 99.96% of all CVD cases (RIGDEN, 1999; SHARPE *et al.*, 1999).

The actual algorithm for simulating anomalous trichromatic vision uses Equations 4.17, 4.18, and 4.19 in conjunction with Equations 4.5 to 4.11. Likewise, the simulation of protanoptic and deutanoptic vision is obtained using Equations 4.20 and 4.21, respectively, in conjunction with Equations 4.8 to 4.11.

$$\begin{bmatrix} WS(\lambda) \\ YB(\lambda) \\ RG(\lambda) \end{bmatrix}_{protanopia} = T_{LMS_2Opp} \begin{bmatrix} L_{protanope}(\lambda) \\ M(\lambda) \\ S(\lambda) \end{bmatrix} \quad (4.20)$$

$$\begin{bmatrix} WS(\lambda) \\ YB(\lambda) \\ RG(\lambda) \end{bmatrix}_{deutanopia} = T_{LMS_2Opp} \begin{bmatrix} L(\lambda) \\ M_{deutanope}(\lambda) \\ S(\lambda) \end{bmatrix} \quad (4.21)$$

where

$$L_{protanope}(\lambda) = 0.96 \frac{Area_L}{Area_M} M(\lambda), \quad (4.22)$$

$$M_{deutanope}(\lambda) = \frac{1}{0.96} \frac{Area_M}{Area_L} L(\lambda) \quad (4.23)$$

Thus, the simulation of any protan or deutan anomaly can be obtained using Equation 4.24, where Γ_{CVD} should be instantiated with the Γ matrix (Equation 4.10) specific for the kind of target CVD.

$$\begin{bmatrix} R_s \\ G_s \\ B_s \end{bmatrix} = \Gamma_{normal}^{-1} \Gamma_{CVD} \begin{bmatrix} R \\ G \\ B \end{bmatrix} \quad (4.24)$$

4.3 Results

The proposed model was incorporated in a visualization system and also implemented in MATLAB. It has been used to simulate the perception of both dichromats and anomalous trichromats (at different degrees of severity). The simulation operator (Equation 4.24)

only requires one matrix multiplication per pixel and can be efficiently implemented on GPUs.

Figure 4.9 compares the results produced by the proposed technique with the ones obtained with the technique of Yang *et al.* (YANG *et al.*, 2008) for the image shown in Figure 4.6 (e). Note that the images simulated using Yang *et al.*'s technique show some green, red and purple shades, for both protanomalous and deuteranomalous at all degrees of severity. This is inconsistent with the perception of these individuals, who after some degree of severity have trouble distinguishing red from green. The last column in Figure 4.9 (Brettel) shows the results simulated using Brettel *et al.*'s algorithm for comparison with the severe case (20 nm).

Figure 4.1 shows a reference image (left) and the simulated perception obtained with the proposed model for different degrees of protanomaly (6 nm and 14 nm) and for protanopia. Note the progressive loss of color contrast as the degree of severity increases. Figure 4.10 shows examples of simulation of anomalous trichromatic vision in scientific visualization. For all examples, there are simulations for both protanomalous and deuteranomalous vision at severity levels corresponding to 2 nm, 8 nm, 14 nm, and 20 nm. Note how the ability to perceive red and green vanishes with the increase of the anomaly severity.

4.3.1 Experimental Validation

To validate the proposed model, some experiments involving both normal trichromats and color vision deficient individuals were performed. All subjects performed two rounds of the color discrimination Farnsworth-Munsell 100-Hue (FM100H) test (FARNSWORTH, 1957). The original test consists of 85 movable color caps and four wooden boxes (trays). One box holds 22 caps, while the other three hold 21 caps each. The tested subject must take one box at a time and arrange its color caps in a continuous color sequence using two extra fixed caps at opposite ends of the box as reference. The color sequences range from red to yellow, yellow to blue-green, blue-green to blue, and blue to purple-red, respectively. The 85 colors are sampled from the Munsell color system (Hue-Value-Chroma space) with equally spaced hue values (starting at red, 5R in Munsell's notation), and equal saturation and brightness control (chroma 6 and value 6 in Munsell's notation).

Each color cap is identified by an indexing number (ranging from 1 to 85) printed on its back. After the arrangement of the caps, the color discrimination aptitude of the subject is verified by computing an error score for each color cap as the sum of the absolute difference between its index and the index of its two adjacent neighbors. The total error score is the sum of the individual error scores less the minimum error score of 170. A plot like the one shown in Figure 4.11 is used to simplify the analysis. In such a plot, the caps are numbered counterclockwise and the individual error scores are plotted radially outward from the circle with an error score of two on the inner circle. The color discrimination aptitude of a subject is analysed over the average scores for all color caps computed from at least two trials, a test and retest.

A computerized version of the FM100H using C++ and OpenGL was implemented. This implementation is based on the Meyer and Greenberg's work (MEYER; GREENBERG, 1988). For the tests, 17-inch CRT flat screen monitors (model LG Flatron E701S, 1024 × 768 pixels, 32-bit color, at 85 Hertz) were used. The monitors were calibrated using a ColorVision Spyder 2 colorimeter (Gamma 2.2 and White Point 6500K). Both calibration and tests were performed with the room lights off. Unlike Meyer and Greenberg, one sequence of color caps was presented at a time (like in the original test). The

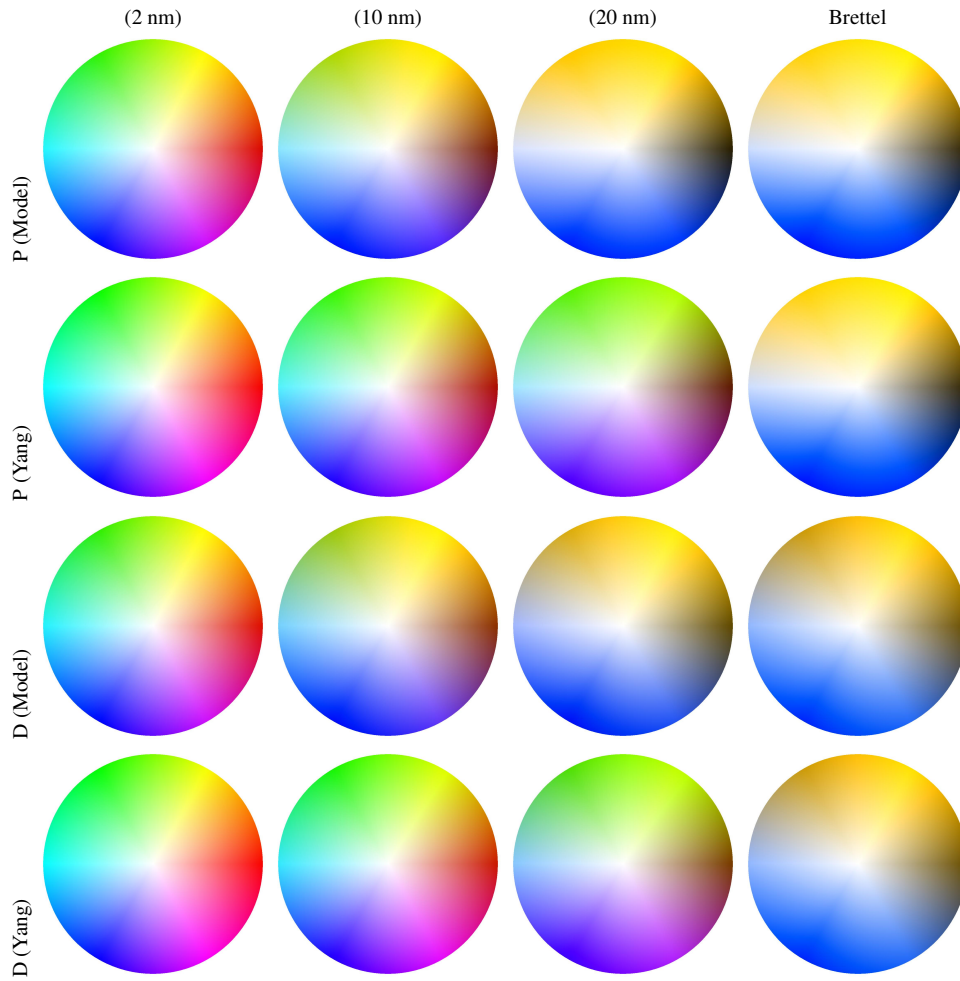


Figure 4.9: Simulation of protanomalous and deuteranomalous vision for several degrees of severity (expressed in nm). Last column: result of Brettel *et al.*'s algorithm for reference. *P/D (Model)*: Protanomaly/Deuteranomaly simulated with the proposed technique. *P/D (Yang)*: Protanomaly/Deuteranomaly simulated with Yang *et al.*'s technique.

user interface consisted of a black screen having the color caps placed horizontally in the central row. Each cap was rendered as a circle with 1 cm of diameter and could be moved using the mouse (except the reference color caps, which are fixed). Both the presentation order of the trays of caps, and the initial arrangement of the caps in each tray were random.

The group of normal trichromats (NT_g group) consisted of 17 male subjects (ages 19 to 29). The group of the color vision deficient individuals (CVD_g group) consisted of 13 male subjects classified as follows: 4 protanomalous (ages 23 to 53), 4 protanopes (ages 22 to 59), 3 deuteranomalous (ages 22 to 28), and 2 deuteranopes (ages 18 to 44). The classification of the subjects in the CVD_g group was done after the application of an Ishihara test (ISHIHARA, 1979).

Each subject in the CVD_g group performed two trials of the FM100H test using the original colors. We then averaged the 16 results of the 8 protans (protanomalous and protanopes) and did the same for the 10 results of the 5 deutans (deuteranomalous and deuteranopes). The results of these averaged tests are shown in Figure 4.12 (b) and (d),

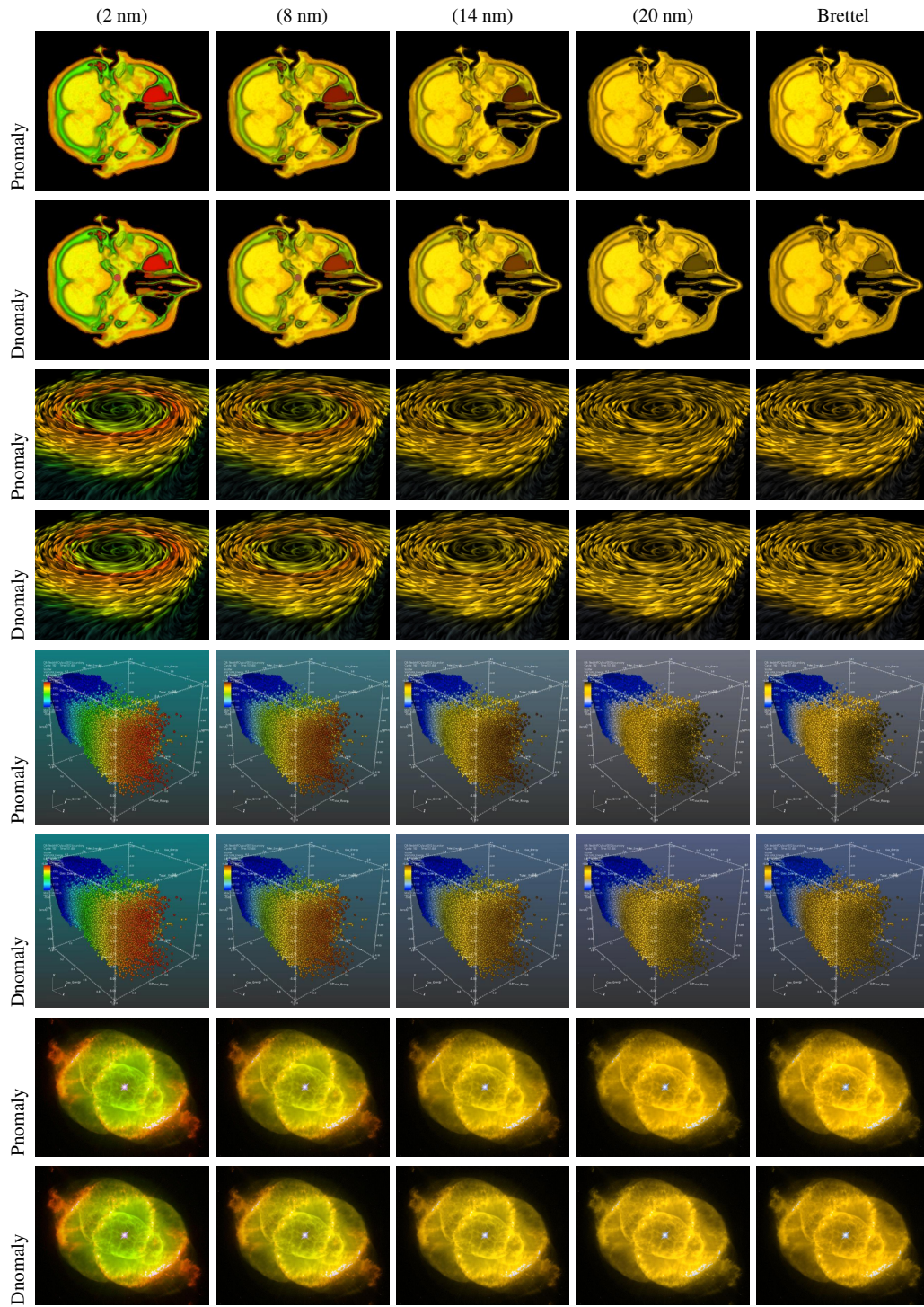


Figure 4.10: Simulation of protanomalous and deuteranomalous vision in scientific visualization. From top to bottom: brain dataset, Tornado, Scatter plot, and Cat's Eye nebula. The degrees of severity are expressed in *nm*. Last column: Brettel *et al.*'s dichromatic simulation for reference. *Pnomaly*: Protanomaly. *Dnomaly*: Deuteranomaly.

for the protans and deutans, respectively.

The subjects in the NT_g group were divided into two subgroups: NT_{gp} (8 individuals, ages 19 to 26) and NT_{gd} (9 individuals, ages 21 to 29). Both subgroups performed two

trials of the FM100H test using the original colors. These 34 results were averaged, which are depicted in the plot shown in Figure 4.11. Then, the proposed model was used to simulate how protanomalous with shifts of 12 nm, 16 nm, and 19 nm, would perceive the original colors of the FM100H test. These sets simulated colors were called CP_{12nm} , CP_{16nm} , and CP_{19nm} , respectively. A similar simulation was performed for the case of deuteranomalous, obtaining sets of simulated colors CD_{12nm} , CD_{16nm} , and CD_{19nm} .

The subgroup NT_{gp} then performed two trials of the FM100H test using the sets CP_{12nm} , CP_{16nm} , and CP_{19nm} , one at a time, instead of the original colors. This should simulate for the normal trichromat the perception of the corresponding degrees of protanomaly. Figure 4.12 (a) shows a plot of averaged 48 results ($8 \times 3 \times 2$). A similar procedure was applied to the 9 members of the NT_{gd} subgroup using the sets CD_{12nm} , CD_{16nm} , and CD_{19nm} of simulated colors. Figure 4.12 (c) shows a plot of averaged 54 results ($9 \times 3 \times 2$).

A comparison of the plots corresponding to the averaged results of the NT_{gp} subgroup (Figure 4.12 a) and the averaged results of the protans (Figure 4.12 b) reveals great similarity. The small blue segment next to the yellow hue represents the eigenvector with largest absolute eigenvalue computed for the covariance matrix of the error scores. A comparison of the averaged results of the NT_{gp} subgroup (Figure 4.12 c) and the averaged results of the deutans (Figure 4.12 d) reveals an even better agreement of the corresponding eigenvectors. Note how these plots are significantly different from the one shown in Figure 4.11. These results indicate that the proposed model provides good simulations for the color perception by individuals with color vision deficiency.

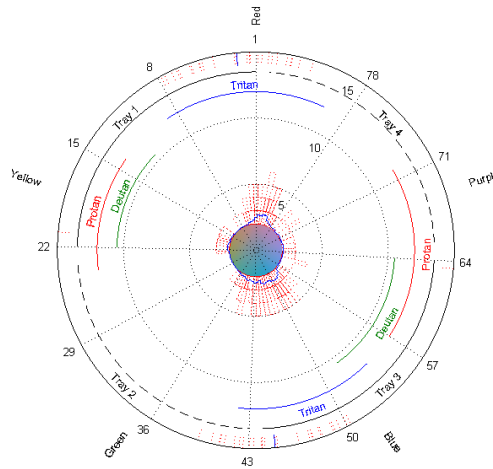


Figure 4.11: Averaged results of the Farnsworth-Munsell 100H test performed by 17 normal trichromats using the test original colors.

4.3.2 Discussion

Once incorporated into visualization systems, the proposed model can provide immediate feedback to visualization designers. As such, it can be a valuable tool for the design of visualizations that are meaningful both for individuals with normal and deficient visual color systems. Note that although one could consider the simpler solution of just adopting color scales that completely fit in the color gamut of dichromats, this might be unnecessar-

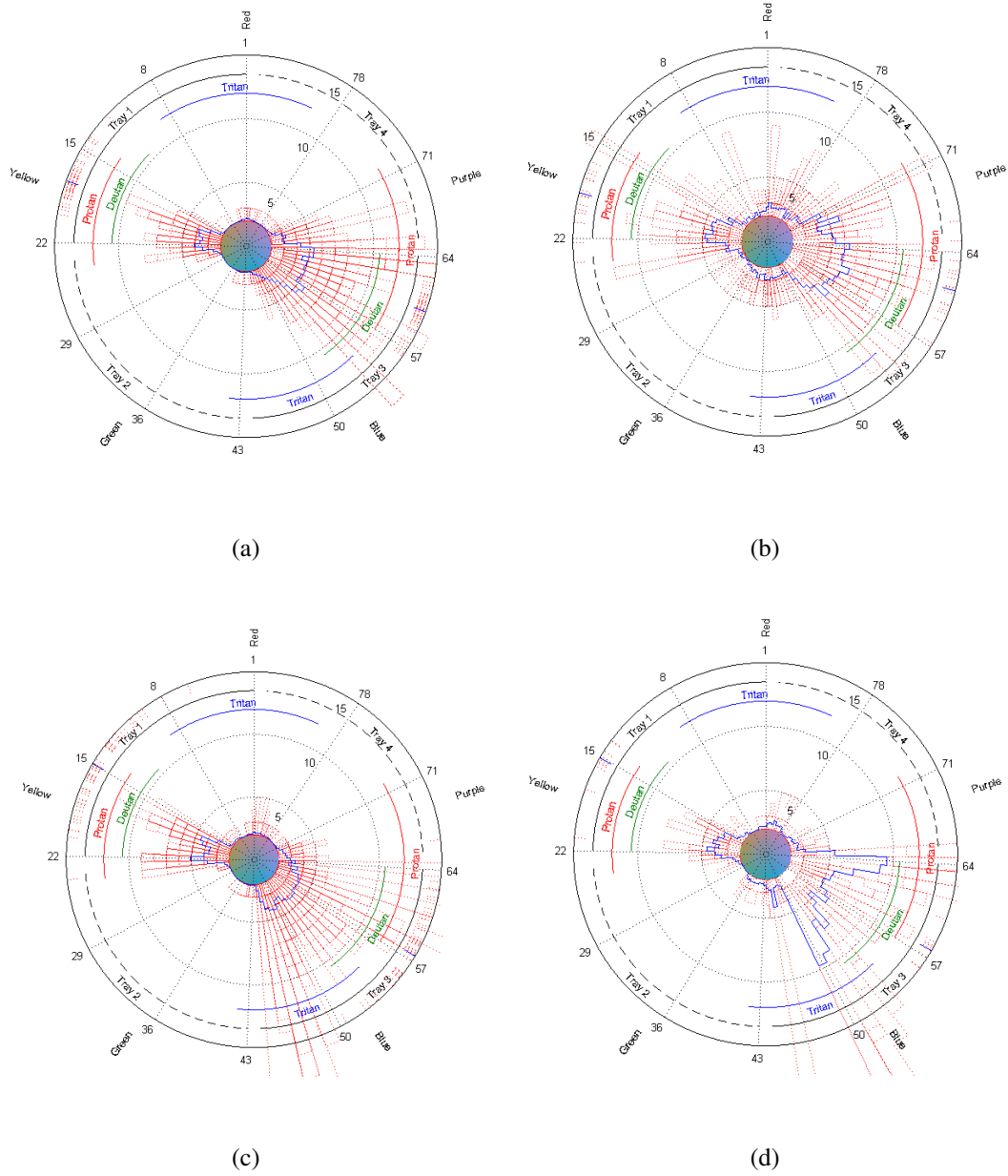


Figure 4.12: Averaged results of the Farnsworth-Munsell 100H test. (a) Normal trichromats simulating protan vision. (b) Protan results for the original colors. (c) Normal trichromats simulating deutan vision. (d) Deutan results for the original colors.

ily restrictive in many situations. In such cases, a larger color gamut could be exploited to obtain more effective results, especially when dealing with multidimensional visualizations. The top row of Figure 4.13 compares the color gamut of normal trichromats, protanomalous with a shift of 10 nm, and protanopes, for two slices of the HSV color space ($V=1.0$ and $V=0.75$). Although the 10-nm protanomalous only perceive a fraction of the HSV disks, they still have a much larger gamut than the protanopes, who only perceive a line across each disk (from blue to yellow). The bottom row of Figure 4.13 shows visualizations of the Visible Male's head using the same transfer function defined over the color gamut of these individuals. Note that the protanomalous' larger color gamut in comparison to the protanope's lends to better color contrast. Such images were captured

using a software for visualization by slicing of 3D texture that incorporates the proposed model and allows switching between normal color vision and the simulation of any degree of anomaly in real-time. The visualization system was provided by Francisco Pinto. The appendix A show the matrices used to incorporate the proposed model in the system.

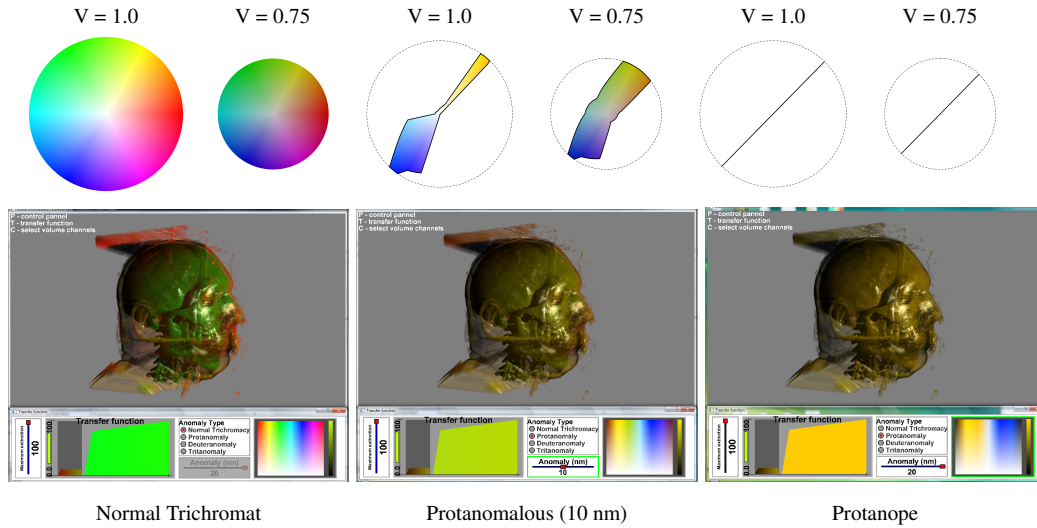


Figure 4.13: Visualization of the Visible Male’s head using the same transfer function (bottom) defined over the color gamut (top row) of a normal trichromat, a protanomalous (10 nm), and a protanope.

The choice of an appropriate color scale for a given visualization should take into account different factors, such as characteristics of the dataset, questions that one would like to answer about the data, the intended viewers and their cultural backgrounds (RHEINGANS, 2000). Thus, the proposed model is not intended to automatically build or guide the construction of color maps, even though it can be used to provide information for approaches that do so (BERGMAN; ROGOWITZ; TREINISH, 1995; HEALEY, 1996; LEVKOWITZ; HERMAN, 1992; WARE, 1988). Instead, it gives visualization designers an understanding of the perceptual limitations of each class of CVD. As such, the proposed model can help designers to refine their visualizations, making them more effective to a wider range of viewers.

More research is needed to develop better color selection methodologies that take into account the limitations of specific groups of observers. Healey (HEALEY, 1996) described a technique for choosing multiple colors for use in visualization. He accomplished this by measuring and controlling perceptual metrics like *color distance*, *linear separation* and *color category* during color selection. Healey’s technique could be used to define sets of colors that provide good differentiation among data elements for both normal trichromats and any given class of CVD.

4.4 Summary and Conclusions

This chapter presented a physiologically-based model for simulating color perception, and showed how it can be used to help designers to produce more effective visualizations. The proposed model is the first to consistently handle normal color vision, anomalous trichromacy, and dichromacy using a unified framework. By means of a con-

trolled user experiment, it was demonstrated that the results produced by the proposed model seem to closely match the perception of individuals with color vision deficiency. It has also compared the proposed model's results to the ones obtained with existing models for simulating the perception of anomalous trichromats (YANG et al., 2008) and of dichromats (BRETTEL; VIÉNOT; MOLLON, 1997). Such comparisons indicate that the model's results are superior to the ones of Yang *et al.* (YANG et al., 2008) for anomalous trichromacy, and equivalent to the ones of Brettel *et al.* (BRETTEL; VIÉNOT; MOLLON, 1997) for the case of dichromacy.

The proposed model also provides a flexible framework for allowing scientists to test different hypotheses about color vision models. This chapter has shown how the plausibility of the three most accepted hypotheses for the causes of dichromatic vision were tested. While it is difficult to verify such hypotheses *in vivo*, the proposed model suggests that pigment substitution is the most plausible one. Moreover, it indicates that pigment substitution would require a renormalization of the spectral sensitivity curve of the affected cones. Such an observation, not yet reported in the vision literature, if verified, would provide some strong evidence in favor of the correctness of the proposed model.

5 A REAL-TIME TEMPORAL-COHERENT COLOR CONTRAST ENHANCEMENT FOR DICHROMATS

This chapter presents a real-time technique for enhancing color contrast for dichromats that guarantees temporal coherence and preserves achromatic colors (gray shades). The cost of this approach is linear on the number of input pixels, and most of the computation can be performed independently for each pixel, lending to an efficient GPU implementation. This chapter demonstrates the effectiveness of the proposed approach by using it to obtain real-time, temporal-coherent, high-quality visualizations for dichromats.

The proposed approach uses the Gaussian pairing technique of Grundland and Dogdson (GRUNDLAND; DODGSON, 2007) for acceleration. However, it differs from their approach in many fundamental aspects. First, it is dealing with recoloring for dichromats, as opposed to color-to-grayscale mappings. Second, it performs all the computation in the $L^*a^*b^*$ color space, which is an approximately perceptually uniform color space, where it makes sense to use distances to represent perceptual differences. Third, it uses PCA, an established technique for estimating the direction of maximum variance in a given dataset, to compute the direction v_{ab} that maximizes the loss of color contrast (in a least-squares sense) in the chromaticity plane (*i.e.*, a^*b^* plane). Fourth, it uses the coordinates of the projected colors onto the plane defined by v_{ab} and the L^* axis as the transformed color coordinates, as opposed to using them to complement the original luminance values. And finally, this approach presents temporal coherence, which is not supported by the technique described in (GRUNDLAND; DODGSON, 2007).

Figure 5.1 illustrates some results generated by the proposed technique and compares them with the ones produced by the state-of-the-art technique for image recoloring for dichromats (KUHN; OLIVEIRA; FERNANDES, 2008a). The reference images represent the perception of normal trichromats. The column *Dichromat* shows the simulated perceptions of dichromats for the corresponding reference images. The next two columns show the recolored images obtained using the proposed technique and its exaggerated contrast version, respectively. The two remaining columns show the results produced by the regular and by the exaggerated-contrast versions of the recoloring technique of Kuhn et al. (KUHN; OLIVEIRA; FERNANDES, 2008a). Note how the proposed technique can satisfactorily recover the contrast lost by dichromats.

The main contributions of this chapter include:

- The first contrast-enhancement image-recoloring technique for dichromats that produces high-quality results in real time (Section 5.1). This solution scales well with

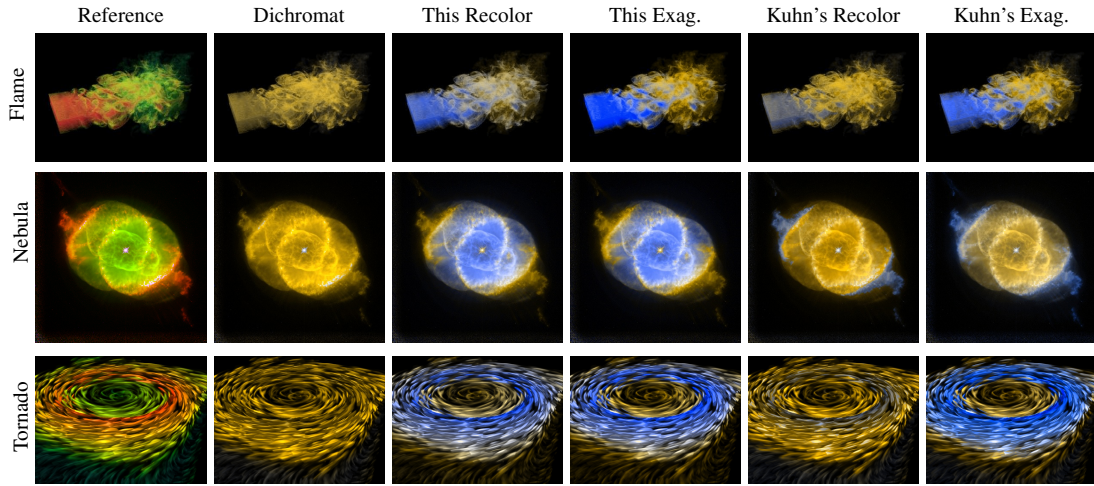


Figure 5.1: Comparison of the results produced by the proposed recoloring technique and by Kuhn et al.'s (KUHN; OLIVEIRA; FERNANDES, 2008a) for a set of scientific visualization images. The "Dichromat" column shows the simulated perception of dichromats for the corresponding "Reference" image obtained using the approach presented in Chapter 4. The simulation and recolorings of the Flame and Nebula images are for deuteranopes, while the Tornado ones are for protanopes.

the number of input pixels, can be efficiently implemented on GPUs, and preserves achromatic colors;

- A technique that enforces temporal coherence in the recolored image sequences (Section 5.1.4);
- The first demonstration of a visualization application with support for real-time high-quality image recoloring for dichromats (Section 5.2);

5.1 The Color-Contrast Enhancing Technique

The proposed approach is based on the key observation that, whenever dichromats experience some significant loss of color contrast, most of this contrast can be recovered by working on a perceptually uniform color space, and orthographically projecting the original colors onto a plane aligned with the direction that maximizes contrast loss (in a least-squares sense). The coordinates of these projections then become the new color coordinates on the reduced (2D) color gamut of the dichromat. Figure 5.3 summarizes this process, which consists of the following steps:

1. Estimation of the vector v_{ab} that represents the direction that maximizes contrast loss in the CIE $L^*a^*b^*$ chromaticity plane, and
2. Projection of the original colors onto the plane defined by v_{ab} and the lightness (L^*) axis. The projected color coordinates are then rotated around L^* to align themselves to the plane of the dichromat, and the resulting colors are used to recolor the image.

In order to guarantee temporal coherence, the algorithm checks and corrects for abrupt changes in the sense of v_{ab} . Sections 5.1.1 to 5.1.4 present the details of these steps.

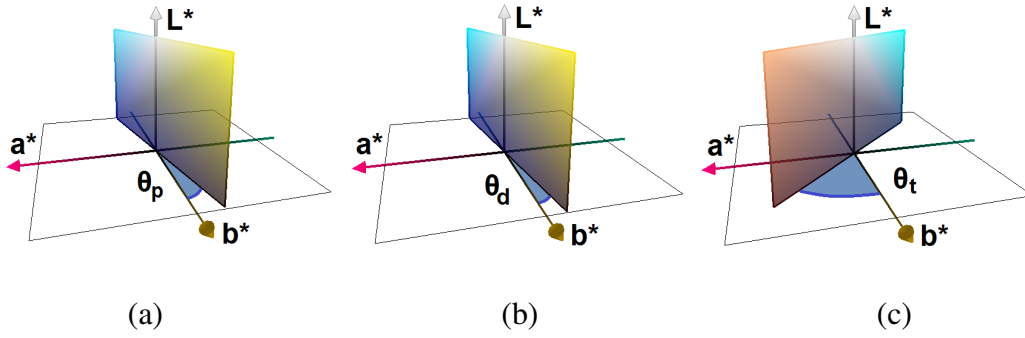


Figure 5.2: Planar approximation for the color gamut of dichromats in the CIE $L^*a^*b^*$ color space (KUHN; OLIVEIRA; FERNANDES, 2008a). (a) Protanope ($\theta_p = -11.48^\circ$). (b) Deutanope ($\theta_d = -8.11^\circ$). (c) Tritanope ($\theta_t = 46.37^\circ$).

5.1.1 Direction that Maximizes Contrast Loss

The color gamut of each class of dichromats can be represented by two half-planes in the LMS color space (BRETTEL; VIÉNOT; MOLLON, 1997), and can be satisfactorily approximated by a single plane (VIÉNOT; BRETTEL; MOLLON, 1999). Figure 5.2 shows these planes mapped to the CIE $L^*a^*b^*$ color space. According to Kuhn *et al.* (KUHN; OLIVEIRA; FERNANDES, 2008a), the angles between such planes and the L^*b^* plane are $\theta_p = -11.48^\circ$, $\theta_d = -8.11^\circ$, and $\theta_t = 46.37^\circ$, for protanopes, deuteranopes, and tritanopes, respectively. The colors shown in Figure 5.2 represent the actual color gamut for each class of dichromacy.

Computing the direction that maximizes the loss of local contrast (in the least-squares sense) for a dichromat observing an image I would require evaluating, for each pixel $p_i \in I$, the contrast lost between p_i and all pixels p_j in a neighborhood N_i around p_i . However, due to spatial coherence, neighbor pixels tend to have similar values. Thus, estimating the loss of local contrast for each pixel p_i against all pixels in N_i tends to result in a significant amount of redundant work. The proposed approach avoids performing this computation on the entire neighborhood N_i by resorting to the Gaussian pairing sampling technique of Grundland and Dogdson (GRUNDLAND; DODGSON, 2007). In this case, for each pixel p_i , its contribution to the loss of local contrast is estimated from a single neighbor p_j . The horizontal and vertical distances between p_i and p_j are randomly defined by univariate Gaussian distributions with zero mean and variance $(2/\pi)\sigma^2$, where $\sigma^2 = \sqrt{2\min(\text{width}, \text{height})}$ (GRUNDLAND; DODGSON, 2007), the function $\min(a, b)$ returns the minimum of a and b , and width and height are the dimensions of the image. Although the direction of maximum loss of local color contrast obtained using this sampling strategy differs from the one computed using the entire neighborhoods, due to spatial coherence these directions tend to be sufficiently close to each other. To avoid flickering during the recoloring of animated or video sequences (Section 5.1.4), it pre-computes the coordinates of the p_j s and stores them in a texture. The same pairs (p_i, p_j) are then used during the entire sequence.

Figures 5.3 (a) and (b) illustrate the process of computing the direction that maximizes the loss of contrast for two pairs of colors, (c_1, c_2) and (c_3, c_4) , represented as small spheres in the $L^*a^*b^*$ color space. c'_1 to c'_4 are the projections of colors c_1 to c_4 , respectively, on the dichromat's plane, and represent his/her perception of colors c_1 to c_4 (Figure 5.3(a)). Since $L^*a^*b^*$ is approximately perceptually uniform, the relative loss of

color contrast experienced by a dichromat observing a pair of colors (c_i, c_j) (with respect to a normal color vision observer) can be estimated as

$$l_{(c_i, c_j)} = \frac{\|c_i - c_j\| - \|c'_i - c'_j\|}{\|c_i - c_j\|}, \quad (5.1)$$

where $\|\cdot\|$ is the vector length operator. For this pair of colors, the direction of contrast loss is given by $\vartheta_{ij} = c_i - c_j$. Since it preserves the lightness coordinate (*i.e.*, L^*) of the

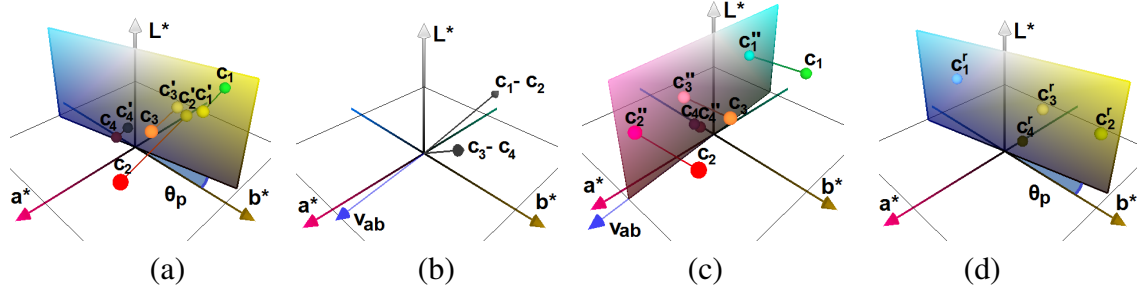


Figure 5.3: The steps of the proposed recoloring algorithm. (a) Colors c_1 to c_4 are perceived by a dichromat as c'_1 to c'_4 , respectively (their projections on the dichromat's gamut plane). The relative loss of contrast experienced by a dichromat for a pair of colors (c_i, c_j) is given by $l_{(c_i, c_j)} = (\|c_i - c_j\| - \|c'_i - c'_j\|) / (\|c_i - c_j\|)$, which happens along the direction $\vartheta_{ij} = c_i - c_j$. (b) Direction v_{ab} (shown in blue) that maximizes the loss of local contrast (in a least-square sense) is computed as the main eigenvector of the matrix $M^T M$, where M is defined in Equation 5.2. (c) Projection of the original colors on the plane defined by v_{ab} and L^* . (d) Final colors obtained after rotating the projected colors c''_k in (c) around L^* so that they align with the dichromat's plane.

original colors to avoid polarity reversal (KUHN; OLIVEIRA; FERNANDES, 2008a), it suffices to compute the direction that maximizes contrast loss on the chromaticity plane. Computing it in the entire $L^*a^*b^*$ space does not improve the results, and would require finding the eigenvectors of a 3×3 matrix instead of a 2×2 . Thus, let $w_i = l_{(c_i, c_j)} \vartheta_{ij}$ be the vector representing the contrast loss along direction ϑ_{ij} associated to pixel p_i . Also let

$$M = \begin{bmatrix} w_1^{a^*} & w_1^{b^*} \\ w_2^{a^*} & w_2^{b^*} \\ \vdots & \vdots \\ w_n^{a^*} & w_n^{b^*} \end{bmatrix} \quad (5.2)$$

be a matrix whose rows contain the coordinates of the chromaticity vectors representing the loss of color contrast for all pixels in image I . The elements of the i -th row of M are the projections of w_i on the a^*b^* plane. v_{ab} can then be obtained as the eigenvector of the 2×2 matrix $M^T M$ whose corresponding eigenvalue has the largest absolute value. In order to solve the resulting characteristic equation, it sets the b^* coordinate of v_{ab} to one and solve for its a^* coordinate.

5.1.2 Computing the Final Colors

When a dichromat experiences a significant loss of color contrast, the orthographic projection of the original colors onto the plane defined by the vectors L^* and v_{ab} tends to spread these colors more than when they are projected onto the dichromat's plane. This

situation is illustrated on Figures 5.3 (a) and (c). If the spatial relationship among the projected colors onto the L^*-v_{ab} plane is transferred to the dichromat's plane, an image with better color contrast will be produced. This is achieved by rotating the projected colors around the L^* axis so that they now align with the plane of the dichromat. Figure 5.3 (d) illustrates this operation, which preserves the achromatic colors from the original image.

5.1.3 Exaggerated Contrast

As one maps the RGB cube to the $L^*a^*b^*$ color space, the maximum length of the resulting chromaticity vectors is 148.47. Thus, it obtains images with exaggerated contrast, similar to the ones produced by Kuhn *et al.*'s technique, simply by rescaling all chromaticity coordinates in the recolored image so that its maximum chroma becomes 148. However, this is not the preferred use for the proposed technique, as images produced with exaggerated contrast tend to contain higher perceptual distortions than images obtained using the regular recoloring technique. Recolorings with exaggerated contrast are shown in Figures 5.1, 5.4 and 5.8 for the sake of comparison.

5.1.4 Enforcing Temporal Coherence

Temporal coherence is an important requirement for image-recoloring techniques, as subtle changes in the color of an object during an interactive visualization session or animation can be quite disturbing. This section explains how the proposed technique enforces temporal coherence.

If the direction of v_{ab} is almost parallel to the a^* axis, a minor change in the input colors might imply a switch in the sign of v_{ab} 's small b^* component (see Figure 5.3(b)). However, for the solution of the characteristic equation associated with the computation of v_{ab} , it was arbitrated its b^* component to 1 (Section 5.1.1), as one possible way to avoid the trivial solution $v_{ab} = 0$. This constrains v_{ab} 's b^* component to be positive, causing its a^* component to change its sign to accommodate the change in v_{ab} 's direction. Such a change would cause recolored pixels to abruptly change colors between consecutive frames (*e.g.*, blue pixels would turn yellow, and vice versa). To avoid the occurrence of these artifacts during an interactive visualization session (or animation) it saves the vector v_{ab} of the current frame and using it for comparison in the next frame. As the angle between the previous and current vectors approaches 180° , it inverts the sense of the current v_{ab} to enforce color consistency. Although simple, this is an effective solution.

5.2 Results

The described technique was implemented both for CPU and for GPU, using C++ and GLSL, and these implementations were used to recolor a large number of images. The GPU implementation was integrated with an existing visualization application using a minimally invasive approach. In this session, the performance and quality of the results produced by our technique are compared with the ones obtained with the approach of Kuhn *et al.* (KUHN; OLIVEIRA; FERNANDES, 2008a), which is currently the state-of-the-art both in terms of performance and image quality. One should note that all recolored images shown in the chapter are perceived similarly both by the class of dichromats they were recolored for and by normal color vision individuals. This comes from the fact that all colors used for recoloring are on the dichromat's plane, which is a subset of the color gamut of a normal trichromat. Also, all images exemplifying results of Kuhn *et al.*'s techniques (regular and exaggerated contrast) were generated with a CPU implementation

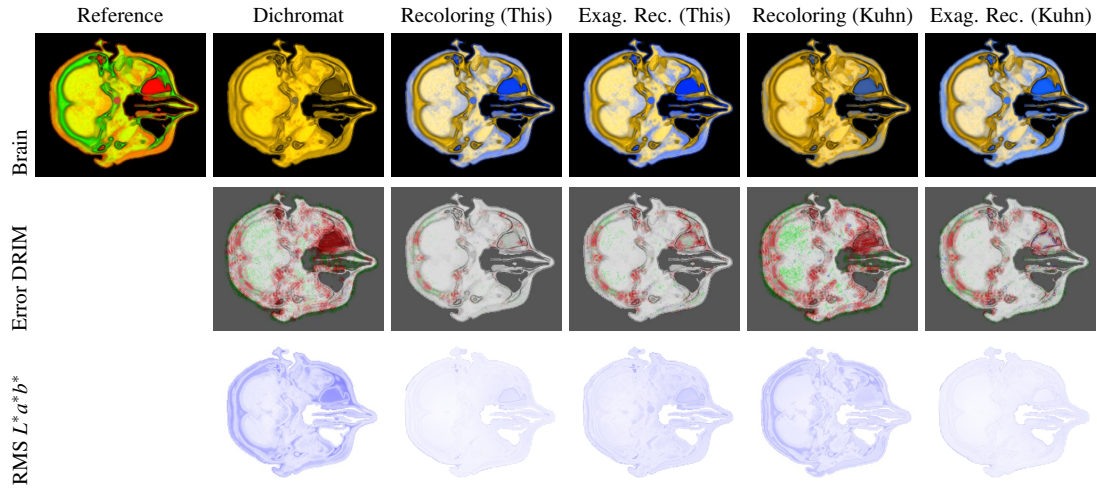


Figure 5.4: Comparison of the results produced by the proposed technique and by Kuhn *et al.*'s. First row, from left to right: reference image, simulated perception of a deuteranope, and recolored images using various algorithms. Second row: Perceptual errors according to the DRIM metric. Third row: Local contrast differences according to the RMS metric of Equation 5.3 (for $k = 100$). According to both metrics, the proposed recoloring technique is less prone to noticeable changes in contrast.

based on K-means (with up to 128 clusters) in order to obtain the best possible image quality. The results reported in this chapter were obtained using a Core 2 Extreme 3.0 GHz PC with 8 GB of memory and a Quadro FX 5800 graphics card.

The quality of the results was assessed using both subjective comparison and a perceptual image quality metric. For this, it was used the dynamic range independent image quality metric (DRIM) of Aydin *et al.* (AYDIN *et al.*, 2008). DRIM uses a model of the human visual system to try to detect visible changes in image structure. Figures 5.1, 5.4, and 5.8 show results produced by the proposed technique and compare them with the ones obtained with Kuhn *et al.*'s approach. In these figures, the reference images illustrate the perception of normal trichromats. The column *Dichromat* shows the simulated perception of dichromats obtained with the algorithm proposed in chapter 4. The remaining columns present the recolored images obtained using the proposed recoloring technique, an exaggerated contrast version of it, Kuhn *et al.*'s (KUHN; OLIVEIRA; FERNANDES, 2008a) technique, and its exaggerated contrast version, respectively. The reference images are from different sources. They illustrate cases of effective visualizations for normal trichromats, but which are challenging for individuals with CVD. As such, they provide good test cases for the proposed technique. Most of these images (*Flame*, *Brain*, *Knee*, *Foot*, *Europe* and *Chart*) have also been used by Kuhn *et al.* (KUHN; OLIVEIRA; FERNANDES, 2008a).

Figure 5.4 shows the results obtained when recoloring the reference *Brain* image for deuteranopes. The second row shows their corresponding color-coded perceptual errors according to DRIM (using its default parameters), computed with respect to the reference image. Green indicates *loss of contrast*, blue represents *contrast amplification*, and red shows regions with *contrast reversal*. The more saturated the colors, the higher the probability of a human observer perceiving these changes in contrast. The DRIM results suggest that the metric cannot fully capture contrast changes that result purely from image

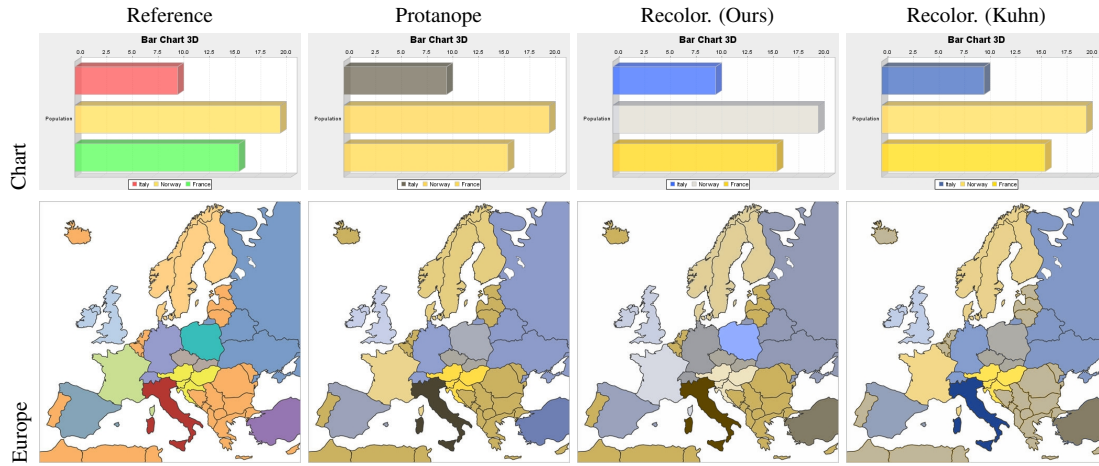


Figure 5.5: Recoloring of information visualization images for protanopes. Reference images are from (WIKIMEDIA COMMONS, 2010).

recoloring.

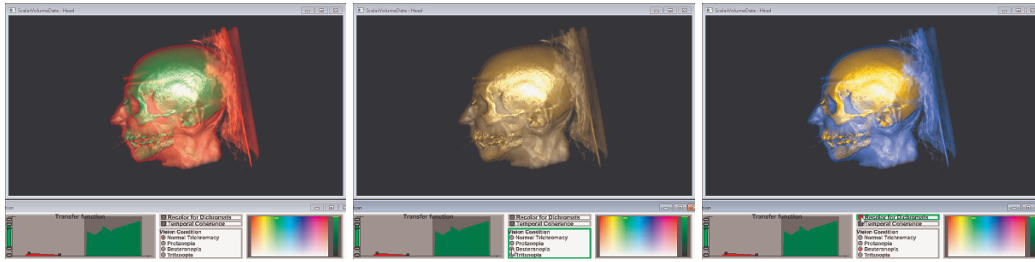


Figure 5.6: Integration of the proposed technique with an existing visualization application. (left) Reference image as perceived by an individual with normal color vision. (center) Simulation of the perception of a deuteranope for the reference image using the model explained in chapter 4. (right) Recolored image for a deuteranope using the proposed technique.

In order to complement DRIM's results, it was defined a simple error metric that tries to capture local differences in color contrast between pairs of images. Such a metric consists in computing a root-mean-square (RMS) error across corresponding neighborhoods in the (pair of) images using the $L^*a^*b^*$ color space. Although it produces plausible results, this metric has not been formally validated as a perceptual error metric. The proposed RMS metric is defined as follows: let $p_i \in I_{ref}$ be a pixel in the reference image I_{ref} , and let $S_{pi} = \{p_j, p_{j+1}, \dots, p_{j+k-1}\}$ be the set of pixels also in I_{ref} in a neighborhood containing k pixels centered at p_i . Likewise, let $q_i \in I_{test}$ be the pixel corresponding to p_i in the test image I_{test} , and let $S_{qi} = \{q_j, q_{j+1}, \dots, q_{j+k-1}\}$ be the set of pixels in the corresponding k -neighborhood around q_i . The difference of local color contrast between I_{ref} and I_{test} at p_i and q_i can be expressed as

$$RMS(q_i) = \sqrt{\frac{1}{k} \sum_{s=j}^{j+k-1} \left(\frac{(p_i - p_s) - (q_i - q_s)}{160} \right)^2}. \quad (5.3)$$

The constant 160 in the denominator keeps the resulting value in the $[0, 1]$ range. The third row of Figure 5.4 shows the resulting error images obtained applying Equation 5.3 to the foreground pixels of the images in the first row (with respect to the reference one). The value 0 is shown in white, and darker shades of blue indicate bigger errors. Note how these errors vary more smoothly over the images. According to both metrics, the results produced by the proposed technique are less prone to noticeable changes in contrast than the regular and exaggerated versions of Kuhn *et al.*'s technique.

Figure 5.8 compares results of the proposed technique and Kuhn *et al.*'s for three medical visualization images. Again, for these examples, the proposed recoloring technique introduced less contrast distortions than both the regular and exaggerated versions of Kuhn *et al.*'s approach. Kuhn *et al.*'s technique (KUHN; OLIVEIRA; FERNANDES, 2008a) is based on the more sounding principle of estimating perceptual differences between pairs of colors in the reference image, and using an optimization procedure to try to enforce such differences in the recolored image. In practice, however, the optimization often is not able to recover the optimal contrast due to the occurrence of local minima. This explains the results shown in Figures 5.1, 5.4, and 5.8. The proposed projection-based approach, on the other hand, tend to produce good results whenever a dichromat experiences significant loss of color contrast.

Figures 5.5 shows the proposed technique's and Kuhn *et al.*'s results for two information visualization examples. In this case, only the results of the regular recoloring techniques are shown. Table 5.1 summarizes the performance of the proposed approach in comparison to both the CPU and GPU versions of Kuhn *et al.*'s approach for seven images shown in this chapter. The entries in the table are ordered by the number of pixels in the images. One can observe that both versions of the proposed technique are up to two orders of magnitude faster than Kuhn *et al.*'s counterparts on images up to 800×800 pixels. Since the cost of the proposed algorithm is linear on the number of pixels, the achieved speedup improves as the image size increases. Although Kuhn *et al.*'s mass-spring optimization applied to a set of quantized colors is quite efficient, it still requires a quantization and a reconstruction steps, which dominate the total cost of the algorithm. Table 5.2 summarizes these costs for some of the images shown in the paper, considering the two quantization and reconstruction strategies described by the authors.

Image (size)	CPU		GPU	
	This Time	Kuhn Time	This Time	Kuhn Time
Flame (288x184)	0.055	1.148	0.019	0.121
Chart (500x300)	0.191	2.707	0.020	0.106
Foot (446x446)	0.252	3.743	0.021	0.307
Brain (532x523)	0.292	5.053	0.023	0.577
Knee (528x528)	0.341	5.217	0.022	0.313
Europe (596x486)	0.385	5.361	0.023	0.565
Nebula (800x800)	0.614	11.73	0.028	1.145

Table 5.1: Performance comparison (in sec.) of the proposed technique and Kuhn *et al.*'s (KUHN; OLIVEIRA; FERNANDES, 2008a) for both CPU and GPU versions of the algorithms executed on several images. Due to the linear cost of the proposed approach, the relative speedup improves as the image size increases.

Image (size)	Clusters	Quant. time	Reconst. time	
Flame (288x184)	88	0.9363	0.0027	K-Means
Foot (446x446)	78	3.5055	0.0082	
Europe (596x486)	70	5.1130	0.0115	
Nebula (800x800)	98	11.2448	0.0255	
Flame (288x184)	77	0.0155	0.0857	Uniform
Foot (446x446)	48	0.0670	0.2764	
Europe (596x486)	48	0.0978	0.5356	
Nebula (800x800)	74	0.2120	1.1130	

Table 5.2: Times (in sec.) for the quantization and reconstruction phases of the technique of Kuhn *et al.* (KUHNS; OLIVEIRA; FERNANDES, 2008a) for several images. K-means used in the CPU version of the technique, and uniform quantization used in its GPU version. The column Clusters shows the number of clusters identified in the quantization phase.

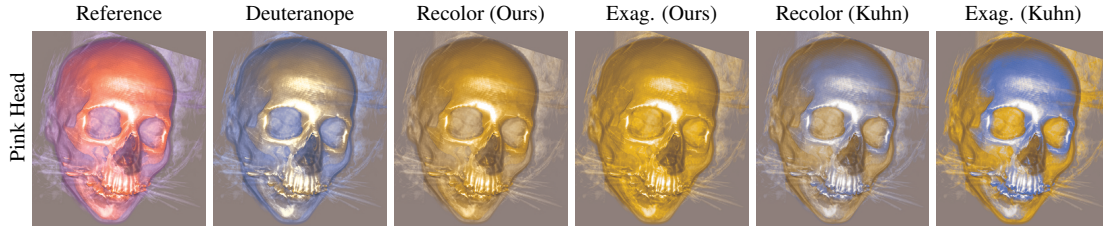


Figure 5.7: Example of a situation that causes the proposed technique to fail. Note that deuteranopes (and protanopes) already perceive the reference image as having sufficient contrast, and no recoloring is necessary.

The proposed technique can be easily integrated with existing applications using a minimally invasive approach. It can be deployed as a few shader programs, which the application should call after rasterizing the scene, but before swapping the back and front buffers. In this case, the shaders simply read the content of the back buffer, recolor it, and write it back, after which the host application swaps the buffers. This strategy was used to integrate the proposed technique to an existing visualization application. Figure 5.6 shows some snapshots of the resulting system.

5.2.1 Limitations

Like all previous image-recoloring techniques for dichromats, this one also has some limitations. For example, let d be the direction of maximum dispersion of the original colors in image I (in $L^*a^*b^*$). If v_{ab} is approximately perpendicular to d and the color dispersion along d is larger than along v_{ab} , the recolored image should exhibit less contrast than the original one. In practice, this requires that the loss of contrast be small, meaning that the dichromat could already perceive the details in the original image. In such a situation, there would be no need for recoloring in the first place. Figure 5.7 illustrates this situation with an image whose colors were carefully chosen to achieve this effect. According to some experiences, such cases should happen only rarely. To handle them, the user can turn the proposed recoloring technique *on* and *off* at any time during an

interactive session.

Although this technique preserves gray shades, it does not provide a mechanism for preserving other colors perceived similarly by dichromats and normal color vision individuals, as does the technique described in (KUHN; OLIVEIRA; FERNANDES, 2008a). Also, as a fundamental limitation of the reduced color gamut of dichromats, no technique, including this, can fully recover the lost contrast in all situations.

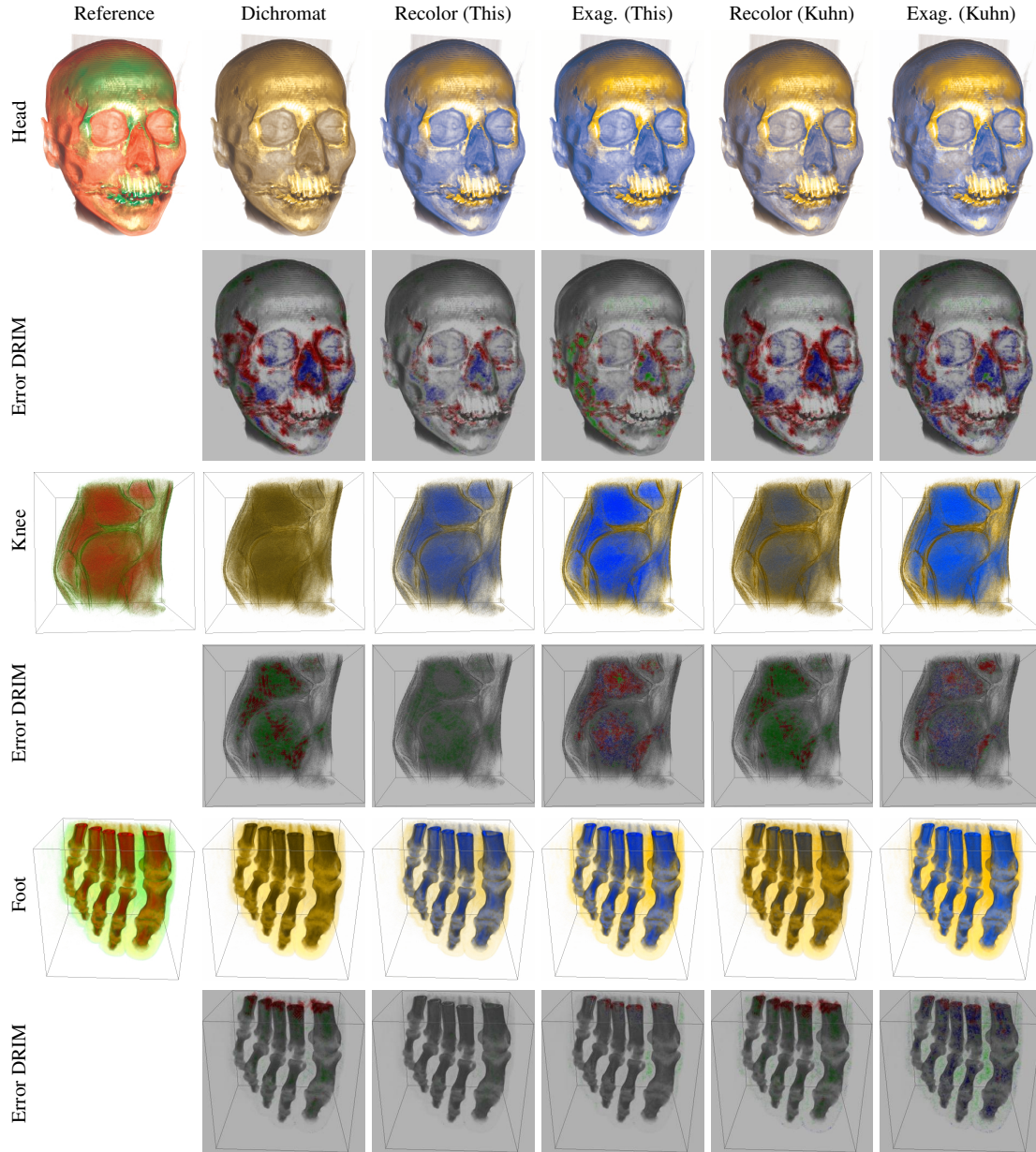


Figure 5.8: Comparison of the results produced by the proposed technique and the ones obtained with Kuhn *et al.*'s approach for a set of medical visualization images. The even rows show the estimated changes in contrast perceived by an observer in the recolored images (with respect to the reference images), according to the DRIM metric. Green indicates *loss of contrast*, blue represents *contrast amplification*, and red shows regions with *contrast reversal*. The metric favors the proposed technique's results in all examples. Reference images Knee and Foot were provided by Francisco Pinto.

5.3 Summary and Conclusions

This chapter presented the first technique to provide real-time, temporal-coherent, high-quality image recoloring for dichromats. Its computational cost varies linearly with the number of input pixels, and it can be efficiently implemented on GPUs. It has shown that the results produced by the proposed technique are at least as good as the ones obtained with the current state-of-the-art technique, while being up to two orders of magnitude faster. It has also shown how to integrate the proposed technique with existing applications using a minimally invasive strategy, and demonstrated its effectiveness producing real-time visualizations for dichromats.

The results of the proposed approach should enable the development of more user-friendly applications for individuals with color vision deficiency. For instance, the low computational cost of this technique makes it a suitable solution for implementation on cell phones and other mobile devices equipped with cameras. On such devices, the recoloring capabilities of this technique can be a useful tool for assisting color vision deficient individuals in several daily tasks.

6 CONCLUSIONS AND FUTURE WORK

Color vision deficiency impacts the professional and personal lives of approximately two hundred million individuals around the world. Thus, it is essential to deeply understand this condition and provide solutions that improve the quality of life of these individuals, as well as their accessibility to technology.

This thesis presented a physiologically-based model of human color vision that allows the simulation of the perception of individuals with CVD. This approach was the first to correctly simulate both dichromacy and anomalous trichromacy in a unified model. Moreover, this simulation technique is capable to simulate the perception of about 99.96% of all cases of color vision deficiency.

This thesis also presented a recoloring technique for dichromats, which is the first to perform high-quality recoloring in real-time and also the first to guarantee temporal coherence. This technique can be integrated in real-time applications and support video recoloring.

Visualizations (information, scientific, and medical) can contain ambiguous contents. Thus, this thesis presented the successful integration of both proposed techniques with a visualization system as a way to demonstrate the practical applications of the models and algorithms proposed in this thesis.

6.1 Future Work

Image-recoloring techniques for dichromats arose from the feedback obtained with techniques for simulation of dichromats perception. Even though, recoloring for dichromats was proven to produce effective results also for anomalous trichromats (KUNH; OLIVEIRA; FERNANDES, 2008a), a recoloring technique specific for anomalous trichromats has never been investigated, and could result in better solutions for these individuals. Now, with the model proposed in Chapter 4, it is possible to simulate the perception of not only dichromats but also anomalous trichromats. Thus, a possible future work consists of image recoloring specifically for anomalous trichromats. The suggestion of recoloring algorithm for anomalous trichromats based on the proposed model consists of the following steps:

1. Conversion of every color $c_i \in C$ to a perceptually uniform color space (*e.g.*, CIE $L^*a^*b^*$), where C is the set of all input colors;
2. analysis of distances between all pairs of colors (c_i, c_j) in the perceptually uniform color space;
3. compute the set of simulated colors s_i using the proposed model;
4. optimization of all pairs of simulated colors (s_i, s_j) aiming to reproduce the original

distances between the pairs (c_i, c_j) constraining the colors to the ones belonging to the gamut of the anomalous trichromat;

5. conversion of the optimized colors back to RGB color space;
6. and compute the final recolored colors r_i by applying the inverse of the simulation matrix to each optimized colors.

The step 4 has been described superficially due to some details that are not yet well defined. Essentially, this step consists of an optimization algorithm and a method to constraint the colors to the gamut of anomalous trichromats in a perceptually uniform color space. A possibility for optimization would be the mass-spring system algorithm which was similarly proposed by Kuhn *et al.* (KUHN; OLIVEIRA; FERNANDES, 2008a). Kuhn *et al.*'s approach is directed for dichromats, therefore they proposed an uni-dimensional optimization and, based on the report of Viénot *et al.* (VIÉNOT; BRETTEL; MOLLON, 1999), approximated the gamut of dichromats to a single plane in CIE $L^*a^*b^*$ color space. For anomalous trichromats the optimization should be at least bi-dimensional and a straightforward method of constraining the colors to the gamut of anomalous trichromats in CIE $L^*a^*b^*$ was not defined yet.

REFERENCES

- ALPERN, M.; WAKE, T. Cone pigments in human deutan colour vision defects. **Journal of Physiology**, [S.l.], v.266, n.3, p.595–612, 1977.
- AYDIN, T. O. et al. Dynamic range independent image quality assessment. In: SIGGRAPH '08: ACM SIGGRAPH 2008 PAPERS. **Anais...** [S.l.: s.n.], 2008. p.1–10.
- BERENDSCHOT, T. T.; KRAATS, J. van de; NORREN, D. van. Foveal cone mosaic and visual pigment density in dichromats. **Journal of Physiology**, [S.l.], v.492.1, p.307–314, 1996.
- BERGMAN, L.; ROGOWITZ, B.; TREINISH, L. A rule-based tool for assisting colormap selection. In: VISUALIZATION '95. **Proceedings...** [S.l.: s.n.], 1995. p.118–125.
- BRAINARD, D. H. **The Psychophysics Toolbox**. 1997.
- BRETTEL, H.; VIÉNOT, F.; MOLLON, J. D. Computerized simulation of color appearance for dichromats. **J. Opt. Soc. Am.**, [S.l.], v.14, n.10, p.2647–2655, 1997.
- BROWN, R. **Photoshop: converting color to black-and-white**. 2006.
- CICERONE, C. M.; NERGER, J. L. The density of cones in the fovea centralis of the human dichromat. **Vision Res.**, [S.l.], v.29, p.1587–1595, 1989.
- DEMARCO, P.; POKORNY, J.; SMITH, V. C. Full-spectrum cone sensitivity functions for X-chromosome-linked anomalous trichromats. **J. Opt. Soc. Am. A**, [S.l.], v.9, n.9, p.1465–1476, 1992.
- DOUGHERTY, R.; WADE, A. **Daltonize**. Accessed on Nov/09, (<http://www.vischeck.com/daltonize>).
- FAIRCHILD, M. D. **Color Appearance Models**. [S.l.]: Addison Wesley, 1997.
- FAIRCHILD, M. D.; WYBLE, D. R. **Colorimetric Characterization of the Apple Studio Display (Flat Panel LCD)**. [S.l.]: Munsell Color Science Laboratory, Center for Imaging Science, Rochester Institute of Technology, 1998. (UCAM-CL-TR-649).
- FARNSWORTH, D. **The Farnsworth-Munsell 100-hue test for the examination of color discrimination**. NY: Munsell Color Company, 1957.
- GOOCH, A. A. et al. Color2Gray: salience-preserving color removal. **ACM Trans. Graph.**, New York, NY, USA, v.24, n.3, p.634–639, 2005.

- GRAHAM, C. H.; HSIA, Y. Studies of Color Blindness: a unilaterally dichromatic subject. **Proc. Natl. Acad. Sci. USA**, [S.l.], v.45, n.1, p.96–99, 1959.
- GRUNDLAND, M.; DODGSON, N. A. Decolorize: fast, contrast enhancing, color to grayscale conversion. **Pattern Recogn.**, New York, NY, USA, v.40, n.11, p.2891–2896, 2007.
- HEALEY, C. G. Choosing effective colours for data visualization. In: IEEE CONFERENCE ON VISUALIZATION, 7. **Proceedings...** [S.l.: s.n.], 1996. p.263–270.
- HUANG, J.-B. et al. Image recolorization for the colorblind. **Acoustics, Speech, and Signal Processing, IEEE International Conference on**, Los Alamitos, CA, USA, v.0, p.1161–1164, 2009.
- HUANG, J.-B.; WU, S.-Y.; CHEN, C.-S. Enhancing Color Representation for the Color Vision Impaired. In: WORKSHOP ON COMPUTER VISION APPLICATIONS FOR THE VISUALLY IMPAIRED, Marseille France. **Anais...** [S.l.: s.n.], 2008.
- IACCARINO, G. et al. Efficient edge-services for colorblind users. In: WWW '06. **Proceedings...** [S.l.: s.n.], 2006. p.919–920.
- ICHIKAWA, M. et al. Web-Page Color Modification for Barrier-Free Color Vision with Genetic Algorithm. **Lecture Notes in Computer Science**, [S.l.], v.2724, p.2134–2146, 2003.
- ICHIKAWA, M. et al. Preliminary study on color modification for still images to realize barrier-free color vision. In: IEEE SMC '06. **Anais...** [S.l.: s.n.], 2004. v.1, p.36–41.
- INGLING JR., C. R.; TSOU, B. H.-P. Orthogonal combination of the three visual channels. **Vision Res.**, [S.l.], v.17, n.9, p.1075–1082, 1977.
- ISHIHARA, S. **Tests for colour-blindness**. [S.l.]: Kanehara Shuppan Co., 1979.
- JEFFERSON, L.; HARVEY, R. Accommodating color blind computer users. In: ASSETS '06. **Proceedings...** [S.l.: s.n.], 2006. p.40–47.
- JESCHKE, E. R. **GIMP**: converting color images to b&w. Accessed in Aug/07, (<http://www.gimp.org/tutorials/Color2BW/>).
- JUDD, D. B. Color perceptions of deuteranopic and protanopic observers. **J. Opt. Soc. Am.**, [S.l.], v.39, n.3, p.252, 1949.
- JUDD, D. B. Response functions for types of vision according to the Müller theory. **J. Res. Natl. Bur. Std.**, [S.l.], v.42, n.1, p.1–16, January 1949.
- JUDD, D. B. Fundamental studies of color vision from 1860 to 1960. **Proc. Natl. Acad. Sci. USA**, [S.l.], v.55, n.6, p.1313–1330, 1966.
- KONDO, S. A Computer Simulation of Anomalous Color Vision. In: COLOR VISION DEFICIENCIES. **Anais...** Kugler & Ghedini, 1990. p.145–159.
- KUHN, G. R.; OLIVEIRA, M. M.; FERNANDES, L. A. F. An Efficient Naturalness-Preserving Image-Recoloring Method for Dichromats. **IEEE Transactions on Visualization and Computer Graphics**, [S.l.], v.14, p.1747–1754, November-December 2008.

- KUHN, G. R.; OLIVEIRA, M. M.; FERNANDES, L. A. F. An improved contrast enhancing approach for color-to-grayscale mappings. **Vis. Comput.**, Secaucus, NJ, USA, v.24, n.7, p.505–514, 2008.
- LEVKOWITZ, H.; HERMAN, G. T. Color Scales for Image Data. **IEEE CG&A**, [S.l.], v.12, n.1, p.72–80, 1992.
- MACHADO, G. M.; OLIVEIRA, M. M. Real-Time Temporal-Coherent Color Contrast Enhancement for Dichromats. **Computer Graphics Forum**, [S.l.], v.29, n.3, p.933–942, June 2010. Proceedings of EuroVis.
- MACHADO, G. M.; OLIVEIRA, M. M.; FERNANDES, L. A. F. A Physiologically-based Model for Simulation of Color Vision Deficiency. **IEEE Transactions on Visualization and Computer Graphics**, [S.l.], v.15, n.6, p.1291–1298, November–December 2009.
- MCINTYRE, D. **Colour Blindness: causes and effects**. [S.l.]: Dalton Publ., 2002.
- MEYER, G. W.; GREENBERG, D. P. Color-defective vision and computer graphics displays. **IEEE Comput. Graph. Appl.**, [S.l.], v.8, n.5, p.28–40, 1988.
- NEITZ, M.; NEITZ, J. Molecular genetics of color vision and color vision defects. **Arch. Ophthalmol.**, [S.l.], v.118, n.3, p.691–700, 2000.
- POKORNY, J.; SMITH, V. C. Evaluation of single-pigment shift model of anomalous trichromacy. **J. Opt. Soc. Am.**, [S.l.], v.67, n.9, p.1196–1209, 1997.
- RASCHE, K.; GEIST, R.; WESTALL, J. Detail Preserving Reproduction of Color Images for Monochromats and Dichromats. **IEEE Comput. Graph. Appl.**, Los Alamitos, CA, USA, v.25, n.3, p.22–30, 2005.
- RASCHE, K.; GEIST, R.; WESTALL, J. Re-coloring Images for Gamuts of Lower Dimension. **Comput. Graph. Forum**, [S.l.], v.24, n.3, p.423–432, 2005.
- RHEINGANS, P. Task-based Color Scale Design. In: SPIE-INT. SOC. OPT. ENG. **Anais...** [S.l.: s.n.], 2000. v.3905, p.33–43.
- RIGDEN, C. The Eye of the Beholder - Designing for Colour-Blind Users. **Br Telecomm Eng**, [S.l.], v.17, 1999.
- RUSHTON, W. A. H. A cone pigment in the protanope. **Journal of Physiology**, [S.l.], v.168, n.2, p.345–359, September 1963.
- SHARPE, L. T. et al. **Color Vision: from genes to perception**. [S.l.]: Cambridge University Press, 1999. p.3–51.
- SLOAN, L. L.; WOLLACH, L. Case of unilateral deuteranopia. **J. Opt. Soc. Am.**, [S.l.], v.38, n.6, p.502, 1948.
- SMITH, V.; POKORNY, J. Spectral sensitivity of the foveal cone photopigments between 400 and 500 nm. **Vision Res.**, [S.l.], v.15, n.2, p.161–171, 1975.

VIÉNOT, F.; BRETTEL, H.; MOLLON, J. D. Digital Video Colourmaps for Checking the Legibility of Displays by Dichromats. **Color Research and Application**, [S.l.], v.24, p.243–252, 1999.

VOS, J. J.; WALRAVEN, P. L. On the derivation of the foveal receptor primaries. **Vision Res.**, [S.l.], v.11, n.8, p.799–818, 1971.

WAKITA, K.; SHIMAMURA, K. SmartColor: disambiguation framework for the color-blind. In: ASSETS '05. **Proceedings...** [S.l.: s.n.], 2005. p.158–165.

WARE, C. Color Sequences for Univariate Maps: theory, experiments and principles. **IEEE C&GA**, [S.l.], v.8, n.5, p.41–49, 1988.

WESNER, M. F. et al. Foveal cone detection statistics in color-normals and dichromats. **Vision Res.**, [S.l.], v.31, n.6, p.1021–1037, 1991.

WIKIMEDIA COMMONS. **Free media repository**. Accessed on Sep/2010, (<http://commons.wikimedia.org>).

WYSZECKI, G.; STILES, W. S. **Color Science**: concepts and methods, quantitative data and formulae. 2nd.ed. [S.l.]: John Wiley and Sons, 2000.

YANG, S. et al. Quantification and standardized description of color vision deficiency caused by anomalous trichromats - Part I: simulation and measurement. **EURASIP Journal on Image and Video Processing**, New York, NY, United States, v.2008, n.1, 2008.

APPENDIX A PRE-COMPUTED MATRICES FOR SIMULATION OF CVD

According to the model presented in this thesis the simulation of the perception of individuals with CVD is given by a single matrix multiplication Φ_{CVD} as in Equation A.1 below. The RGB vector on the right represents the reference RGB color, which is multiplied by the matrix Φ_{CVD} to compute the simulated color $R_s G_s B_s$.

$$\begin{bmatrix} R_s \\ G_s \\ B_s \end{bmatrix} = \Phi_{CVD} \begin{bmatrix} R \\ G \\ B \end{bmatrix} \quad (\text{A.1})$$

This matrix can be computed for all severities of protanomaly, deuteranomaly, and tritanomaly. Aiming efficiency, one can pre-compute the matrices for many severities and use them in the application allowing to switching between many severities and types of CVDs. Table A.1 contains a set of pre-computed matrices for severities in the range $[0.0, 1.0]$ where 1.0 represents the highest severity or a case of dichromacy, and 0.0 represents absence of CVD (identity matrix).

The matrices in Table A.1 were computed for severities growing with a step of 0.1. If you want to simulate colors with higher precision severities values, for example, a severity of 0.873, you can use the model in the article to compute the specified matrix. This is the most accurate approach, but it is also possible to interpolate between the two matrices with nearest severities. For example, to compute the matrix for a case of severity 0.873, the matrices 0.8 and 0.9 can be interpolated with a weight of 0.73. This approach is a fast approximation and also very accurate for a set of pre-computed matrices with severity step of 0.1.

Table A.1: Simulation matrices Φ_{CVD}

Severity	Protonomaly	Deuteranomaly	Tritanomaly
0.0	$\begin{bmatrix} 1.000 & 0.000 & 0.000 \\ 0.000 & 1.000 & 0.000 \\ 0.000 & 0.000 & 1.000 \end{bmatrix}$	$\begin{bmatrix} 1.000 & 0.000 & 0.000 \\ 0.000 & 1.000 & 0.000 \\ 0.000 & 0.000 & 1.000 \end{bmatrix}$	$\begin{bmatrix} 1.000 & 0.000 & 0.000 \\ 0.000 & 1.000 & 0.000 \\ 0.000 & 0.000 & 1.000 \end{bmatrix}$
0.1	$\begin{bmatrix} 0.856 & 0.182 & -0.038 \\ 0.029 & 0.955 & 0.016 \\ -0.003 & -0.002 & 1.004 \end{bmatrix}$	$\begin{bmatrix} 0.866 & 0.178 & -0.044 \\ 0.050 & 0.939 & 0.011 \\ -0.003 & 0.007 & 0.996 \end{bmatrix}$	$\begin{bmatrix} 0.927 & 0.093 & -0.019 \\ 0.021 & 0.965 & 0.014 \\ 0.008 & 0.055 & 0.937 \end{bmatrix}$
0.2	$\begin{bmatrix} 0.735 & 0.335 & -0.070 \\ 0.052 & 0.919 & 0.029 \\ -0.005 & -0.004 & 1.009 \end{bmatrix}$	$\begin{bmatrix} 0.761 & 0.319 & -0.080 \\ 0.091 & 0.889 & 0.020 \\ -0.006 & 0.013 & 0.993 \end{bmatrix}$	$\begin{bmatrix} 0.896 & 0.133 & -0.029 \\ 0.030 & 0.945 & 0.025 \\ 0.013 & 0.105 & 0.882 \end{bmatrix}$
0.3	$\begin{bmatrix} 0.630 & 0.466 & -0.096 \\ 0.069 & 0.890 & 0.041 \\ -0.006 & -0.008 & 1.014 \end{bmatrix}$	$\begin{bmatrix} 0.675 & 0.434 & -0.109 \\ 0.125 & 0.848 & 0.027 \\ -0.008 & 0.019 & 0.989 \end{bmatrix}$	$\begin{bmatrix} 0.906 & 0.128 & -0.034 \\ 0.027 & 0.941 & 0.032 \\ 0.013 & 0.148 & 0.838 \end{bmatrix}$
0.4	$\begin{bmatrix} 0.539 & 0.579 & -0.118 \\ 0.083 & 0.866 & 0.051 \\ -0.007 & -0.012 & 1.019 \end{bmatrix}$	$\begin{bmatrix} 0.606 & 0.529 & -0.134 \\ 0.155 & 0.812 & 0.032 \\ -0.009 & 0.023 & 0.986 \end{bmatrix}$	$\begin{bmatrix} 0.948 & 0.089 & -0.038 \\ 0.014 & 0.947 & 0.039 \\ 0.011 & 0.194 & 0.795 \end{bmatrix}$
0.5	$\begin{bmatrix} 0.458 & 0.680 & -0.138 \\ 0.093 & 0.846 & 0.061 \\ -0.007 & -0.017 & 1.024 \end{bmatrix}$	$\begin{bmatrix} 0.547 & 0.608 & -0.155 \\ 0.182 & 0.782 & 0.037 \\ -0.010 & 0.027 & 0.983 \end{bmatrix}$	$\begin{bmatrix} 1.017 & 0.027 & -0.044 \\ -0.006 & 0.958 & 0.048 \\ 0.006 & 0.249 & 0.745 \end{bmatrix}$
0.6	$\begin{bmatrix} 0.385 & 0.769 & -0.154 \\ 0.101 & 0.830 & 0.070 \\ -0.007 & -0.022 & 1.030 \end{bmatrix}$	$\begin{bmatrix} 0.499 & 0.675 & -0.174 \\ 0.205 & 0.755 & 0.040 \\ -0.011 & 0.031 & 0.980 \end{bmatrix}$	$\begin{bmatrix} 1.105 & -0.047 & -0.058 \\ -0.032 & 0.972 & 0.061 \\ 0.001 & 0.318 & 0.681 \end{bmatrix}$
0.7	$\begin{bmatrix} 0.320 & 0.850 & -0.169 \\ 0.106 & 0.816 & 0.078 \\ -0.007 & -0.028 & 1.035 \end{bmatrix}$	$\begin{bmatrix} 0.458 & 0.732 & -0.190 \\ 0.226 & 0.731 & 0.043 \\ -0.012 & 0.034 & 0.977 \end{bmatrix}$	$\begin{bmatrix} 1.193 & -0.110 & -0.083 \\ -0.058 & 0.979 & 0.079 \\ -0.002 & 0.403 & 0.599 \end{bmatrix}$
0.8	$\begin{bmatrix} 0.259 & 0.923 & -0.182 \\ 0.110 & 0.804 & 0.085 \\ -0.006 & -0.034 & 1.041 \end{bmatrix}$	$\begin{bmatrix} 0.423 & 0.781 & -0.204 \\ 0.246 & 0.710 & 0.045 \\ -0.012 & 0.037 & 0.974 \end{bmatrix}$	$\begin{bmatrix} 1.258 & -0.140 & -0.118 \\ -0.078 & 0.975 & 0.103 \\ -0.003 & 0.501 & 0.502 \end{bmatrix}$
0.9	$\begin{bmatrix} 0.204 & 0.990 & -0.194 \\ 0.113 & 0.795 & 0.092 \\ -0.005 & -0.041 & 1.046 \end{bmatrix}$	$\begin{bmatrix} 0.393 & 0.824 & -0.217 \\ 0.264 & 0.690 & 0.046 \\ -0.012 & 0.040 & 0.972 \end{bmatrix}$	$\begin{bmatrix} 1.279 & -0.125 & -0.154 \\ -0.085 & 0.958 & 0.127 \\ -0.001 & 0.601 & 0.400 \end{bmatrix}$
1.0	$\begin{bmatrix} 0.152 & 1.053 & -0.205 \\ 0.115 & 0.786 & 0.099 \\ -0.004 & -0.048 & 1.052 \end{bmatrix}$	$\begin{bmatrix} 0.367 & 0.861 & -0.228 \\ 0.280 & 0.673 & 0.047 \\ -0.012 & 0.043 & 0.969 \end{bmatrix}$	$\begin{bmatrix} 1.256 & -0.077 & -0.179 \\ -0.078 & 0.931 & 0.148 \\ 0.005 & 0.691 & 0.304 \end{bmatrix}$

APPENDIX B EXPERIMENTAL DATA

The model for simulating the perception of individuals with CVD presented in this thesis uses as resource data the spectral power distribution (SPD) of an typical CRT monitor (Table B.1) and the spectral sensitivity functions of cone cells of individuals with normal color vision (Table B.2). Such data were obtained with the Psychtoolbox (BRAINARD, 1997) which is a set of data and functions for vision research. The data for cone cells sensitivity functions refers to the data reported after Smith and Pokorny (SMITH; POKORNY, 1975) and were used to simulate CVD as explained in Chapter 4.

Table B.1: SPD of a typical CRT display (BRAINARD, 1997).

Wavelength	Red	Green	Blue	Wavelength	Red	Green	Blue
380	0.0025	0.0018	0.0219	585	0.1220	0.1769	0.0051
385	0.0017	0.0016	0.0336	590	0.1861	0.1407	0.0047
390	0.0017	0.0020	0.0524	595	0.2173	0.1155	0.0043
395	0.0011	0.0021	0.0785	600	0.0777	0.0938	0.0029
400	0.0017	0.0025	0.1130	605	0.0531	0.0759	0.0023
405	0.0028	0.0030	0.1624	610	0.2434	0.0614	0.0036
410	0.0037	0.0043	0.2312	615	0.5812	0.0522	0.0061
415	0.0046	0.0059	0.3214	620	0.9354	0.0455	0.0088
420	0.0064	0.0079	0.4263	625	1.6054	0.0437	0.0141
425	0.0079	0.0104	0.5365	630	0.6464	0.0278	0.0060
430	0.0094	0.0126	0.6296	635	0.1100	0.0180	0.0015
435	0.0105	0.0147	0.6994	640	0.0322	0.0136	0.0008
440	0.0113	0.0170	0.7470	645	0.0207	0.0107	0.0006
445	0.0115	0.0191	0.7654	650	0.0194	0.0085	0.0006
450	0.0113	0.0220	0.7519	655	0.0196	0.0067	0.0007
455	0.0113	0.0267	0.7151	660	0.0166	0.0055	0.0006
460	0.0115	0.0340	0.6619	665	0.0173	0.0044	0.0005
465	0.0164	0.0462	0.5955	670	0.0220	0.0039	0.0006
470	0.0162	0.0649	0.5177	675	0.0186	0.0033	0.0005
475	0.0120	0.0936	0.4327	680	0.0377	0.0030	0.0007
480	0.0091	0.1345	0.3507	685	0.0782	0.0028	0.0010
485	0.0119	0.1862	0.2849	690	0.0642	0.0023	0.0010
490	0.0174	0.2485	0.2278	695	0.1214	0.0028	0.0016
495	0.0218	0.3190	0.1809	700	0.7169	0.0078	0.0060
500	0.0130	0.3964	0.1408	705	1.1098	0.0113	0.0094
505	0.0123	0.4691	0.1084	710	0.3106	0.0039	0.0030
510	0.0260	0.5305	0.0855	715	0.0241	0.0011	0.0007
515	0.0242	0.5826	0.0676	720	0.0180	0.0009	0.0009
520	0.0125	0.6195	0.0537	725	0.0149	0.0008	0.0008
525	0.0119	0.6386	0.0422	730	0.0108	0.0009	0.0011
530	0.0201	0.6414	0.0341	735	0.0097	0.0011	0.0010
535	0.0596	0.6348	0.0284	740	0.0091	0.0009	0.0010
540	0.0647	0.6189	0.0238	745	0.0093	0.0010	0.0012
545	0.0251	0.5932	0.0197	750	0.0083	0.0011	0.0013
550	0.0248	0.5562	0.0165	755	0.0073	0.0013	0.0012
555	0.0325	0.5143	0.0143	760	0.0081	0.0015	0.0016
560	0.0199	0.4606	0.0119	765	0.0067	0.0018	0.0015
565	0.0161	0.3993	0.0099	770	0.0070	0.0021	0.0028
570	0.0128	0.3297	0.0079	775	0.0073	0.0015	0.0046
575	0.0217	0.2719	0.0065	780	0.0066	0.0018	0.0058
580	0.0693	0.2214	0.0057				

Table B.2: Spectral sensitivity functions of cone types concerning normal trichromats (after Smith and Pokorny (SMITH; POKORNY, 1975)).

Wavelength	L Cone	M Cone	S Cone	Wavelength	L Cone	M Cone	S Cone
380	0.0000	0.0000	0.0000	585	0.9340	0.5640	0.0010
385	0.0000	0.0000	0.0000	590	0.8940	0.4770	0.0008
390	0.0000	0.0000	0.0000	595	0.8480	0.3930	0.0007
395	0.0000	0.0000	0.0000	600	0.7950	0.3180	0.0006
400	0.0027	0.0028	0.1080	605	0.7350	0.2500	0.0005
405	0.0044	0.0047	0.1790	610	0.6700	0.1930	0.0003
410	0.0069	0.0077	0.2850	615	0.6020	0.1470	0.0002
415	0.0108	0.0124	0.4530	620	0.5300	0.1100	0.0002
420	0.0158	0.0189	0.6590	625	0.4540	0.0808	0.0001
425	0.0200	0.0254	0.8130	630	0.3800	0.0583	0.0001
430	0.0233	0.0317	0.9080	635	0.3150	0.0418	0.0001
435	0.0268	0.0395	0.9770	640	0.2560	0.0296	0.0001
440	0.0301	0.0477	1.0000	645	0.2040	0.0207	0.0000
445	0.0324	0.0555	0.9700	650	0.1590	0.0144	0.0000
450	0.0343	0.0635	0.9100	655	0.1220	0.0101	0.0000
455	0.0368	0.0731	0.8500	660	0.0914	0.0070	0.0000
460	0.0412	0.0860	0.7990	665	0.0670	0.0049	0.0000
465	0.0502	0.1070	0.7750	670	0.0482	0.0033	0.0000
470	0.0627	0.1300	0.6890	675	0.0350	0.0023	0.0000
475	0.0798	0.1570	0.5820	680	0.0257	0.0016	0.0000
480	0.1020	0.1890	0.4680	685	0.0180	0.0011	0.0000
485	0.1280	0.2240	0.3620	690	0.0124	0.0008	0.0000
490	0.1620	0.2670	0.2760	695	0.0087	0.0005	0.0000
495	0.2060	0.3240	0.2120	700	0.0062	0.0004	0.0000
500	0.2630	0.3960	0.1640	705	0.0000	0.0000	0.0000
505	0.3370	0.4910	0.1280	710	0.0000	0.0000	0.0000
510	0.4230	0.5950	0.0956	715	0.0000	0.0000	0.0000
515	0.5200	0.7060	0.0676	720	0.0000	0.0000	0.0000
520	0.6170	0.8080	0.0474	725	0.0000	0.0000	0.0000
525	0.7000	0.8840	0.0347	730	0.0000	0.0000	0.0000
530	0.7730	0.9410	0.0256	735	0.0000	0.0000	0.0000
535	0.8340	0.9780	0.0182	740	0.0000	0.0000	0.0000
540	0.8830	0.9970	0.0124	745	0.0000	0.0000	0.0000
545	0.9230	0.9990	0.0083	750	0.0000	0.0000	0.0000
550	0.9540	0.9870	0.0055	755	0.0000	0.0000	0.0000
555	0.9770	0.9610	0.0037	760	0.0000	0.0000	0.0000
560	0.9930	0.9220	0.0025	765	0.0000	0.0000	0.0000
565	1.0000	0.8700	0.0018	770	0.0000	0.0000	0.0000
570	0.9970	0.8060	0.0014	775	0.0000	0.0000	0.0000
575	0.9860	0.7320	0.0013	780	0.0000	0.0000	0.0000
580	0.9650	0.6510	0.0012				

APPENDIX C SIMULATION OF CVD USING SPD OF AN LCD

Although spectral power distributions (SPD) of different models and types of displays vary, RGB colors representations are approximately equivalent between them. But there are small variations which can interfere in the results of the technique for simulation presented in this thesis. Figure C.1 (left) illustrates the SPD of an typical CRT monitor. Such SPD was used as resource for the development of the proposed technique. Figure C.1 (right) illustrates an example of SPD for an LCD (FAIRCHILD; WYBLE, 1998). Note the differences between both graphics. Resource data regarding the LCD is available in Table C.1.

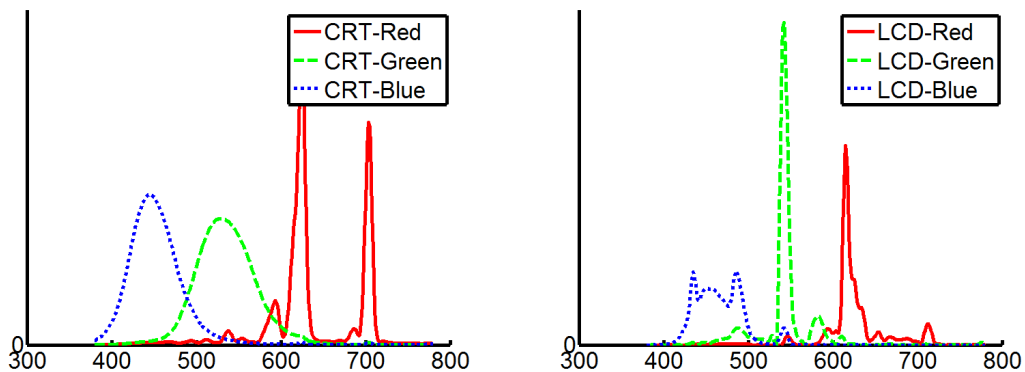


Figure C.1: Illustration of monitors' SPDs. (left) SPD of a typical CRT monitor (BRAINARD, 1997). (right) SPD of an LCD according to Fairchild (FAIRCHILD; WYBLE, 1998).

The results obtained when using the proposed model (Chapter 4) with the SPD data for the LCD presents small variations to the ones based on the CRT data. But Equations 4.22 and 4.23 present a scaling factor of 0.96 which consists of an adjustment to the resource data used. These different SPDs result in approximately the same simulated result, as can be seen in Figure C.2. A new scaling factor of 0.94 for the LCD replaces the 0.96 factor used for the CRT (Figure C.2 center column).

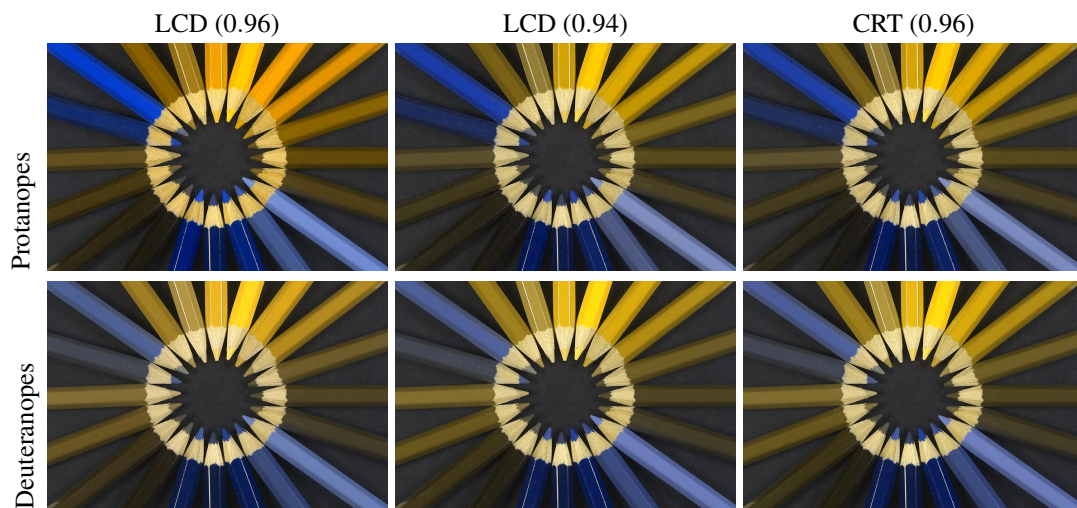


Figure C.2: Illustration comparing the results of the technique's implementations with different SPDs. (left column) Simulation for an LCD using the 0.96 scaling factor. (center column) Simulation for an LCD using the 0.94 scaling factor. (right column) result from the original implementation based on the CRT's SPD.

Table C.1: SPD of a LCD monitor (Fairchild (FAIRCHILD; WYBLE, 1998)).

Wavelength	Red	Green	Blue	Wavelength	Red	Green	Blue
380	0.0000	0.0000	0.0000	585	0.0198	0.1468	0.0000
385	0.0000	0.0000	0.0000	590	0.0635	0.0754	0.0000
390	0.0000	0.0000	0.0000	595	0.0873	0.0357	0.0000
395	0.0000	0.0000	0.0000	600	0.0635	0.0159	0.0000
400	0.0000	0.0000	0.0040	605	0.0714	0.0040	0.0000
405	0.0000	0.0000	0.0040	610	0.2619	0.0476	0.0000
410	0.0000	0.0000	0.0079	615	1.0714	0.0159	0.0000
415	0.0000	0.0000	0.0238	620	0.4881	0.0040	0.0000
420	0.0000	0.0000	0.0516	625	0.3532	0.0040	0.0000
425	0.0000	0.0000	0.0992	630	0.2103	0.0000	0.0000
430	0.0000	0.0040	0.1865	635	0.1944	0.0000	0.0000
435	0.0000	0.0119	0.3929	640	0.0556	0.0000	0.0000
440	0.0040	0.0000	0.2540	645	0.0238	0.0000	0.0000
445	0.0040	0.0119	0.2738	650	0.0476	0.0000	0.0000
450	0.0000	0.0119	0.3016	655	0.0675	0.0000	0.0000
455	0.0040	0.0079	0.3016	660	0.0238	0.0000	0.0000
460	0.0000	0.0198	0.2976	665	0.0397	0.0040	0.0000
465	0.0040	0.0238	0.2698	670	0.0397	0.0040	0.0000
470	0.0040	0.0317	0.2460	675	0.0278	0.0000	0.0000
475	0.0040	0.0357	0.2103	680	0.0278	0.0000	0.0000
480	0.0040	0.0516	0.2460	685	0.0317	0.0000	0.0000
485	0.0040	0.0873	0.3929	690	0.0317	0.0000	0.0000
490	0.0040	0.0873	0.3333	695	0.0198	0.0000	0.0000
495	0.0040	0.0675	0.2024	700	0.0159	0.0000	0.0000
500	0.0040	0.0437	0.0913	705	0.0119	0.0000	0.0000
505	0.0000	0.0357	0.0437	710	0.0952	0.0040	0.0000
510	0.0000	0.0317	0.0238	715	0.0952	0.0000	0.0000
515	0.0000	0.0317	0.0119	720	0.0159	0.0000	0.0000
520	0.0000	0.0238	0.0079	725	0.0040	0.0000	0.0000
525	0.0000	0.0238	0.0040	730	0.0000	0.0000	0.0000
530	0.0000	0.0317	0.0040	735	0.0000	0.0000	0.0000
535	0.0000	0.1944	0.0159	740	0.0000	0.0000	0.0000
540	0.0000	1.5794	0.0794	745	0.0000	0.0000	0.0000
545	0.0437	1.4048	0.0754	750	0.0000	0.0000	0.0000
550	0.0317	0.4127	0.0079	755	0.0000	0.0000	0.0000
555	0.0040	0.0952	0.0040	760	0.0000	0.0000	0.0000
560	0.0000	0.0317	0.0000	765	0.0000	0.0000	0.0000
565	0.0000	0.0159	0.0000	770	0.0000	0.0000	0.0000
570	0.0000	0.0079	0.0000	775	0.0000	0.0119	0.0000
575	0.0000	0.0952	0.0000	780	0.0000	0.0000	0.0000
580	0.0040	0.1429	0.0000				

APPENDIX D UM MODELO PARA SIMULAÇÃO DAS DEFICIÊNCIAS NA PERCEPÇÃO DE CORES E UMA TÉCNICA DE AUMENTO DO CONTRASTE DE CORES PARA DICROMÁTAS

Resumo da Dissertação em Português

As Deficiências na Percepção de Cores (DPC) afetam cerca de 200.000.000 (duzentos milhões) de pessoas em todo o mundo, provocando dificuldade ou incapacidade de distinção entre determinadas cores, o que impacta suas vidas pessoais e profissionais. A Figura D.1 ilustra um exemplo de problema enfrentado por estes indivíduos. A imagem à esquerda consiste de um mapa ilustrando o crescimento populacional da Europa no ano de 2006, enquanto a imagem à direita mostra a simulação da percepção do mapa da esquerda por indivíduos com deuteranopia¹. Note como a DPC pode afetar a capacidade destes indivíduos identificarem dados em ilustrações simples. Neste caso, deuteranopos apresentariam dificuldades para distinguir entre as cores que representam crescimento e redução populacional de até 0.5%. Este exemplo demonstra uma situação recorrente em trabalhos de visualização de informação e visualização científica.

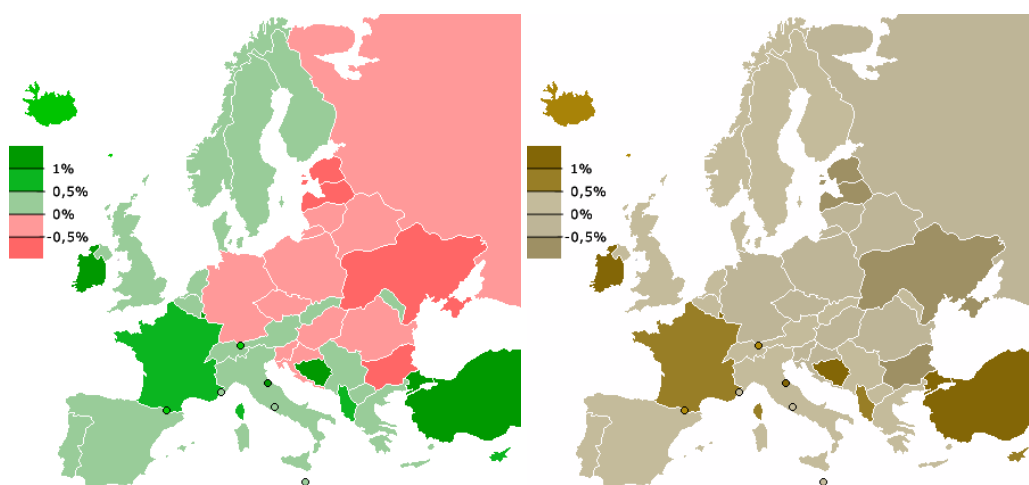


Figure D.1: (esquerda) um mapa da Europa em que cores foram usadas para codificar o percentual de alteração populacional de diferentes países no ano de 2006. (direita) simulação da percepção da imagem à esquerda por indivíduos com deuteranopia.

¹ Deuteranopia é um tipo de DPC caracterizado pela ausência de cones do tipo *M* na retina.

Os cones são as células fotoreceptoras responsáveis pela percepção de cores. Na retina humana existem três tipos de cones, que são chamados de *L*, *M* e *S*, devido às suas sensibilidades às regiões do espectro com comprimentos de onda longos (*Long*), médios (*Medium*) e curtos (*Short*), respectivamente. Portanto, a visão de cores normal é chamada de *tricromática normal*. As sensibilidades espectrais dos cones são determinadas pelas propriedades dos fotopigmentos contidos. As deficiências na percepção de cores são causadas por anomalias nesta configuração e são classificadas em *tricromacia anômala*, *dicromacia* e *monocromacia*. A tricromacia anômala é caracterizada pela presença de três tipos de fotopigmentos na retina, sendo um desses anômalo, e é ainda classificada em protanomia, deuteranomalia e tritanomia, dependendo se o fotopigmento anômalo refere-se ao cone do tipo *L*, *M* ou *S*, respectivamente. Já os casos de dicromacia se caracterizam pela presença de apenas dois tipos de fotopigmentos na retina e são classificados em protanopia, deuteranopia e tritanopia, caso o fotopigmento ausente seja referente aos cones do tipo *L*, *M* ou *S*, respectivamente. A monocromacia consiste de um caso extremamente raro e se caracteriza pela ausência de qualquer tipo ou a presença de apenas um tipo de fotopigmento na retina. As DPC *red-green* (vermelho-verde em inglês), englobam os seguintes tipos: protanopia, protanomalia, deuteranopia e deuteranomalia. Juntos estes tipos representam cerca de 99,96% dos casos de DPC, cujas causas envolvem fatores hereditários relacionados a genes recessivos localizados no cromossomo X. Por consistirem de seqüências genéticas neste cromossomo sem alelos no cromossomo Y, as DPC *red-green* são mais incidentes entre os homens (ca. 7,9%) do que entre as mulheres (ca. 0,42%). A Tabela D.1 demonstra a incidência dos diversos tipos de DPC na população Caucasiana. Acredita-se que os demais tipos de DPC podem ser adquiridos por acidentes neurológicos.

Tipo de DPC	Incidência (%)	
	Homens	Mulheres
Tricromacia anômala	5,71	0,39
Protanomia	1,08	0,03
Deuteranomalia	4,63	0,36
Tritanomalia	0,0001	0,0001
Dicromacia	2,28	0,03
Protanopia	1,01	0,02
Deuteranopia	1,27	0,01
Tritanopia	0,002	0,001
Monocromacia	0,003	0,00001

Table D.1: Incidência dos tipos de DPC na população Caucasiana (RIGDEN, 1999; SHARPE et al., 1999).

Os trabalhos mais relevantes voltados para indivíduos com DPC se classificam em *técnicas de simulação* e *técnicas de recoloração*. As técnicas de simulação visam apresentar a percepção de indivíduos com DPC para indivíduos tricromatas normais². Tais técnicas fornecem um entendimento sobre como as dificuldades em tarefas relacionadas com cores são vivenciadas por estes indivíduos. Além disto, permite o estudo de melhorias em trabalhos (e.g., de designers, de visualização científica ou de visualização de informação) visando ampliar seus públicos. Já os trabalhos de recoloração têm como objetivo

²Tricromacia normal refere-se a visão de cores normal, ou seja, que não apresenta nenhum tipo de DPC.

realçar os contrastes em imagens para que as características destas sejam percebidas pelos indivíduos com DPC. Por exemplo, algumas imagens de visualização podem apresentar perda de informações dependendo da percepção destes indivíduos. As técnicas de recoloração deveriam recuperar estas informações de forma automática, atribuindo autonomia em situações muitas vezes constrangedoras para estes indivíduos.

Este trabalho apresenta um modelo baseado na fisiologia para simular a percepção de indivíduos com DPC. As técnicas anteriores só foram capazes de simular efetivamente a percepção de indivíduos com dicromacia, o que representa cerca de 27,46% dos casos de DPC. Este modelo, além de simular a percepção de dicromatas, possibilitou também a simulação da percepção de tricromatas anômalos, que representam cerca de 72,50% dos casos de DPC. Com isto, tem-se uma técnica que, baseada no mesmo modelo, simula a percepção de cerca de 99,96% de todos os casos de DPC.

Além disto, este trabalho apresenta uma técnica de recoloração em tempo-real que também permite coerência temporal. A implementação em GPU do algoritmo proposto permitiu recoloração de alta qualidade com eficiência de até duas ordens de magnitude mais rápida do que as técnicas anteriores, que não eram capazes de recolorir em tempo-real. Com isto, tem-se de forma inédita uma técnica capaz de recolorir vídeos e telas de aplicações interativas. Além disto, visando evitar *flickering*, esta técnica fornece uma abordagem que permite coerência temporal.

D.1 O Modelo para Simulação da Percepção de Cores

A teoria mais aceita para explicar a percepção de cores pelos humanos é chamada de *teoria dos estágios*. Esta é capaz de explicar e prever diversos fenômenos importantes da visão de cores, como, por exemplo, equiparação de cores, discriminação de cores, aparência de cores, adaptação cromática, entre outros, referentes tanto a observadores tricromáticos normais quanto a indivíduos com DPC (WYSZECKI; STILES, 2000). De acordo com esta teoria, os estímulos visuais, captados pelos cones, resultam em sinais que são posteriormente processados em estágios subseqüentes. Esta combinação leva à percepção de cores, em determinados estágios, através de canais oponentes, sendo um canal de luminância (WS) e dois de crominância (YB para amarelo-azul e RG para vermelho-verde). Esta teoria fornece o melhor modelo da visão de cores nos humanos, e uma discussão acerca de algumas variações desta pode ser encontrada em (JUDD, 1966).

Este trabalho propõe um modelo que se baseia na teoria dos estágios e, portanto, envolve uma transformação de sensibilidade espectral das células fotoreceptoras (L , M e S) para funções referentes aos canais oponentes (WS , YB e RG). Os coeficientes desta transformação não são facilmente obtidos, mas, felizmente, Ingling e Tsou (INGLING JR.; TSOU, 1977) forneceram tais dados. A forma *suprathreshold* da transformação apresenta vantagens sobre a *threshold*, pois tenta considerar resultados de estudos psicofísicos e eletrofisiológicos considerando a adaptação à luz. A Equação D.1 descreve a transformação na forma *suprathreshold* proposta por Ingling e Tsou:

$$\begin{bmatrix} V_\lambda \\ y - b \\ r - g \end{bmatrix} = \begin{bmatrix} 0.600 & 0.400 & 0.000 \\ 0.240 & 0.105 & -0.700 \\ 1.200 & -1.600 & 0.400 \end{bmatrix} \begin{bmatrix} L \\ M \\ S \end{bmatrix} \quad (D.1)$$

onde V_λ representa o canal de luminância WS , enquanto $r - g$ e $y - b$ representam os dois canais oponentes de crominância RG e YB , respectivamente. A Figura D.2 ilustra graficamente a transformação apresentada. À esquerda, três curvas ilustrando as funções de

sensibilidade espectrais dos três tipos de cones relativos à indivíduos tricromatas normais e, à direita, três curvas resultantes da transformação das curvas à esquerda de acordo com a Equação D.1 proposta por Ingling e Tsou.

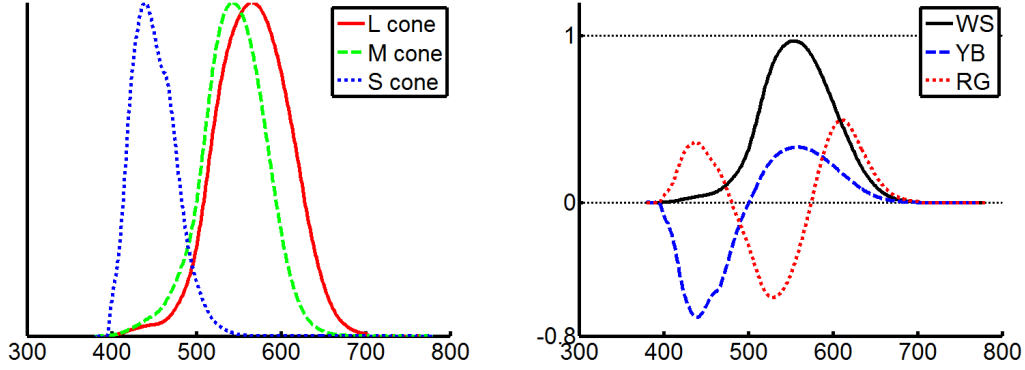


Figure D.2: (esquerda) funções de sensibilidade espectrais dos cones referentes a indivíduos tricromatas normais (após Smith e Pokorny (SMITH; POKORNY, 1975)). (direita) funções de resposta espectrais dos canais oponentes de acordo com modelo *suprathreshold* proposto por Ingling e Tsou (INGLING JR.; TSOU, 1977) assumindo como base os dados das curvas à esquerda.

O modelo proposto neste trabalho simula as deficiências na percepção de cores como alterações na absorção espectral dos fotopigmentos dos cones. Embora, para isto, a modelagem se dê essencialmente no estágio retinal dos fotoreceptores, o estágio oponente é crucial para produzir os resultados corretos e não pode ser subestimado. Portanto, o modelo proposto usa a equação do modelo de Ingling e Tsou, cuja transformação de LMS para espaço oponente é representada pela matriz 3×3 mostrada na Equação D.1, que será referenciada como T_{LMS_2Opp} . Portanto, assume-se que as conexões neurais que ligam as próprias células fotoreceptoras ao resto do sistema visual não são afetadas pelas DPC. Logo, o modelo proposto usa a transformação T_{LMS_2Opp} para obter as funções de resposta espectrais dos canais oponentes, como mostrado nas seguintes equações:

$$\begin{bmatrix} WS(\lambda) \\ YB(\lambda) \\ RG(\lambda) \end{bmatrix}_p = T_{LMS_2Opp} \begin{bmatrix} L_a(\lambda) \\ M(\lambda) \\ S(\lambda) \end{bmatrix} \quad (D.2)$$

$$\begin{bmatrix} WS(\lambda) \\ YB(\lambda) \\ RG(\lambda) \end{bmatrix}_d = T_{LMS_2Opp} \begin{bmatrix} L(\lambda) \\ M_a(\lambda) \\ S(\lambda) \end{bmatrix} \quad (D.3)$$

$$\begin{bmatrix} WS(\lambda) \\ YB(\lambda) \\ RG(\lambda) \end{bmatrix}_t = T_{LMS_2Opp} \begin{bmatrix} L(\lambda) \\ M(\lambda) \\ S_a(\lambda) \end{bmatrix} \quad (D.4)$$

Onde $L(\lambda)$, $M(\lambda)$ e $S(\lambda)$ são as funções de sensibilidade espectrais dos cones normais e $L_a(\lambda)$, $M_a(\lambda)$ e $S_a(\lambda)$ são as simulações das funções de sensibilidade espectrais dos cones anômalos. Nestas equações, p se refere a protanopia e protanomalia, d se refere a deuteranopia e deuteranomalia, e t se refere a tritanopia e tritanomia. Note que a transformação referente à tricromacia normal está representada na Equação D.1.

Uma transformação do espaço de cores RGB para um espaço de cores oponentes é obtida simplesmente ao projetar-se as distribuições de emissões espectrais $\varphi_R(\lambda)$, $\varphi_G(\lambda)$ e $\varphi_B(\lambda)$ das primárias RGB no conjunto de funções base $WS(\lambda)$, $YB(\lambda)$ e $RG(\lambda)$ que definem o espaço de cores oponentes, como mostrado na Equação D.5. Ao usar o conjunto apropriado de funções base, a Equação D.5 transforma triplas RGB em cores oponentes referentes a tricromacia normal, tricromacia anômala e dicromacia.

$$\begin{aligned}
 WS_R &= \rho_{WS} \int \varphi_R(\lambda) WS(\lambda) d\lambda, \\
 WS_G &= \rho_{WS} \int \varphi_G(\lambda) WS(\lambda) d\lambda, \\
 WS_B &= \rho_{WS} \int \varphi_B(\lambda) WS(\lambda) d\lambda, \\
 YB_R &= \rho_{YB} \int \varphi_R(\lambda) YB(\lambda) d\lambda, \\
 YB_G &= \rho_{YB} \int \varphi_G(\lambda) YB(\lambda) d\lambda, \\
 YB_B &= \rho_{YB} \int \varphi_B(\lambda) YB(\lambda) d\lambda, \\
 RG_R &= \rho_{RG} \int \varphi_R(\lambda) RG(\lambda) d\lambda, \\
 RG_G &= \rho_{RG} \int \varphi_G(\lambda) RG(\lambda) d\lambda, \\
 RG_B &= \rho_{RG} \int \varphi_B(\lambda) RG(\lambda) d\lambda
 \end{aligned} \tag{D.5}$$

Os fatores de normalização ρ_{WS} , ρ_{YB} e ρ_{RG} são escolhidos para satisfazer as restrições na Equação D.6. Elas garantem que as cores acromáticas (tons de cinza) tenham exatamente as mesmas coordenadas variando de (0,0,0) a (1,1,1) em ambos RGB assim como em todas as possíveis versões do espaço de cores oponentes (tricromático normal, todos tricromáticos anômalos e todos dicromáticos). Esta restrição é fundamental para o algoritmo de simulação.

$$\begin{aligned}
 WS_R + WS_G + WS_B &= 1, \\
 YB_R + YB_G + YB_B &= 1, \\
 RG_R + RG_G + RG_B &= 1
 \end{aligned} \tag{D.6}$$

Logo, a classe geral de matrizes de transformação Γ que mapeiam o espaço de cores RGB para as várias instâncias do espaço de cores oponentes podem ser expressas como:

$$\Gamma = \begin{bmatrix} WS_R & WS_G & WS_B \\ YB_R & YB_G & YB_B \\ RG_R & RG_G & RG_B \end{bmatrix} \tag{D.7}$$

Seja Γ_{normal} a matriz que mapeia RGB para o espaço de cores oponentes de um tricromata normal a simulação para um tricromata normal da percepção de cores de um indivíduo com DPC é obtida com a Equação D.8.

$$\begin{bmatrix} R_s \\ G_s \\ B_s \end{bmatrix} = \Gamma_{normal}^{-1} \Gamma \begin{bmatrix} R \\ G \\ B \end{bmatrix} \tag{D.8}$$

Os resultados obtidos com o modelo proposto podem ser observados na Figura D.3. Esta compara o resultado da simulação da percepção de protanômalos e deuteranômalos referente a diversos graus de severidade (expressos em *nm*) com o resultado obtido para protanopos e deuteranopos de acordo com a técnica proposta por Brettel *et al.* (BRETTEL; VIÉNOT; MOLLON, 1997). Os casos severos de tricromacia anômala se equivalem a dicromacia, o que é reproduzido pelos resultados do modelo proposto. A Figura D.3 também compara esses resultados com os obtidos com a técnica proposta por Yang *et*

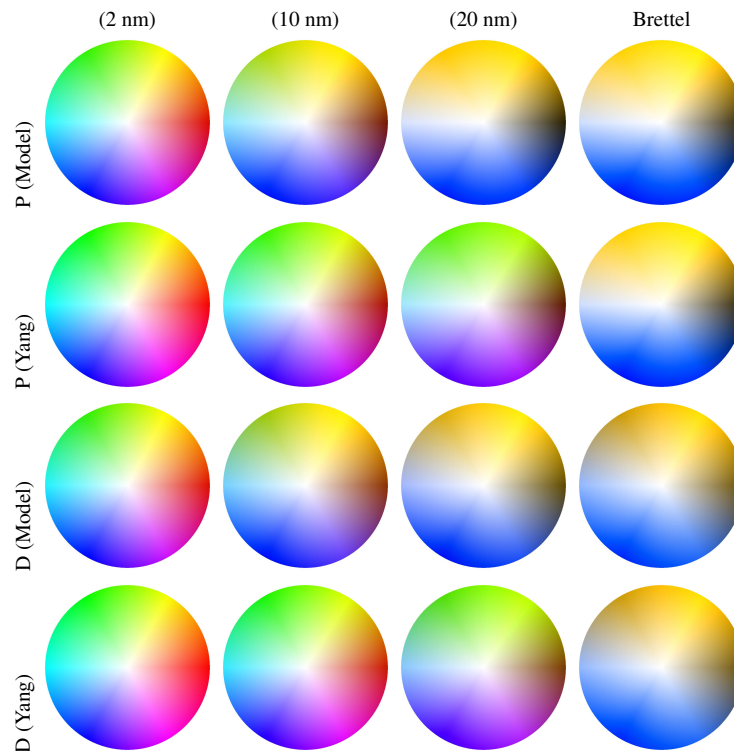


Figure D.3: Simulação da visão de protanômalos e deuteranômalos para diversos graus de severidade (expressos em *nm*). Última coluna: resultado do algoritmo de Brettel *et al.* tido como referência de precisão para casos de dicromacia. *P/D (Model)*: simulações de Protanomia/Deuteranomalia com a técnica proposta. *P/D (Yang)*: simulações de Protanomia/Deuteranomalia com a técnica proposta por Yang *et al.*.

al. (YANG *et al.*, 2008). Note como os resultados do modelo proposto são mais consistentes do que os resultados de Yang *et al.*.

O modelo proposto foi validado através de experimentos envolvendo o teste Farnsworth-Munsell 100-Hue (FM100H) (FARNSWORTH, 1957). Foi implementada uma versão computadorizada do teste para aplicação em indivíduos tricromatas normais e indivíduos com DPC. No caso, também se aplicou em tricromatas normais uma versão do teste que usava o modelo proposto para simular a percepção de indivíduos com DPC, simulando a aplicação do teste nestes indivíduos. Os resultados dos testes simulados foram equivalentes aos resultados do teste original aplicado a indivíduos com DPC.

D.2 A Técnica de Realce de Contraste de Cores

A técnica de recoloração proposta se baseia na seguinte observação: sempre que indivíduos portadores de dicromacia sofrem alguma perda significativa na percepção de contraste de cor, boa parte deste contraste pode ser recuperado se, ao trabalhar num espaço de cores perceptualmente uniforme, as cores originais forem projetadas num plano alinhado com a direção que maximiza a perda de contraste (no sentido de mínimos quadrados). As coordenadas dessas projeções se tornam as coordenadas da nova cor no gamut reduzido (2D) dos dicromatas. A Figura D.5 resume este processo, que consiste dos seguintes passos:

1. o vetor v_{ab} que representa a direção que maximiza a perda de contraste no plano de cromaticidade CIE $L^*a^*b^*$ é estimado e
2. as cores originais são projetadas no plano definido por v_{ab} e o eixo de luminosidade (L^*). As coordenadas das cores projetadas são então rotacionadas em torno de L^* para que se alinhem ao plano aproximado ao gamut dos dicromatas. As cores resultantes são usadas na imagem recolorida.

Visando garantir coerência temporal, o algoritmo verifica e corrige mudanças abruptas no sentido de v_{ab} .

O gamut de cores referente a cada classe de dicromacia pode ser representada por dois semi-planos no espaço de cores LMS (BRETTEL; VIÉNOT; MOLLON, 1997) e pode ser satisfatoriamente aproximada a um plano (VIÉNOT; BRETTEL; MOLLON, 1999). A Figura D.4 mostra esses planos mapeados para o espaço de cores CIE $L^*a^*b^*$. De acordo com Kuhn *et al.* (KUHN; OLIVEIRA; FERNANDES, 2008a) os ângulos entre tais planos e o plano L^*b^* são $\theta_p = -11.48^\circ$, $\theta_d = -8.11^\circ$ e $\theta_t = 46.37^\circ$ para protanopia, deuteranopia e tritanopia, respectivamente. As cores ilustradas na Figura D.4 representam os gamuts de cores presentes em cada classe de dicromacia.

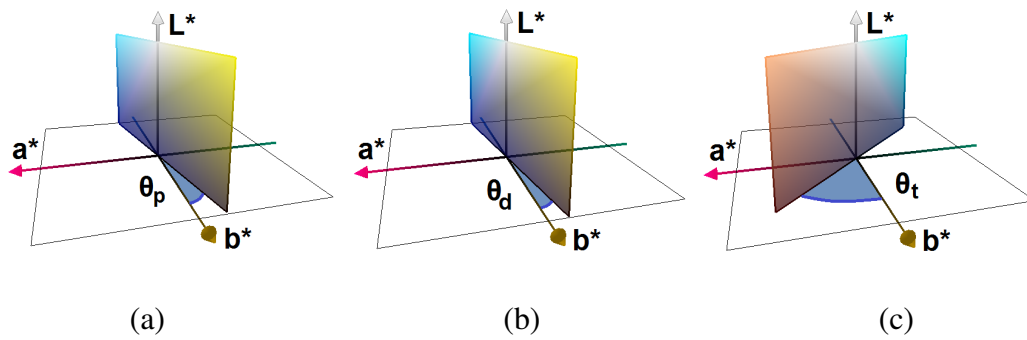


Figure D.4: Planos que se aproximam aos gamuts de cores referentes às percepções dos dicromatas no espaço de cores CIE $L^*a^*b^*$ (KUHN; OLIVEIRA; FERNANDES, 2008a). (a) Protanopia ($\theta_p = -11.48^\circ$). (b) Deuteranopia ($\theta_d = -8.11^\circ$). (c) Tritanopia ($\theta_t = 46.37^\circ$).

Calcular a direção que maximiza a perda de contraste local (no sentido de mínimos quadrados) referente à percepção de uma imagem I por um indivíduo portador de dicromacia pode requerer a avaliação, para cada pixel $p_i \in I$, da perda de contraste entre p_i e todos os pixels p_j numa vizinhança N_i em torno de p_i . Entretanto, devido à coerência espacial, os pixels vizinhos tendem a apresentar valores semelhantes. Logo, a estimativa de perda de contraste local para cada pixel p_i contra todos os pixels em N_i tende a resultar em trabalho reduntante. A técnica proposta evita efetuar este cálculo em toda a vizinhança N_i ao recorrer à abordagem para amostragem por pareamento Gaussiano proposta por Grundland e Dogdson (GRUNDLAND; DODGSON, 2007). Neste caso, a contribuição de cada pixel p_i para a perda de contraste local é estimada para apenas um vizinho p_j . As distâncias horizontais e verticais entre p_i e p_j são definidas aleatoriamente de acordo com uma distribuição Gaussiana univariada com mediana zero e variância $(2/\pi)\sigma^2$, onde $\sigma^2 = \sqrt{2\min(\text{width}, \text{height})}$ (GRUNDLAND; DODGSON, 2007). A função $\min(a, b)$ retorna o menor valor entre a e b , e width e height referem-se às dimensões da imagem. Embora a direção que maximiza a perda de contraste local obtida usando esta estratégia de amostragem difira da calculada quando se usa a vizinhança inteira, devido a coerência

espacial essas direções tendem a ser suficientemente próximas umas das outras. Visando evitar *flickering* durante a recoloração de seqüências de vídeos ou animadas, o algoritmo proposto pré-calcula as coordenadas dos p_j s e as salva numa textura. Durante toda a seqüência, os mesmos pares (p_i, p_j) são usados.

As Figuras D.5 (a) e (b) ilustram o processo de cálculo da direção que maximiza a perda de contraste para dois pares de cores, (c_1, c_2) e (c_3, c_4) , representados como pequenas esferas no espaço de cores $L^*a^*b^*$. c'_1 a c'_4 ilustram as projeções das cores c_1 a c_4 , respectivamente, no plano do dicromata, e representam suas percepções de cores pelos dicromatas (Figure D.5(a)). Sendo $L^*a^*b^*$ aproximadamente perceptualmente uniforme, a relativa perda de contraste de cor vivenciada pelo dicromata ao observar um par de cores (c_i, c_j) (referente a um observador com visão de cores normal) pode ser estimado como

$$l_{(c_i, c_j)} = \frac{\|c_i - c_j\| - \|c'_i - c'_j\|}{\|c_i - c_j\|}, \quad (D.9)$$

onde $\|\cdot\|$ é o operador de comprimento de vetores. Para este par de cores, a direção de perda de contraste é dada por $\vartheta_{ij} = c_i - c_j$. Para evitar inversão de polaridade (KUHN; OLIVEIRA; FERNANDES, 2008a), o algoritmo proposto preserva a coordenada de luminosidade (*i.e.*, L^*) das cores originais. Logo, é suficiente calcular a direção que maximiza a perda de contraste apenas no plano de cromaticidade. Não há vantagens em efetuar este cálculo nas três dimensões do espaço $L^*a^*b^*$, além disso, seria requerido calcular os autovetores numa matrix 3×3 em vez de numa 2×2 . Portanto, seja $w_i = l_{(c_i, c_j)} \vartheta_{ij}$ o vetor que representa a perda de contraste ao longo da direção ϑ_{ij} associada ao pixel p_i e seja

$$M = \begin{bmatrix} w_1^{a^*} & w_1^{b^*} \\ w_2^{a^*} & w_2^{b^*} \\ \dots & \dots \\ w_n^{a^*} & w_n^{b^*} \end{bmatrix} \quad (D.10)$$

uma matriz cujas linhas contêm as coordenadas dos vetores de cromaticidade referentes à perda de contraste de todos os pixels na imagem I , os elementos da i -ésima linha de M representam as projeções de w_i no plano a^*b^* , logo, v_{ab} pode ser obtido como o autovetor da matriz $2 \times 2 M^T M$ cujos autovalores correspondentes têm o maior valor absoluto. A fim de resolver a equação característica correspondente, o algoritmo atribui o valor um à coordenada b^* de v_{ab} e soluciona para sua coordenada a^* .

Quando a percepção de um dicromata sofre com uma significativa perda de contraste de cor, a projeção ortográfica das cores originais no plano definido pelos vetores L^* e v_{ab} tendem a proporcionar um maior espalhamento das cores se comparado à projeção direta no plano dicromático. Esta situação é ilustrada na Figura D.5 (a) e (c). Ao transferirmos a relação espacial entre as cores projetadas no plano L^*-v_{ab} para o plano dicromático, uma imagem com melhor contraste de cores é produzida. Para isto, rotaciona-se as cores projetadas em torno do eixo L^* visando o alinhamento destas com o plano dicromático. A Figura D.5 (d) ilustra esta operação, que preserva as cores acromáticas da imagem original.

Coerência temporal é um requisito importante para as técnicas de recoloração de imagens, já que mudanças sutis na cor de um objeto durante uma sessão interativa de visualização ou animação pode incomodar bastante os observadores. Se a direção de v_{ab} é praticamente paralela ao eixo a^* , uma pequena mudança nas cores de entrada pode implicar na inversão do sinal do componente b^* de v_{ab} (veja Figura D.5(b)). Entretanto, para

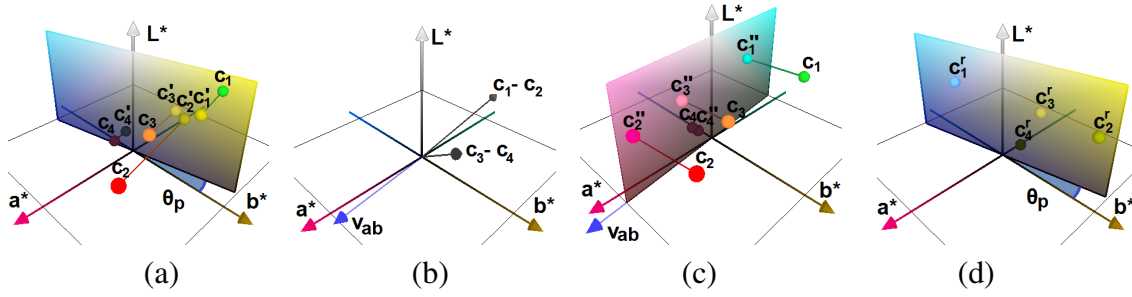


Figure D.5: Ilustração dos passos do algoritmo de recoloração proposto. (a) As cores c_1 a c_4 são percebidas por um dicromata como c'_1 a c'_4 , respectivamente (suas projeções no plano referente ao gamut do dicromata). A relativa perda de contraste, quando um par de cores (c_i, c_j) é percebido por um dicromata, é dada por $l_{(c_i, c_j)} = (\|c_i - c_j\| - \|c'_i - c'_j\|) / (\|c_i - c_j\|)$, o que acontece ao longo da direção $v_{ij} = c_i - c_j$. (b) A direção v_{ab} (em azul) que maximiza a perda de contraste local (no sentido de mínimos quadrados) é calculada como o principal autovetor da matriz $M^T M$, onde M está definido na Equação D.10. (c) A projeção das cores originais no plano definido por v_{ab} e L^* . (d) As cores finais obtidas após a rotação das cores projetadas c''_k em (c) em torno de L^* para que se alinhem com o plano do dicromata.

a solução da equação característica associada com o cálculo de v_{ab} , foi arbitrado o valor 1 ao seu componente b^* , como uma maneira possível de evitar a solução trivial $v_{ab} = 0$. Isto restringe o sinal do componente b^* de v_{ab} como positivo, causando a inversão do sinal do componente a^* para adaptar a mudança na direção de v_{ab} . Esta inversão pode provocar mudanças abruptas nas cores dos pixels recoloridos entre quadros consecutivos (*e.g.*, pixels azuis poderiam virar amarelos e vice-versa). Para evitar a ocorrência destes artefatos durante uma sessão interativa de visualização (ou animação) o algoritmo registra as coordenadas do vetor v_{ab} referentes ao quadro atual para comparação com as coordenadas do vetor obtido no próximo quadro. Caso o ângulo entre ambos os vetores (atual e anterior) se aproxime de 180° , o algoritmo inverte o sentido do v_{ab} atual, visando forçar consistência de cor. Apesar de simples, esta é uma solução eficaz.

Os resultados do algoritmo proposto estão apresentados na Figura D.6 que os compara com os resultados obtidos pela técnica de Kuhn *et al.*. A Tabela D.2 resume o ganho de performance alcançado pelo algoritmo proposto ao comparar os tempos de execução de ambas as versões (CPU e GPU) com a técnica de Kuhn *et al.* para um conjunto de sete imagens de diversos tamanhos. Os registros na tabela estão apresentados em ordem crescente pelo número de pixels das imagens. Como pode-se observar, em ambas as versões (CPU e GPU), a técnica proposta apresenta ganhos de performance de até duas ordens de magnitude mais rápidas do que a técnica de Kuhn *et al.* para imagens de até 800×800 pixels. Como o custo do algoritmo proposto é linear no número de pixels, a aceleração alcançada apresentará ganhos em performance ainda mais significativos para imagens com maiores dimensões.

D.3 Conclusões

Este capítulo apresentou resumidamente as técnicas propostas nesta dissertação de mestrado que consistem de um modelo para simulação da percepção de cores e uma técnica de realce de contraste de cores.

Imagem (tamanho)	CPU		GPU	
	Proposta Tempo	Kuhn Tempo	Proposta Tempo	Kuhn Tempo
Flame (288x184)	0,055	1,148	0,019	0,121
Chart (500x300)	0,191	2,707	0,020	0,106
Foot (446x446)	0,252	3,743	0,021	0,307
Brain (532x523)	0,292	5,053	0,023	0,577
Knee (528x528)	0,341	5,217	0,022	0,313
Europe (596x486)	0,385	5,361	0,023	0,565
Nebula (800x800)	0,614	11,73	0,028	1,145

Table D.2: Comparação entre as performances (em segundos) da técnica proposta e a técnica apresentada por Kuhn *et al.* (KUHN; OLIVEIRA; FERNANDES, 2008a) para suas versões CPU e GPU. Devido ao custo linear da técnica proposta, a aceleração relativa é ainda melhor para imagens de maiores dimensões.

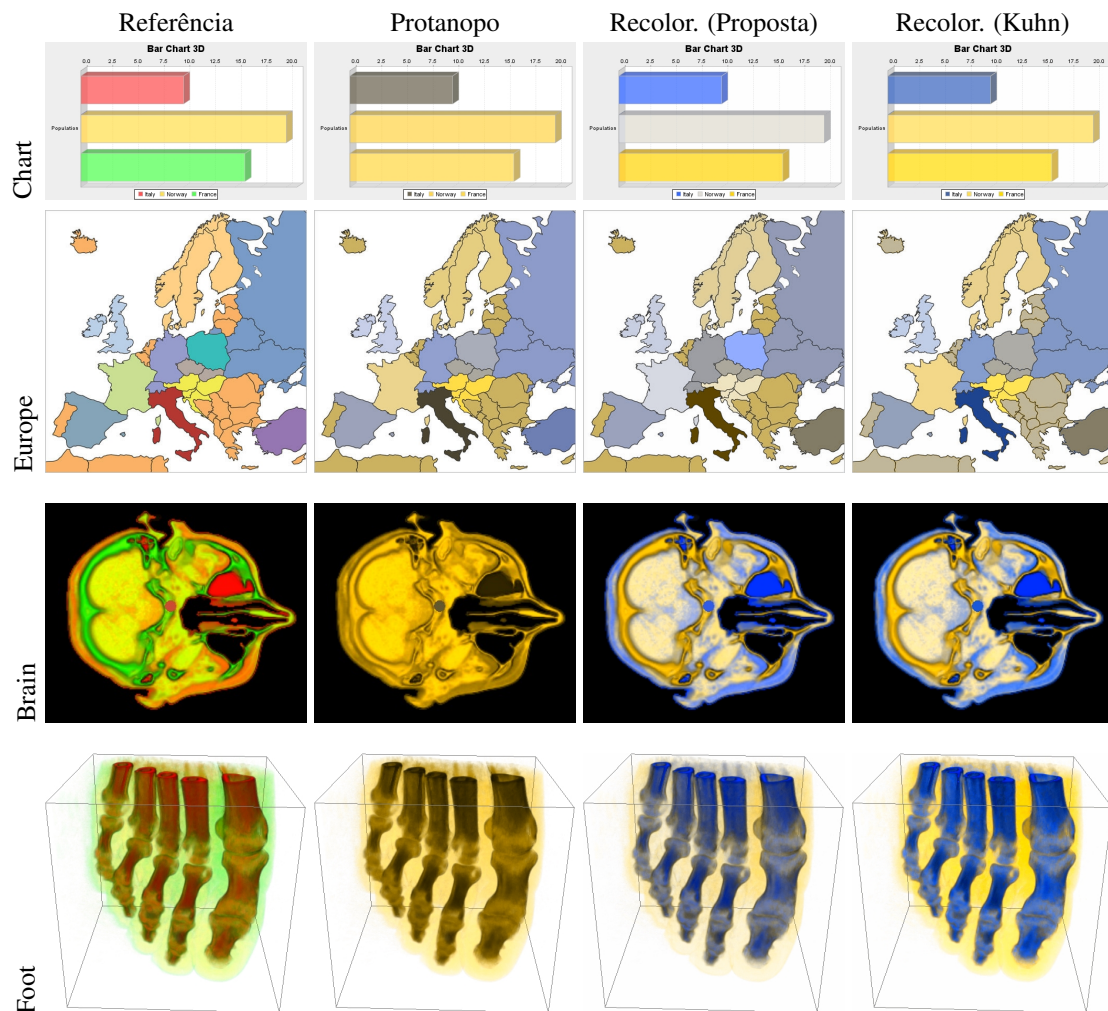


Figure D.6: Imagens comparando os resultados de recolorações da técnica proposta com a técnica apresentada por Kuhn *et al.* (KUHN; OLIVEIRA; FERNANDES, 2008a).

O modelo proposto é o primeiro a consistentemente tratar visão de cores normal, tricromacia anômala e dicromacia usando um *framework* unificado. Por meio de experimentos controlados com usuários, foi demonstrado que os resultados produzidos pelo modelo proposto se equiparam à percepção de indivíduos com deficiências na percepção de cores. Os resultados do modelo proposto foram comparados com os obtidos com modelos existentes para simulação da percepção de tricromatas anômalos (YANG et al., 2008) e dicromatas (BRETTEL; VIÉNOT; MOLLON, 1997). Tais comparações indicaram que os resultados do modelo são superiores aos de Yang *et al.* (YANG et al., 2008) para tricromacia anômala e equivalentes aos de Brettel *et al.* (BRETTEL; VIÉNOT; MOLLON, 1997) para dicromacia.

A técnica de recoloração apresentada é a primeira a oferecer recoloração de imagens para dicromatas em tempo-real, com coerência temporal e alta qualidade. Seu custo computacional varia linearmente com o número de pixels de entrada e pode ser eficientemente implementado em GPUs. Foi mostrado que os resultados produzidos com a técnica proposta apresentam resultado pelo menos tão bons quanto os obtidos com as técnicas estado-da-arte, sendo que com tempos de execução até duas ordens de magnitude mais rápidos. Além disso, os resultados da técnica proposta permitem o desenvolvimento de aplicações mais amigáveis para indivíduos com deficiência na percepção de cores, já que o baixo custo computacional desta técnica faz dela uma solução adequada para implementação em telefones celulares e outros dispositivos móveis equipados com câmeras. Em tais dispositivos, a capacidade de recoloração desta técnica pode ser uma ferramenta útil para auxiliar indivíduos com deficiência na percepção de cores em diversas tarefas cotidianas.

A integração de ambas as técnicas com um sistema de visualização foi bem sucedida, utilizando uma abordagem minimamente invasiva através de suas implementações voltadas para GPUs. A Figura D.7 exibe algumas telas deste aplicativo com as opções para simular a percepção de indivíduos com DPC (Figura D.7 centro) e recolorir para realçar contraste de cores para estes indivíduos (Figura D.7 direita).

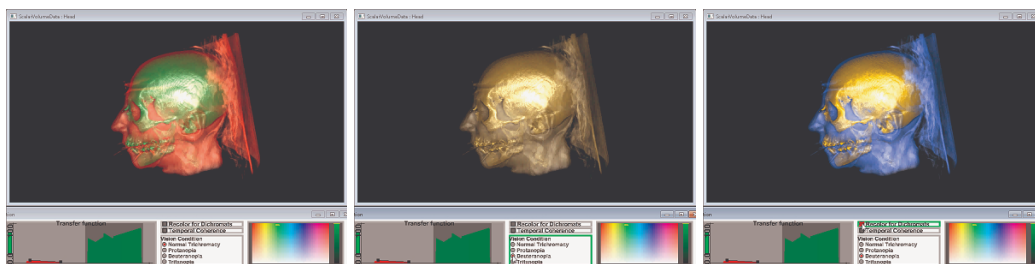


Figure D.7: Integração das técnicas propostas com um sistema de visualização existente. Esquerda: imagem de referência como percebida por um indivíduo com visão de cores normal. Centro: simulação da percepção de deuteranopos da imagem de referência usando o modelo proposto. Direita: imagem recolorida para deuteranopos usando a técnica proposta. Implementações minimamente invasivas voltadas para GPUs.

“ A Model for Simulation of Color Vision Deficiency and a Color Contrast
Enhancement Technique for Dichromats”

por

Gustavo Mello Machado

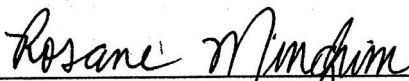
Dissertação Apresentada aos Senhores:



Profa. Dra. Carla Maria Dal Sasso Freitas
(UFRGS)



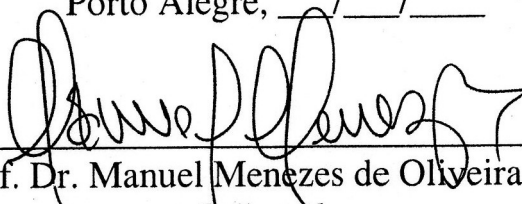
Prof. Dr. Marcelo Walter
(UFRGS)



Profa. Dra. Rosane Minghim
(ICMC - USP)

Vista e permitida a impressão.

Porto Alegre, ____/____/____



Prof. Dr. Manuel Menezes de Oliveira Neto
Orientador